The potential of lightweight materials and advanced engines to reduce life cycle energy and greenhouse gas emissions for ICVs and EVs using design harmonization techniques

by

Anne Marie Lewis

A dissertation submitted in partial fulfillment
of the requirements for the degree of
Doctor of Philosophy
(Mechanical Engineering and Natural Resources and Environment)
in the University of Michigan
2013

Doctoral Committee:

Professor Dionissios N. Assanis, Co-Chair
Professor Claus Borgnakke, Co-Chair
Professor Gregory A. Keoleian, Co-Chair
Professor John M. DeCicco
Assistant Research Scientist Jarod C. Kelly
Research Scientist George A. Lavoie
Professor Huei Peng

Acknowledgements

I am deeply grateful to many people for their support and guidance during my doctoral studies. I would like to thank my advisors in Mechanical Engineering and Natural Resources and Environment, Provost Dennis Assanis, Prof. Greg Keoleian, and Prof. Claus Borgnakke, who have shared their expertise and challenged and inspired me in many ways. I am especially thankful for their support of my joint PhD through the Student Initiated Degree Program, without which I could not have pursued the research topic that I was most interested in.

I am also extremely thankful to my dissertation committee members for offering their guidance and many insightful conversations as the dissertation research evolved. In particular, I would like to thank Dr. George Lavoie for sharing his expertise and offering his tremendous assistance with co-authoring a journal paper (Chapter 4). Also, I am grateful to Dr. Jarod Kelly for sharing his insight on a weekly basis and always making time to discuss details of the dissertation with me. I have also learned a great deal from Prof. John DeCicco and am very grateful for the time he taken to meet with me throughout the years. Last but not least, I am thankful to Prof. Huei Peng for sharing his expertise of hybrid powertrains and supporting the research as Director of the US-China Clean Energy Research Center (CERC).

I have been fortunate to be a member of two terrific labs during my doctoral research: the Automotive Laboratory in Mechanical Engineering and Center for Sustainable Systems in Natural Resources and Environment. I cannot express enough how grateful I am to have met such wonderful people and developed friendships with some of the smartest people I have known. Their support, both intellectually and emotionally, has been invaluable.

Lastly, I am eternally grateful to my parents for providing me with the best education and opportunities they could since I was young. I could not have made it nearly this far without their support and love!

Table of Contents

List of Figures

List of Tables

List of Notations

ΔVM_{nonpwt}	change in vehicle mass due to non-powertrain subsystems
Da	Damkohler number
ρ	density
μ	dynamic viscosity
x_{EGR}	EGR mass fraction
E	elastic modulus
x_{EV}	percent change in mass for powertrain-dependent subsystems
ϕ	fuel air equivalence ratio
τ_{ID}	ignition delay (ms)
K	Karlovitz stretch factor
S_L	laminar flame speed
δ_L	laminar flame thickness
M	material index
γ_i	mass influence coefficient for subsystem *i*
γ_V	mass influence coefficient for the vehicle
$M_{bodystruc}$	mass of the body structure subsystem
$m_{frontsusp}$	mass of the front suspension subsystem
$m_{fuelexh}$	mass of the fuel and exhaust subsystem
M_{RS}	mass of the vehicle after lightweight (re-sizing)
M_0	mass of the vehicle before lightweighting
η_{OTC}	overall turbocharger efficiency
P	pressure (bar)
Δ	primary mass change
β	ratio of S_L for ethanol to iso-octane
γ	ratio of specific heats
τ_{RES}	residence time (ms)
T	temperature (K)
ΔCA50	the difference between the CA50 that does not knock and CA50 for MBT timing
L	turbulence integral length scale
u’	turbulence intensity
Re_t	turbulent Reynolds number

List of Abbreviations

A/HSS	advanced/high strength steel
ATDC	after top dead center
BIW	body-in-white
BMEP	brake mean effective pressure (bar)
BSFC	brake specific fuel consumption (g/kWh)
BTE	brake thermal efficiency
CA50	crank angle at 50% mass fraction burned
CAD	crank angle degrees
E85	85% ethanol, 15% gasoline (by volume)
EGR	exhaust gas recirculation (mass fraction)
EVO	Exhaust Valve Open
EVC	Exhaust Valve Close
GDI	gasoline direct injection
GHG	greenhouse gas
HCCI	homogeneous charge compression ignition
HEDGE	high-efficiency dilute gasoline engine
HEG	high efficiency gasoline
HEV	hybrid electric vehicle
ICV	internal combustion vehicle
IVO	Intake Valve Open
IVC	Intake Valve Close
LCA	life cycle assessment
LHV	lower heating value
MBT	maximum brake torque
MPG	miles per gallon
MPGe	miles per gallon equivalent
NA	naturally aspirated
ON	octane number
PHEV	plug-in hybrid electric vehicle
RPM	revolutions per minute
SI	spark ignition
TDC	top dead center
WOT	wide open throttle

Abstract

Lightweight materials and advanced combustion engines are being used with conventional and electrified vehicles to increase fuel economy, but such technologies may require more energy to produce and the impact of plug-in hybrid electric vehicles (PHEVs) is dependent on the electric grid. In this study, life cycle assessment (LCA) is used to evaluate the total energy and GHG emissions for baseline and lightweight internal combustion vehicles (ICVs), hybrid electric vehicles (HEVs) and PHEVs when they are operated with baseline and advanced gasoline and ethanol engines. Also, design harmonization techniques are developed to enable a comparison across diverse vehicle platforms by creating functionally equivalent conventional and hybrid vehicle models that account for increased structural support required for heavier, electrified powertrains. Lightweight vehicle models include primary and secondary mass reductions (including powertrain re-sizing) and are evaluated with body-in-white mass reduction scenarios with aluminum-intensive and advanced/high strength steel (A/HSS) designs. Advanced engine/fuel strategies are incorporated in the vehicle models with fuel economy maps, which were developed with a novel method to ensure combustion limits are not violated under boosted and dilute conditions for high compression ratio engines.

The harmonized vehicle models show that the structural mass required per kg of powertrain mass for electrified vehicles is 0.2-0.3 kg. As compared to lightweight materials, more significant life cycle improvements are achieved by using advanced gasoline and E85 engines, as fuel consumption is reduced up to 24%. As compared to A/HSS, more mass can be removed from the vehicle with aluminum, leading to greater fuel consumption and life cycle reductions. However, due to the higher energy and GHG emissions associated with aluminum production, more significant life cycle reductions occur for an equivalent decrease in vehicle mass with A/HSS. Also, life cycle impacts are reduced more for ICVs as compared to hybrid vehicles because fuel economy is most sensitive to mass for ICVs. Considering the same vehicle platform, the combination of

lightweight materials and advanced engines yields the most life cycle energy and GHG reductions of the scenarios considered in this work, as the technologies provide complimentary results due to engine downsizing. The least life cycle energy and GHG emissions occur for the lightest weight hybrid vehicles using the downsized/turbocharged gasoline or E85 engine.

Chapter 1: Introduction, Motivation, Objectives and Approach

1.1 Motivation

In an effort to increase energy security and mitigate impacts of global warming, advanced vehicle technologies are being developed to increase vehicle efficiency and decrease greenhouse gas (GHG) emissions. In particular, lightweight materials and advanced combustion engines are being used to increase fuel economy for both conventional and electrified vehicles, especially as automobile manufacturers are required to meet fuel economy targets for 2017-2025 CAFE [1], [2]. Vehicle electrification is also increasing in popularity as more conventional vehicles are equipped with stop/start technology and hybrid and plug-in hybrid electric vehicles (HEV, PHEV) are gaining market share [3]. While these technologies are effective at reducing fuel consumption during the vehicle operation, the energy and emissions upstream of vehicle use may increase. For instance, lightweight materials are often more energy intensive to produce and vehicle electrification is dependent on the electricity from the grid, which varies according to fuel source [4], [5]. Also, highly efficient engines often require additional hardware (e.g. turbocharger system) or advanced fuels which could increase the material production energy consumption and GHG emissions. Since life cycle assessment (LCA) evaluates vehicle production, operation and end-of-life management, it is a useful tool to evaluate the impact of lightweight vehicles with advanced conventional and electrified powertrains [6].

1.2 Lightweight vehicles

The reduction in life cycle energy and GHG emissions that results from using lightweight materials to reduce vehicle mass is dependent on the following inputs: 1) the total mass that may be reduced from the vehicle, 2) the energy and GHG emissions required to produce and dispose of the lightweight materials and 3) the energy consumed and GHGs emitted during operation and upstream of the vehicle use. Also, assumptions

regarding vehicle miles traveled (VMT) and the lifetime of the vehicle are important for the analysis since vehicles that are more energy intensive to produce have a longer payback period, but may be more beneficial in the long-term.

1.2.1 Mass reduction potential

Methods of vehicle mass reduction include material substitution, vehicle redesign, and vehicle downsizing [7], [8]. Mass is reduced through material substitution by replacing standard materials, such as steel, with lighter weight, higher strength materials. The amount of mass that can be reduced through this substitution alone depends on the lightweight material properties and the function of the original component [9]. Vehicle redesign, the second method to mass reduction, is achieved by either optimizing the vehicle design in some way (e.g. redesign the body structure with optimization techniques) or by downsizing vehicle subsystems after a primary mass reduction occurs, known as a secondary mass reduction [10], [11]. The third method to mass reduction, vehicle downsizing, requires changing the dimensions of the vehicle to provide weight savings. While vehicle downsizing can be a significant method to mass reduction (e.g. downsizing from one EPA size-class to the next size-class results in a 8-11% weight reduction [7]), it is not considered in this work because vehicle mass reductions are assumed to occur without altering the original vehicle dimensions. Thus, primary mass reductions through material substitution and secondary mass reductions through subsystem resizing are the focus of this work.

Since lightweighting is applicable to vehicles that use any powertrain technology, the mass reduction potential of diverse powertrain vehicles must be determined in a consistent manner. Previous work has done this by ensuring that vehicle performance is constant by re-sizing powertrain components [12], [13]. Also, some studies have accounted for structural support required for heavier, electrified powertrains [8], [14]. This work expands upon previous work by developing a novel design harmonization method that maintains functional equivalency (including vehicle performance) for diverse powertrain vehicles and accounts for additional structural support for heavier powertrains based on vehicle teardown data.

1.2.1.1 Material substitution (Primary mass reductions)

Lightweight automotive materials, such as aluminum, advanced/high strength steel (A/HSS), magnesium and plastics and polymer composites, such as carbon fiber reinforced plastic (CFRP), have the potential to replace conventional steel and reduce vehicle weight. However, due to cost and manufacturing limitations of magnesium and non-metals, the percentage of HSS and aluminum in the light-duty vehicle fleet is increasing at a far faster rate [15]. Since HSS enables structural designs that are simultaneously stronger and lower in mass, it is currently being used to replace mild steel in a variety of subsystems, such as the powertrain, suspension, chassis, front-end and body-in-white (BIW), which is the bare body shell after welding but before painting [16]. Aluminum has a much lower density than steel and is being used to replace steel in parts such as the engine blocks, cylinder heads, wheels, closures and BIW. In fact, all-aluminum bodies have been used in production vehicles such as the Audi A2 and A8, Jaguar XJ, Mercedes SL, Land Range Rover, and Tesla Model S [16], [17]. Based on these trends, this work focuses on HSS and aluminum as a means to reduce vehicle mass.

The mass reduction potential of aluminum and A/HSS has been assessed using engineering analysis including computer aided engineering (CAE) and optimization [18], [19], [20], [21], [22]. For instance, recent studies by NHTSA, The Aluminum Industry and WorldAutoSteel have evaluated the potential to reduce mass of the BIW [18], [21], [22]. NHTSA found that by using an aluminum-intensive design (modeled after Audi's spaceframe concept), the BIW mass could be reduced by 35% [18]. However, The Aluminum Industry found that up to a 42% reduction could be made while maintaining structure requirements [21]. With regards to A/HSS, NHTSA determined a 22% BIW mass reduction was possible, while WoldAutoSteel found a 35% reduction using a combination of current and near-future steels [18], [22].

1.2.1.2 Secondary mass reductions

After an initial mass is removed from the vehicle, other subsystems may be downsized while performance is maintained. The magnitude of these secondary mass savings is typically assessed using regression analysis of vehicle teardown data [11], [23]. Based on this data, mass influence coefficients are calculated for each subsystem, defined as ratio of change in subsystem mass per unit change in gross vehicle mass. Previous

studies have found that secondary mass savings, which include powertrain resizing, range from 23% to 180% of the initial mass change [23], [24].

1.2.1.3 Design harmonization of conventional and electrified vehicles

As conventional and electrified vehicles are expected to utilize lightweight vehicle designs, there is a need to assess their combined impact on reducing life cycle energy and GHG emissions. Accordingly, the mass reduction potential of these vehicles must be evaluated with baseline and lightweight vehicle models that preserve the same functional equivalency across diverse vehicle platforms. It is necessary to define the functional equivalency to ensure that life cycle results are comparable, but this definition may differ according to the scope and objective of the study.

While previous work relating to design harmonization techniques is limited, recent studies have assessed the vehicle use phase of the life-cycle for conventional and electrified vehicles by ensuring that performance requirements are equivalent for all vehicles [12], [25]. For instance, Argonne National Laboratory (ANL) has compared the vehicle operation of conventional and electrified vehicles by sizing powertrain components based on performance criteria (e.g. engines are sized for gradeability and acceleration, HEV motors are sized to capture drive cycle regenerative energy) [12]. Also, previous work has determined the mass of electrified vehicle by adding/subtracting the mass of (P)HEV components to an ICV model as necessary [8], [26], [27].

Since (P)HEVs are likely to have a heavier powertrain mass than conventional vehicles which must be managed in a crash, possible structural design changes must be considered. Previous work has addressed this with a number of approaches, ranging from detailed modeling with finite element analysis (FEA) to a constant glider method, which assumes no additional structure is required [20], [26]. Additionally, studies have assumed a structural mass multiplier, such as 0.5 kg of structural mass per 1 kg increase in powertrain mass [8]. While detailed modeling techniques provide the most technical accuracy, they are often beyond the scope of LCAs. On the other hand, there is no certainty that the other approaches yield appropriate results, given a certain powertrain mass increase. Thus, this work provides an alternative approach to determine the structural mass required for heavy powertrains as part of the design harmonization techniques in Chapters 2-3.

1.2.2 Material production energy intensity

As shown in Table 1, the energy and GHG emissions due to material production vary substantially for aluminum and steel. Due to the energy intensive process of reducing alumina to aluminum, the energy and emissions of primary aluminum are significantly higher than steel [5], [28]. However, by recycling aluminum, this process is eliminated and the energy required is much more similar to steel [28]. Since the majority of energy required to produce aluminum is in the form of electricity, the GHG intensity varies greatly according to the fuel mix of the grid and electricity allocation protocol [28], [29]. On the other hand, the production of A/HSS requires little to no additional energy as compared to conventional steel. Steel is strengthened mainly by alloying elements or thermally treating the metal, which are reported by the steel industry to be less than 5% of the overall production impacts [30], [31].

Table 1. Energy and GHG emission intensities

		MJ/kg	kgGHG/kg
Primary steel/AHSS		26.10 [32]	2.36 [32]
Secondary steel/AHSS		13.06 [32]	0.88 [32]
Primary wrought aluminum	Extruded	147 [33]	10.74 [33]
	Cold rolled sheet	218 [33]	15.94 [33]
Primary cast aluminum		168 [33]	12.22 [33]
Secondary wrought aluminum	Extruded	11.56 [34]	0.84 [34]
	Cold rolled sheet	28.26 [34]	2.08 [34]
Secondary cast aluminum		19.06 [34]	1.37 [34]

1.2.3 Vehicle efficiency

Vehicle mass reduction increases vehicle efficiency by reducing the tractive effort required to move the vehicle. As shown in Equation 1, tractive force, F_t, is a function of vehicle mass and is the sum of rolling resistances, F_{roll}, inertial forces, F_i, aeordynamic drag, F_{aero}, and forces due to the grade of the road, F_g [N]:

$$\boldsymbol{F_t = F_{roll} + F_i + F_{aero} + F_g = C_R(mg) + ma + \frac{1}{2}C_D\rho v^2 A + mg\sin\theta}$$

Equation 1: Vehicle tractive force

where C_R is the rolling resistance coefficient [-]

m is the vehicle mass [kg]

g is the gravitational acceleration	[m/s^2]
a is vehicle acceleration	[m/s^2]
C_D is the drag coefficient	[-]
ρ is the air density	[kg/m^3]
v is the vehicle velocity	[m/s]
A is the vehicle frontal area	[m^2]
θ is the grade of the road	[deg]

Accordingly, as mass decreases less effort is required to accelerate the vehicle, overcome friction at the wheels, and meet the desired vehicle speed at a non-zero road grade.

Many studies have assessed the fuel consumption reductions possible due to vehicle lightweighting for an internal combustion vehicle (ICV) [10], [13], [35], [36], [37], [38]. This is commonly reported as an elasticity of mass and fuel consumption, or the percent change in fuel consumption (or MPG) per percent change in vehicle mass [35]. Previous work has found that for a conventional vehicle, a 10% mass reduction results in a fuel consumption reduction of between 1.9-8.2% [10], [13], [16], [35], [36], [37], [38]. The disparity in these results is due to assumptions regarding the vehicle size, drive cycle characteristics (e.g. the frequency of acceleration events), and powertrain re-sizing [10], [36]. The maximum improvements occur when the powertrain is re-sized to maintain performance, as fuel consumption is reduced between 5.5-8.2% [10], [13], [36], [37].

Previous work has shown that the relationship between vehicle mass and fuel consumption is highly dependent on powertrain architecture [13], [35], [36], [38], [39]. For instance, a study by An et al. found that with a constant vehicle mass, a "vertical leap" in fuel economy is possible when switching from a conventional to electric hybrid powertrain [35]. However, once this change is made the benefit of mass reduction is less for the HEV (i.e. for the same mass change on an ICV and HEV, the change in fuel consumption is less for the HEV) [35]. These two trends are due to the fact that HEVs are able to capture kinetic energy through regenerative braking and eliminate engine idling, which is a significant source of efficiency losses for ICVs. Recent work by Carlson et al. has validated these modeling results through on-road validation by comparing the energy

consumption of a Ford Fusion (ICV), Ford Fusion Hybrid (HEV) and Nissan Leaf (BEV) when weight is incrementally added to the vehicle [38]. Results showed that for the same mass change, the absolute change in energy consumption for the vehicle operation is greatest for the ICV and least for the BEV [38].

Recent work has also assessed the importance of powertrain downsizing for vehicles with diverse powertrains and found that when powertrains are re-sized to maintain performance, fuel consumption is reduced much more for ICVs as compared to HEVs [13], [36]. HEV powertrain efficiency is very dependent on the control strategy as this determines when and how to use the engine and motor to deliver power to the wheels [13]. Also, since HEVs rely on regenerative energy to increase powertrain efficiency, downsizing the motor and battery may limit the amount of energy that can be regenerated [13], [36]. However, ICV powertrains benefit significantly from downsizing because smaller engines have less losses associated with friction and throttling (see Section 1.3.2 High Efficiency Gasoline Engine for a more detailed explanation) [13], [36], [37]. In fact, the mass elasticity of fuel consumption has been shown to be very low for ICVs if the powertrain is not re-sized [13], [36], [38]. This is because as mass is reduced from the vehicle, the load required from the engine is less and these low load operating conditions are less efficient [13], [36]. Thus, downsizing is needed to shift the operating condition to higher loads that have a higher efficiency [13], [36]. Accordingly, recent modeling work has shown that powertrain re-sizing for an ICV reduces fuel consumption by an equivalent or greater amount than vehicle mass reduction alone [36].

1.2.4 Life cycle results

Previous LCAs have assessed the energy and GHG reduction potential of aluminum and HSS for light-duty vehicles [5], [40]. These studies have shown that the life cycle results are a function of the increase in energy and emissions during vehicle production, which is offset by reductions during the vehicle use [5], [40]. For instance, Kim et al. compared aluminum and HSS in a life cycle model, assuming that the vehicle mass can be reduced at most 23% with aluminum substitutions and 19% with a combination of HSS substitutions and secondary mass reductions [4]. A range of emission factors associated with material production was considered for each material, including information for recycled materials (assuming a closed-loop recycling scenario) [4]. Due

to the increased vehicle production burden of aluminum as compared to HSS, the total life cycle GHG emissions are higher for the lightweight aluminum vehicle, despite lower GHG emissions produced during the vehicle operation. However, if closed-loop recycling is considered, the payback period of the lightweight aluminum vehicle is significantly reduced. Overall, previous work has shown that aluminum and A/HSS can reduce life cycle energy and GHG emissions, but the significance of these reductions is highly dependent on assumptions regarding material intensities (i.e. gCO2/kg, MJ/kg), vehicle modeling methods and the vehicle lifetime [5], [40], [41].

1.3 Advanced combustion engines

1.3.1 Thermodynamic review

The potential of advanced combustion engines to reduce fuel consumption, and therefore life cycle energy and GHG emissions, is a function of the thermodynamic potential of these engine/fuel strategies. Engine efficiency can be expressed in a number of ways, including fuel conversion, combustion, or thermal efficiency. Fuel conversion efficiency, η_f, is a measure of the work output per unit energy supplied and is a function of combustion and thermal efficiency, as shown in Equation 2. Combustion efficiency, η_c, which quantifies the energy released per energy supplied, is generally very close to 100% for stoichiometric spark-ignited (SI) engines [42]. Thermal efficiency is a measure of the work output per energy released. As shown in Equation 3, thermal efficiency increases as compression ratio, r_c, and the ratio of specific heats, γ, increase for an ideal cycle. Thus, to develop highly efficient engines, a thermodynamic understanding of γ, as well as the main sources of efficiency losses, is essential.

$$\eta_f = \eta_c \eta_{th}$$

Equation 2: Fuel conversion efficiency

$$\eta_{th} = 1 - \frac{1}{r_c^{\gamma-1}}$$

Equation 3: Thermal efficiency

Mixture composition and temperature has a significant impact on γ, which is a function of the mixture gas constant, R, and constant pressure specific heat capacity, c_P, as shown in Equation 4. Lower combustion temperatures are desirable to increase thermal

efficiency because as temperature decreases, the average molecular energy of the mixture decreases, which decreases c_P and increases γ. Also, a mixture with a low molecular weight is beneficial, as R is inversely proportional to molecular weight. Molecules with a lower energy (e.g. diatomic vs. triatomic) also lower the specific heat capacity of the mixture, which provides further increases to γ. As γ increases, more work can be done on the mixture during compression and the maximum attainable thermal efficiency increases.

$$\gamma = \frac{1}{1 - \frac{R}{c_P}}$$

Equation 4: Ratio of specific heats (gamma)

To illustrate the impact of temperature and composition on thermal efficiency, consider the case of exhaust gas recirculation (EGR), a process in which exhaust gas is either recycled externally into the intake stream or kept in the cylinder until the next cycle. In the unburned mixture, the c_P of exhaust gas species offsets the high c_P of the fuel, thus increasing γ. Likewise, γ increases in the burned gas zone due to lower temperatures which cause c_P to decrease. However, this trend is somewhat offset by the increased concentration of triatomic molecules which increase c_P. If dilution is achieved with air instead of EGR, the concentration of triatomic molecules does not increase and efficiency is further increased.

Heat transfer decreases engine efficiency, particularly at low engine speeds where there is more time for heat transfer to occur. To reduce these losses, combustion temperatures can be lowered by use of dilution, such as cooled EGR. Also, the proper combustion phasing is required to mitigate heat transfer losses while maximizing work output during expansion. Previous simulation work has shown that a CA50 (the location of 50% mass fraction burned) of 10 crank angle degrees (CAD) after top dead center (aTDC) achieves maximum efficiency [43]. 10%-90% burn duration is another important consideration since longer combustion durations lowers the work output. For instance, burn durations up to 20 CAD have minimal thermal efficiency losses, but efficiency decreases very rapidly for burn durations greater than 20 CAD [43].

Friction is also a significant source of efficiency losses and is most highly correlated to engine load. As described by the Chen-Flynn expression, friction increases

linearly with peak pressure and exponentially with piston speed [44]. Accordingly, for boosted conditions or high engine speeds, absolute friction increases. However, the relative impact of friction decreases as load increases due to the higher output of work [43]. Thus, assuming that the engine is not knock limited at high loads, the maximum efficiency occurs at peak load due to the decreased impact of friction.

1.3.2 High Efficiency Gasoline Engine

Engine efficiency can be significantly improved, with no reduction in performance, by downsizing and turbocharging spark-ignited gasoline engines [45]. For a given engine torque output, smaller engines must operate at higher load regimes where the relative impacts of friction are less significant [43]. Thus, efficiency is improved for the same vehicle performance conditions. Also, from a vehicle perspective, there is the possibility that smaller engines could reduce vehicle mass and lead to further increases in fuel economy [46]. However, since turbocharger systems are also required, it is difficult to generalize if total engine and vehicle mass will increase or decrease when such engines are used [46].

While downsized/turbocharged engines have the potential to significantly increase engine efficiency, they remain limited by knock, caused by higher cylinder temperatures and pressures. To mitigate knock, spark timing is adjusted from maximum brake torque (MBT) timing or excess fuel is injected in the cylinder to cool the charge. Alternatively, the compression ratio could be lowered, but this would also decrease the thermal efficiency of the engine. Another option is to use cooled exhaust gas recirculation (EGR) to dilute the mixture. As previously mentioned, EGR has the combined benefit of lowering peak temperatures and consequently increasing the ratio of specific heats, γ, for unburned and burned mixtures. Advantages of EGR also include reducing pumping work at low loads, eliminating fuel enrichment at high loads and enabling MBT spark timing, as demonstrated by Alger et al. [47]. However, the application of EGR is limited because it also increases burn rates which can increase the chance of misfire or partial burning [42], [48], [49]. Advanced ignition systems have demonstrated the ability to extend the lean limit, as an ignition system developed by Southwest Research Institute (SwRI) has been shown to increase combustion stability by emitting a continuous current at a high energy level. For instance, experimental results have shown that when used with the

SwRI high-efficiency dilute gasoline engine (HEDGE), the 0-50% MFB duration decreases and combustion stability is improved for 0-25% external EGR compared to the stock ignition system [50].

The HEDGE engine, which also utilizes advanced boosting and an increased compression ratio, is an excellent demonstration of the efficiency benefits of dilution, as results show that fuel consumption decreases between 5-30% compared to a typical port-injected engine [51]. The most improvements are obtained at high loads due to reduced knock, improved combustion phasing, and eliminating the need for fuel enrichment [51].

1.3.3 High Efficiency Ethanol Engines

Due to the high octane number (ON) and heat of vaporization of ethanol, it can also be used to increase engine efficiency by reducing the likelihood of knock, increasing volumetric efficiency and lowering heat transfer losses [52], [53]. For instance, previous research has shown that even with increased compression ratios (e.g. up to 16.5:1) and higher load conditions, ethanol-gasoline blends can enable MBT timing with no occurrences of knock [54], [55], [56]. Ethanol remains limited by high peak cylinder pressures that exceed typical peak pressures for gasoline, about 100 bar [57], [58]. However, this is not a technical limit, as diesel engines are designed to tolerate much higher cylinder pressures.

Previous research has investigated the efficiency and power improvements possible through using ethanol-gasoline blends with an increased compression ratio. In particular, Szybist et al. performed a thorough investigation of the impact on power, efficiency, and fuel consumption for ethanol blends at difference compression ratios (9.2, 11.85, and 12.87), achieved by changing pistons on a 2.0 L Ecotec GM engine [53]. Experiments were run with regular gasoline (RG), high octane gasoline, and ethanol blends of 10%, 50%, and 85% with RG. Each fuel was run at stoichiometric conditions, as shown in Equation 5-Equation 6, and spark timing was adjusted for maximum brake torque (MBT). Similar to other studies, their results show that indicated mean effective pressure (IMEP) and indicated thermal efficiency (ITE) is higher for E85 as compared to RG for similar engine conditions and increases with compression ratio [55], [56], [59]. Indicated specific fuel consumption (ISFC) is also higher for E85 due to the lower energy content of ethanol. However, fuel consumption decreases with increasing compression

ratio due to the improved power and efficiency for higher compression ratios [53], [60]. These results indicate two things: 1) switching from gasoline to E85 increases power and efficiency by making more optimal engine conditions possible (increased compression ratio without spark retard), and 2) ethanol increases the power and efficiency for very similar engine conditions (compression ratio of 9.2 with no changes in spark timing) [53].

$$C_8H_{18} + 12.5\,(O_2 + 3.76N_2) \rightarrow 8CO_2 + 9H_2O + 47N_2$$

Equation 5: Combustion of iso-octane [53]

$$C_2H_6O + 3\,(O_2 + 3.76N_2) \rightarrow 2CO_2 + 3H_2O + 11.28N_2$$

Equation 6: Combustion of ethanol [53]

Under similar engine conditions, increased IMEP for ethanol is a result of charge cooling as well as a thermodynamic composition effects. Since ethanol has a higher heat of vaporization as compared to gasoline, more heat is required to vaporize the fuel. Thus, the specific volume of the intake charge is reduced and volumetric efficiency increases. Szybist et al. quantified this effect by measuring the air flow for each fuel [53]. Air flow increases about 2% for E85, leading to a higher heating value per unit mass of air (for a stoichiometric mixture) [53]. Accordingly, more energy per mass of air is induced to the cylinder and IMEP increases.

Previous work has shown the efficiency improvements possible with E85, as compared to conventional gasoline [53], [58], [60], [61], [62], [63]. For instance, Szybist et al. found that with the same compression ratio, switching from gasoline to E85 increases indicated thermal efficiency (ITE) by about 7% at mid loads and close to 8% at wide open throttle (WOT) [53]. If the compression ratio is increased from 9.2 to 12.87, ITE increases by 7.9%-8.4% [53]. These results are consistent with work by Caton et al. that measured the thermal efficiency of using E85 with compression ratios ranging from 9 to 16.5 [61]. They found that the relative thermal efficiency increases by 2% for each compression ratio increase [61]. Experimental work by Gingrich et al. shows most significant improvements with using E85, as BTE is increased by 9-10 percentage points when increasing the compression ratio from 9 to 11 and using E85 instead of 92 RON gasoline [62]. A portion of these improvements are due to the use of EGR, which eliminates the need for fuel enrichment and ensure that MBT timing is possible, resulting in a 3-4% BTE improvement [62].

1.3.4 Previous thermodynamic studies

Previous work has shown that thermodynamic models are a useful tool to assess the potential of advanced combustion strategies [43], [64]. For instance, a study by Caton analyzed the thermodynamics of a high efficiency engine by incrementally incorporating the following changes to a baseline engine model: higher compression ratio, shorter combustion duration, lean equivalence ratio, EGR, and increased wall temperature [64]. For each case, Caton assess the thermodynamic tradeoffs associated with pressure, friction, temperature, γ, thermal efficiency and exergy destroyed [64]. Results show that while each technology increases the net efficiency, diluting the mixture (with air or EGR) and increasing the compression ratio achieve the greatest improvements. Efficiency improvements due to dilution are due to the increased work that can be extracted from combustion gases due to increased γ and reductions in heat transfer. Furthermore, by examining the impact of γ for an adiabatic engine model, Caton concluded that increased γ is responsible for half of the efficiency gains for dilute cases considered [64].

Recent work by Lavoie et al. also used thermodynamic models to evaluate the potential of advanced combustion strategies using dilution with downsized/turbocharged engines [43]. Lavoie et al. expanded the range of advanced combustion techniques considered by Caton to include higher dilution regimes (up to 80%) and homogeneous charge compression ignition (HCCI) combustion [43]. Results indicate that efficiency gains with advanced combustion (defined as using between 30% and 60% dilution) and downsizing are additive, not overlapping [43]. Also, drive cycle simulations show that a naturally aspirated (NA) advanced combustion and downsized/turbocharged SI engine increase CAFE fuel economy by 23% and 36%, respectively, while a downsized/turbocharged advanced combustion engine results in a 58% improvement as compared to a baseline NA engine [43]. Dilution with air achieves the highest engine efficiency due to improved composition properties and reduced temperatures, while engine downsizing increases efficiency by reducing frictional losses and increasing brake efficiency [43]. Turbocharging contributes significantly to net efficiency improvements by reducing pumping losses. Since these results have not considered combustion limitations such as knock or flammability limits, the fuel economy improvements represent the maximum potential of each strategy to reduce fuel consumption [43].

1.4 Objectives, contribution and approach

1.4.1 Objectives

The objective of this work is to evaluate the individual and combined potential of advanced internal combustion engines and lightweight vehicle materials to reduce life cycle energy and GHG emissions for an internal combustion vehicle (ICV), hybrid electric vehicle (HEV), and plug-in hybrid electric vehicle (PHEV). Also, fuel cycle energy and GHG emissions will be assessed parametrically by considering diverse liquid and electric fueling options.

The main objectives are as follows:

1. Lightweight vehicles: Determine the life cycle energy and GHG emissions reductions that are possible by using material substitution and secondary mass reductions for diverse vehicle platforms.
2. Advanced combustion engines: Evaluate the realistic potential of advanced combustion engines to increase engine efficiency and vehicle fuel economy.
3. Lightweight vehicles and advanced combustion engines: Assess the synergies and tradeoffs of using advanced combustion engines and lightweight materials to reduce life cycle energy and GHG emissions.
4. Diverse fuels: Determine the total life cycle energy and GHG emissions of these systems when used with diverse liquid fuels and electricity.

1.4.2 Contribution

Unlike previous LCAs, this work will incorporate a consistent method to model vehicles with diverse powertrains and include a novel method for assessing the realistic efficiency potential of advanced gasoline and ethanol engines. Also, this work will evaluate the impact of mass reduction on fuel consumption for each vehicle architecture (i.e. ICV, HEV, and PHEV), thereby providing a more accurate description of vehicle efficiency. A range of possible impacts from each fuel will be considered, which enables scenario analyses beyond the scope of what is typically considered in a vehicle LCA.

In summary, this work advances current LCAs by incorporating:

1. Mass reduction potential models that capture the tradeoffs associated with heavier powertrains, vehicle efficiency and lightweight material production
2. Conceptual engine models that preserve physical insight while demonstrating the potential of internal combustion engines to reduce life cycle energy and GHG emissions

1.4.3 Approach

To satisfy the objectives listed above, the potential of vehicle mass reduction and advanced engines are assessed in both individual and combined models using the modeling tools listed in Table 2. An overview of the method and models used for the dissertation is provided in Figure 1. As shown, each technology option is incorporated to the vehicle design for an ICV, HEV and PHEV. Vehicle performance and fuel economy results are obtained using Autonomie, a forward-facing vehicle simulation software [65]. Lastly, the life cycle energy and GHG emissions for the vehicle systems are determined based on the vehicle material composition, fuel economy results, and fuel type. These life cycle results are obtained using GREET 1 and 2, vehicle and fuel lifecycle modeling tools, respectively, and previous literature to determine a range of energy and GHG emissions intensities associated with lightweight materials and liquid fuels [66], [67]. The energy and GHG emissions due to electrical consumption are determined with eGrid, a database for power sector environmental impacts provided by the US Environmental Protection Agency [68]. Further details on the model inputs, data sources and model outputs are included in Table 3-Table 4 in the Appendix.

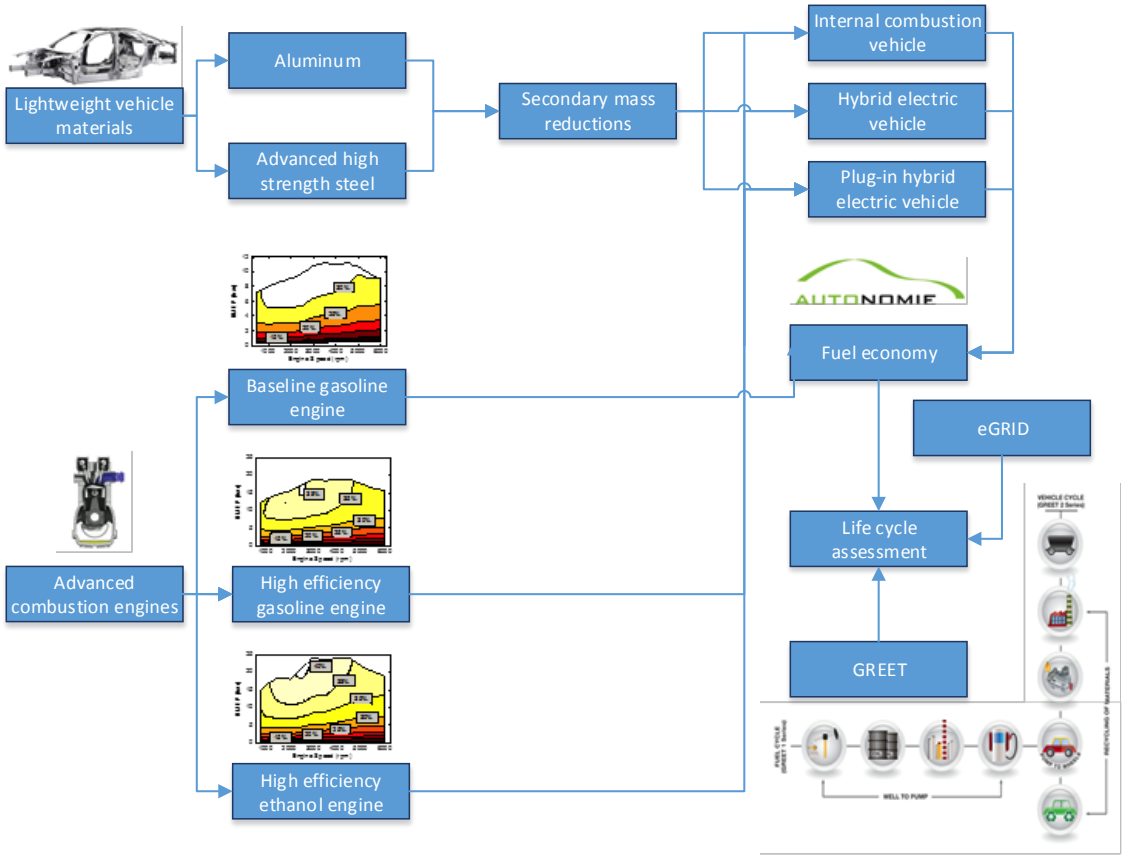

Figure 1: Dissertation model overview (Chapters 2-5)

Table 2: Dissertation modeling tools for engines, vehicles and life cycle energy and GHG emissions

Software	Purpose	Author
GT-Power	engine modeling	Gamma Technologies
Autonomie	vehicle modeling	Argonne National Laboratory
GREET	vehicle and fuel cycle modeling	Argonne National Laboratory
eGrid	database for power sector environmental parameters	U.S. Environmental Protection Agency

It is important to note that optimizing vehicle efficiency through methods such as controls or gear ratios selection is beyond the scope of this work. Accordingly, the standard controller in Autonomie is used for each powertrain-type vehicle without modification. Gear ratios are selected for the baseline vehicles using engineering judgment but are not modified for the lightweight vehicles. As a result of these assumptions, the mass elasticities of fuel consumption in this work are expected to be lower than if the vehicle was optimized for the new vehicle mass. However, such

assumptions are consistent with previous studies that have evaluated the impact of mass reduction for diverse vehicle types [13], [35], [36], [37].

Within the scope of the lightweight vehicle analysis, a new method is developed to compare the impacts of mass reduction across diverse powertrain vehicles. These design harmonization techniques provide a systematic method to model baseline vehicles by accounting for increased structural mass required for heavier powertrains. Also, design changes associated with electric vehicles are incorporated by downsizing the fuel and exhaust subsystem. Lightweight vehicle models are designed with the following assumptions: 1) material substitution of steel with aluminum and AHSS results in body-in-white (BIW) mass reductions of 32-45% and 22-35%, respectively, and 2) secondary mass reductions, including powertrain re-sizing, are incorporated early to the vehicle design process. Based on these methods and assumptions, baseline and lightweight vehicle models are developed and evaluated in a LCA.

The internal combustion engine analysis requires a novel method to assess the potential of advanced gasoline and ethanol combustion strategies to decrease fuel consumption. This method enables knock and flammability limits to be identified using scaling methods that preserve physical insight and are validated against experimental results. These combustion limits are applied to a high efficiency gasoline and E85 engine under boosted and dilute operation conditions and compared to a baseline naturally aspirated gasoline engine. Within knock and flammability constraints, each operating condition is optimized for efficiency and fuel economy maps are generated for each engine. Also, ideal versions of these maps are generated, assuming the engine is not constrained by knock or flammability limits. Lastly, fuel economy and life cycle results are obtained to assess the potential of the high efficiency gasoline and E85 engines to reduce energy and GHG emissions.

To assess the synergies and tradeoffs of integrating lightweight materials and advanced engines in the vehicle design, the following questions are identified to focus the scope of the analysis:

1. What level of mass reduction is required to match the life cycle GHG emissions reductions for a contemporary ICV due to downsizing/boosting an advanced gasoline engine?
2. What are the maximum life cycle energy and GHG reductions possible when lightweighting a contemporary ICV and replacing a baseline engine with an advanced gasoline or ethanol downsized/boosted engine?
3. What are the life cycle energy and GHG emissions reductions due to using an advanced downsized/boosted ethanol engine in a HEV and PHEV as compared to an ICV with a baseline engine?

The following chapters are organized according to individual or combined use of the technologies considered in this work. Chapter 2 focuses on vehicle design and describes design harmonization techniques used to model baseline and lightweight versions of an ICV, HEV, and PHEV. Chapter 3 uses the framework presented in Chapter 2 to evaluate the life cycle energy and greenhouse gas emissions of a baseline and lightweight ICV, HEV, and PHEV. Chapter 4 provides technical details regarding engine fuel economy maps and presents life cycle results for each engine/fuel strategy. Chapter 5 provides an integrated assessment of the potential of lightweight materials and advanced engines to reduce life cycle energy and GHG emissions by answering the questions listed above. Lastly, Chapter 6 discusses the major findings of the dissertation and presents suggestions for future work. Chapters 2-4 have been prepared as journal papers: Chapters 2-3 are a 2-part paper (to be submitted to Applied Energy) and Chapter 4 is an individual paper (under review with the International Journal of Engines Research).

1.5 References

[1] Paramount Research, “WardsAuto / DuPont Survey of Auto Industry Challenges,” www.paramountresearch.com, 2011.

[2] T. V. Johnson, “Review of CO2 emissions and technologies in the road transportation sector,” SAE Paper 2010–01–1276, 2010.

[3] S. C. Davis, S. W. Diegel, and R. G. Boundy, *Transportation Energy Data Book, Edition 31*. 2012, pp. 6–7.

[4] A. Elgowainy, J. Han, L. Poch, A. Wang, M. Mahalik, and A. Rousseau, “Well-to-Wheels Analysis of Energy Use and Greenhouse Gas Emissions of Plug-In Hybrid Electric Vehicles,” *Argonne National Laboratory*, 2010.

[5] H.-J. Kim, C. McMillan, G. A. Keoleian, and S. J. Skerlos, “Greenhouse Gas Emissions Payback for Lightweighted Vehicles Using Aluminum and High-Strength Steel,” *Journal of Industrial Ecology*, vol. 14, no. 6, pp. 929–946, Dec. 2010.

[6] ISO, *ISO 14040 Environmental management - Life cycle assessment - Principles and framework*. 1997.

[7] L. Cheah, C. Evans, A. Bandivadekar, and J. Heywood, “Factor of Two : Halving the Fuel Consumption of New U . S . Automobiles by 2035,” *MIT Laboratory for Energy and Environment*, LFEE 2007–04 RP, 2007.

[8] A. Bandivadekar, K. Bodek, L. Cheah, C. Evans, T. Groode, J. Heywood, E. Kasseris, M. Kromer, and M. Weiss, “On the Road in 2035,” 2008.

[9] M. F. Ashby, *Materials Selection, Second Edititon*. 1999.

[10] L. W. Cheah, “Cars on a Diet : The Material and Energy Impacts of Passenger Vehicle Weight Reduction in the U.S.,” MIT, Doctoral Dissertation, 2010.

[11] D. E. Malen, R. Gobbels, and R. Wohlecker, “Estimation of Secondary Mass Changes in Vehicle Design,” SAE Paper 2013–01–0655, 2013.

[12] A. Moawad, A, Sharer, P, Rousseau, “Light-Duty Vehicle Fuel Consumption Displacement Potential up to 2045,” *Argonne National Laboratory*, 2011.

[13] S. Pagerit, P. Sharer, and A. Rousseau, “Fuel economy sensitivity to Vehicle Mass for Advanced Vehicle Powertrains,” SAE Paper 2006–01–0665, 2006.

[14] C.-S. N. Shiau, C. Samaras, R. Hauffe, and J. J. Michalek, "Impact of battery weight and charging patterns on the economic and environmental benefits of plug-in hybrid vehicles," *Energy Policy*, vol. 37, no. 7, pp. 2653–2663, Jul. 2009.

[15] A. I. Taub, P. E. Krajewski, A. A. Luo, and J. N. Owens, "The Evolution of Technology for Materials Processing over the Last 50 Years : The Automotive Example," *JOM*, vol. 59, no. 2, pp. 48–57, 2007.

[16] N. Lutsey, "Review of technical literature and trends related to automobile mass-reduction technology," *California Air Resources Board*, May, 2010.

[17] DriveAluminum Presentation, "The Vehicle Race to Lose Weight," *Aluminum Industry*, 2013.

[18] H. Singh, "Mass Reduction for Light-Duty Vehicles for Model Years 2017-2025," *Report No. DOT HS 811 666*, Program Reference: DOT, 2012.

[19] EPA, "Light-Duty Vehicle Mass Reduction and Cost Analysis — Midsize Crossover Utility Vehicle," *U.S. Environmental Protection Agency*, EPA-420-R-12-026, 2012.

[20] FKA, "Investigation of the Trade-off Between Lightweight and Battery Cost for an Aluminium-Intensive Electric Vehicle," Project No. 106330, 2012.

[21] EDAG, "Venza aluminum BIW concept study," 2013.

[22] H. Shaw, J., Singh, "Overview Report - FutureSteelVehicle Phase 2," World Auto Steel, 2011.

[23] C. Bjelkengren, "The Impact of Mass Decompounding on Assessing the Value of Vehicle Lightweighting," MIT, Doctoral Dissertation, 2006.

[24] K. D. Malen, E, K., Reddy, "Preliminary Vehicle Mass Estimation Using Empirical Subsystem Influence Coefficients," Auto-Steel Partnership, http://www.a-sp.org/en/LightweightPrograms.aspx, 2007.

[25] V. Freyermuth, E. Fallas, and A. Rousseau, "Comparison of Powertrain Configuration for Plug-in HEVs from a Fuel Economy Perspective," SAE Paper, 2008–01–0461, 2008.

[26] T. R. Hawkins, B. Singh, G. Majeau-Bettez, and A. H. Strømman, "Comparative Environmental Life Cycle Assessment of Conventional and Electric Vehicles," *Journal of Industrial Ecology*, vol. 17, no. 1, pp. 53–64, Feb. 2013.

[27] D. Malen, "Design Advisor User Guide", WorldAutoSteel, http://www.worldautosteel.org/projects/, 2012.

[28] F. Stodolsky, A. Vyas, R. Cuenca, and L. Gaines, "Life-Cycle Energy Savings Potential from Aluminum- Intensive Vehicles," in *1995 Total Life Cycle Conference & Exposition*, 1995.

[29] J. S. Colett, J. C. Kelly, and G. A. Keoleian, "Impacts of regional variation and electricity allocation protocol on aluminum production GHG emissions," *Draft submitted to Environmental Science & Technology*, 2013.

[30] C. Tamarelli, "AHSS 101: The evolving use of advanced high-strength steels for automotive applications," 2011.

[31] WorldSteel, "GHG emissions of high strength steels versus conventional steels," http://old.worldsteel.org/pictures/storyfiles/GHGemissionsandAHSS.pdf, 2010.

[32] R. Geyer, "Life Cycle Energy and Greenhouse Gas (GHG) Assessments of Automotive Material Substitution: WorldAutoSteel Energy and GHG Model," 2012.

[33] P. Americas, "Final Report Life Cycle Impact Assessment of Aluminum Beverage Cans, for Aluminum Association, Inc.," 2010.

[34] I. Roy F. Weston, "Life cycle inventory report for the North American aluminum industry," 1998.

[35] F. An and D. J. Santini, "Mass Impacts on Fuel Economies of Conventional vs . Hybrid Electric Vehicles," *Society of Automotive Engineers Technical Paper*, vol. 2004–01–0572.

[36] I. J. Wohlecker, R., Wallentowitz, H., Johannaber, M., Espig, M., Leyers, "Determination of Weight Elasticity of Fuel Economy for Conventional ICE Vehicles, Hybrid Vehicles and Fuel Cell Vehicles," *FKA*, Report 555.

[37] A. Casadei and R. Broda, "Impact of Vehicle Weight Reduction on Fuel Economy for Various Vehicle Architectures," Ricardo Project FB769, 2010.

[38] R. B. Carlson, J. Diez, and J. Gibbs, "The Measured Impact of Vehicle Mass on Road Load Forces and Energy Consumption for a BEV, HEV, and ICE Vehicle," SAE Paper 2013–01–1457, 2013.

[39] C. Reynolds and M. Kandlikar, "How hybrid-electric vehicles are different from conventional vehicles: the effect of weight and power on fuel consumption," *Environmental Research Letters*, vol. 2, no. 014003, Jan. 2007.

[40] S. Das, "The life-cycle impacts of aluminum body-in-white automotive material," *Jom*, vol. 52, no. 8, pp. 41–44, Aug. 2000.

[41] H. C. Kim and T. J. Wallington, "Life-Cycle Energy and Greenhouse Gas Emission Bene fits of Lightweighting in Automobile : Review and Harmonization," *Environmental Science & Technology*, vol. 47, no. 12, pp. 6089–6097, 2013.

[42] J. B. Heywood, *Internal Combustion Engine Fundamentals*. New York, 1998.

[43] G. Lavoie, E. Ortiz-Soto, A. Babajimopoulos, J. B. Martz, and D. N. Assanis, "Thermodynamic sweet spot for high-efficiency, dilute, boosted gasoline engines," *Int J of Engine Res*, vol. 14, no. 3, pp. 260-278, Aug. 2012.

[44] S. Chen and P. Flynn, "Development of a Single Cylinder Compression Ignition Research Engine," SAE Paper 650733, 1965.

[45] F. Richard, S., Font, G., Le Berr, "On the use of system simulation to explore the potential of innovative combustion systems: methodology and application to highly downsized SI engines running with ethanol-gasoline blends," SAE Paper 2011–01–0408, 2011.

[46] P. Leduc, B. Dubar, A. Ranini, and G. Monier, "Downsizing of gasoline engine: an efficient way to reduce CO2 emissions," *Oil & Gas Science and Technology*, vol. 58, no. 1, pp. 115–127, 2003.

[47] M. Hedge, P. Weber, J. Gingrich, T. Alger, and I. Khalek, "Effect of EGR on Particle Emissions from a GDI Engine," SAE Paper 2011–01–0636, 2011.

[48] W. Dai, S. G. Russ, N. Trigui, and K. V Tallio, "Regimes of premixed turbulent combustion and misfire modeling in SI engines," SAE Paper 982611, 1998.

[49] R. J. Middleton, J. B. Martz, G. A. Lavoie, A. Babajimopoulos, and D. N. Assanis, "A computational study and correlation of premixed isooctane air laminar reaction fronts diluted with EGR," *Combustion and Flame*, vol. 159, no. 10, pp. 3146–3157, 2012.

[50] T. Alger, J. Gingrich, B. Mangold, and C. Roberts, "A Continuous Discharge Ignition System for EGR Limit Extension in SI Engines," SAE Paper 2011–01–0661, 2012.

[51] T. Alger and J. Gingrich, "Cooled EGR for Fuel Economy and Emissions Improvement in Gasoline Engines," JSAE Paper 20105013, 2010.

[52] E. Kasseris and J. Heywood, "Charge Cooling Effects on Knock Limits in SI DI Engines Using Gasoline / Ethanol Blends: Part 2-Effective Octane Numbers," SAE Paper 2012–01–1284, 2012.

[53] J. Szybist, M. Foster, W. R. Moore, K. Confer, A. Youngquist, and R. Wagner, "Investigation of Knock Limited Compression Ratio of Ethanol Gasoline Blends," SAE Paper 2010–01–0619, 2010.

[54] P. Grabner, H. Eichlseder, and G. Eckhard, "Potential of E85 Direct Injection for Passenger Car Application," SAE Paper 2010–01–2086, 2012.

[55] S. Utsumi, A. Ota, K. Kawatake, T. Kawai, and T. Tsunooka, "The Effect of Ethanol Fuel on a Spark Ignition Engine," SAE Paper 2006–01–3380, 2006.

[56] P. A. Caton, L. J. Hamilton, and J. S. Cowart, "Experimental and Modeling Investigation into the Comparative Knock and Performance Characteristics of E85, Gasohol [E10] and Regular Unleaded Gasoline [87 (R+M)/2]," SAE Paper 2007–01–0473, 2007.

[57] K. S. Hoyer, W. R. Moore, and K. Confer, "A Simulation Method to Guide DISI Engine Redesign for Increased Efficiency using Alcohol Fuel Blends," SAE Paper 2010–01–1203, 2010.

[58] M. J. Christie, N. Fortino, and R. B. Llc, "Parameter Optimization of a Turbo Charged Direct Injection Flex Fuel SI Engine Hakan Yilmaz," SAE Paper 2009–01–0238, 2009.

[59] K. Moore, W., Foster, M., Hoyer, "Engine Efficiency Improvements Enabled by Ethanol Fuel Blends in a GDi VVA Flex Fuel Engine," SAE Paper 2011–01–0900, 2011.

[60] N. Maji, S., Gajendra Babu., M.K., Gupta, "A Single Cylinder Engine Study of Power, Fuel Consumption and Exhaust Emissions with Ethanol," SAE Paper 2001–28–0029, 2001.

[61] P. A. Caton, L. J. Hamilton, and J. S. Cowart, "An Experimental and Modeling Investigation into the Comparative Knock and Performance Characteristics of E85, Gasohol [E10] and Regular Unleaded Gasoline [87 (R+M)/2]," SAE Paper 2007–01–0473, 2007.

[62] J. Gingrich, T. Alger, and B. Sullivan, "Ethanol Flex-fuel Engine Improvements with Exhaust Gas Recirculation and Hydrogen Enrichment," SAE Paper 2009–01–0140, 2009.

[63] K. Nakata, S. Utsumi, A. Ota, K. Kawatake, T. Kawai, and T. Tsunooka, "The Effect of Ethanol Fuel on a Spark Ignition Engine," SAE Paper 2006–01–3380, 2006.

[64] J. A. Caton, “An Assessment of the Thermodynamics Associated With High-Efficiency Engines,” in *Proceedings of the ASME 2010 Internal Combustion Engine Division Fall Technical Conference*, 2010.

[65] Argonne National Laboratory, “Autonomie.” UChicago Argonne, LLC, 2009.

[66] Argonne National Laboratory, “GREET 1 rev2.” UChicago Argonne, LLC, 2012.

[67] Argonne National Laboratory, “GREET 2 rev1.” UChicago Argonne, LLC, 2012.

[68] US Environmental Protection Agency, “eGRID2012 year 2009 Summary Tables,” 2012.

[69] Gamma Technologies, “GT-Power, v. 7.1,” 2010.

[70] www.A2Mac1.com, Automotive Benchmarking, Yipsilanti, MI, 2013.

1.6 Appendix

An overview of the inputs required for GT-Power, Autonomie and GREET 1 and 2 is shown in Table 3 [65], [66], [67], [69]. As indicated in the table, the following inputs were determined in this work: CA50 timing for maximum brake torque (MBT), engine fuel economy maps, vehicle fuel economy, vehicle and subsystem mass, and vehicle material composition. Further detail on the sources of model inputs and the associated outputs is provided in Table 4. Dates of data sources are included so that future research may easily identify the data that requires updating.

Table 3. Inputs for each modeling software

GT-Power	• Single cylinder engine parameters (e.g. bore, stroke, compression ratio, valve timing) • Fuel specifications for ethanol and iso-octane • Turbocharger model • Heat transfer model (Woschni) • Friction model (Chen-Flynn) • Parameters for Wiebe function (including CA50 for MBT timing)*
Autonomie	• Engine fuel economy maps* • MATLAB/Simulink models for powertrain components, automatic or continuously variable transmissions, wheels and body • Drag and rolling resistance coefficients • Driver model and vehicle controls • Total vehicle mass* • Velocity profiles for EPA drive cycles, 0-60 MPG acceleration test and gradeabiltiy test
GREET 1 (fuel-cycle)	• Energy and GHG emissions for each process required to produce ethanol and gasoline • Fuel economy*
GREET 2 (vehicle-cycle)	• Energy and GHG emissions for each process required to produce the vehicle (including material data, battery manufacturing, and vehicle assembly) • Energy and GHG emissions for vehicle end-of-life processes (vehicle disassembly and disposal/recycling) • Assumptions regarding vehicle maintenance over its lifetime (e.g. number of battery replacements) • Total vehicle and subsystem mass (from teardown data)* • Total vehicle material composition (from teardown data)*

*Determined/created in this work

Table 4. Model inputs (with sources) and outputs

Input	Source of input data	Model	Output
Powertrain mass and front track width (Ch 2)	Vehicle teardown data, 2007-2013 [70]	Design harmonization model (Ch 2)	Baseline vehicle mass (Ch 2)
Subsystem mass fractions, powertrain mass (Ch 2)	Vehicle teardown data, 2007-2013 [70]	Design harmonization model (Ch 2)	Vehicle subsystem mass and material composition (Ch 2)
Primary mass reduction: Closures (Ch 2); BIW (Ch 3)	Ashby, 1999 [9]; NHTSA, 2012 [18]	Design harmonization model (Ch 2, 3, 5)	Lightweight vehicle mass (Ch 2, 3, 5)
Subsystem mass influence coefficients (Ch 2, 3, 5)	Don Malen, 2013 [11]		
Gasoline and ethanol fuel properties (Ch 4); engine specifications (Ch 4)	GT-Power, 2010 [69]; Previous literature	GT-Power engine/fuel models (Ch 4)	Engine fuel economy maps (Ch 4)
Engine fuel economy maps (Ch 4)	GT-Power engine models in Ch 4 of this work	Vehicle drive cycle models: Autonomie (Ch 3, 5), Matlab (Ch 4)	Fuel economy (Ch 3-5)
Fuel economy (Ch 3, 5)	Vehicle drive cycle models in Ch 3, 5 of this work	Life cycle model (Ch 3, 5)	Well-to-tank energy and GHG emissions (Ch 3, 5)
Energy and GHG emissions to produce and transport gasoline and ethanol to the vehicle (Ch 3, 5)	GREET 1, 2012 [66]		
Energy and GHG emissions from electricity (Ch 3, 5)	eGrid, 2012 [68]		
Fuel economy (Ch 4)	Autonomie vehicle drive cycle models in Ch 3, 5 of this work	Life cycle model (Ch 3, 5)	Tank-to-wheel energy and GHG emissions (Ch 3, 5)
Energy and GHG emissions from combustion (Ch 3, 5)	GREET 1, 2012 [66]		
Vehicle subsystem mass and material composition (Ch 2)	Vehicle teardown data, 2007-2013 [70]; GREET 2, 2012 [67]	Life cycle model (Ch 3, 5)	Vehicle-cycle energy and GHG emissions (Ch 3,5)
Steel and aluminum energy intensity and GHG emissions intensity (Ch 3)	WorldAutoSteel, 2012 [32]; Aluminum Association, 1998, 2012 [33], [34]		
Energy and GHG emissions to produce naturally aspirated and turbocharged engines (Ch 5)	Vehicle teardown data, 2010, 2013 [70]		

Chapter 2. Vehicle lightweighting vs. electrification: Part 1 – Design harmonization techniques to model vehicles with diverse powertrains

2.1 Abstract

Vehicle electrification and mass reduction have the potential to increase fuel economy and decrease life cycle energy and greenhouse gas (GHG) emissions. However, life cycle assessment (LCA) is required to fully understand these impacts due to electricity and lightweight material production burdens. While recent work has compared conventional, electrified and lightweight vehicles in a LCA, there remains a need for an appropriate method to examine comparable vehicles across diverse vehicle platforms (e.g. conventional internal combustion engine vs. hybrid electric), particularly as structural mass requirements may change depending on powertrain mass. This work develops such design harmonization techniques to model the vehicle mass, powertrain specifications, and material composition of an internal combustion vehicle (ICV), hybrid electric vehicle (HEV) and plug-in hybrid electric vehicle (PHEV), including lightweight versions of these vehicles. Baseline vehicle models are harmonized with functional equivalency requirements and by accounting for the structural support required for heavier powertrains, while lightweight vehicles are harmonized with mass compounding models that include powertrain re-sizing. The lightweight design method is demonstrated with a moderate material replacement scenario (steel is replaced with aluminum in the closures and bumpers) and subsystem downsizing (i.e. secondary mass reductions). Part 2 of this work (presented in Chapter 3) uses this design method to evaluate the life cycle energy and GHG emissions of the baseline vehicles presented in the current chapter and lightweight vehicles designed with more significant material substitution scenarios. Results of the current work demonstrate the utility of the design harmonization framework, as differences in powertrain-dependent subsystems are incorporated into the

vehicle model and functional equivalency is maintained for all baseline and lightweight vehicles.

2.2 Introduction

In an effort to increase energy security and mitigate impacts of global warming, advanced vehicle technologies are being developed to increase vehicle efficiency and decrease greenhouse gas (GHG) emissions. For instance, lightweight materials are being used to increase fuel economy for both conventional and electrified vehicles, particularly as automobile manufacturers are required to meet fuel economy targets for 2017-2025 CAFE [1]. Vehicle electrification is also increasing in popularity as more conventional vehicles are equipped with stop/start technology and hybrid and plug-in hybrid electric vehicles (HEV, PHEV) are gaining market share [2]. However, these technologies are known to increase the energy and emissions upstream of the vehicle use, as lightweight materials are often more energy intensive to produce and vehicle electrification is dependent on the electricity from the grid [3], [4]. Since life cycle assessment (LCA) evaluates vehicle production, operation and end-of-life management, it is a useful tool to evaluate the impact of lightweight, electrified vehicles [5].

Previous work has modeled lightweight vehicles by accounting for primary and secondary mass reductions, including powertrain resizing to maintain performance [6]. Primary reductions are considered either by detailed engineering assessment of part re-design or by substitution ratios found with material indices. Since material indices are determined based on the material properties and function of the part, the ratio of the material indices for the baseline and lightweight material yields a part-specific substitution ratio [7]. Secondary mass reductions, or the mass change due to subsystem resizing, are evaluated using mass influence coefficients for each subsystem. These coefficients are the ratio of change in subsystem mass per unit change in gross vehicle mass and are found using regression analysis of vehicle teardown data [8], [9]. Previous studies have found that secondary mass savings, including powertrain resizing, range from 23% to 180% of the initial mass change [9], [10].

Since lightweight vehicle technologies will likely be used with both conventional and electrified vehicles to reduce vehicle load, there is a need to assess their combined impact on reducing life cycle energy and GHG emissions. Accordingly, previous studies

have designed methods to create comparable models for vehicles with diverse powertrains. For instance, Argonne National Laboratory (ANL) has compared conventional and electrified vehicles by sizing powertrain components based on performance criteria (e.g. engines are sized for gradeability and acceleration, HEV motors are sized to capture drive cycle regenerative energy) [11]. Previous work has also assessed the total vehicle mass for each powertrain architecture, since electrified vehicles are likely to have heavier powertrains than conventional vehicles [12], [13]. The powertrain mass for these vehicles is determined by accounting for the weight of new components and downsizing the existing infrastructure as necessary [12], [13], [14].

Once the new powertrain weight is determined, the structural design of the vehicle must be considered since this extra weight must be managed in a crash. Methods to account for the additional structural mass required for electric powertrains vary widely in the literature, from using finite element analysis (FEA) and finding the mass necessary for crash test approval to using the same glider and assuming the vehicle is designed for the heaviest powertrain [14], [15]. Other studies have used structural mass multipliers (e.g. 0-2 kg structural weight per 1 kg battery weight [16], 0.5 kg structural weight per 1 kg extra powertrain weight [12]) based on industry input. While a FEA approach provides the most technical detail, it is beyond the scope for most LCAs. On the other hand, a constant glider approach likely underpredicts vehicle weight and therefore overpredicts the benefits due to electrification. Structural mass multiplier values are perhaps a better compromise, but may lead to inflated vehicle weights and have a limited application (e.g. up to a 2:1 ratio from Shiau et al. applies to battery weight only [16]). Thus, there remains a need for a method to determine the structural mass required for heavy powertrains with a simple, but robust method.

The objective of this work is to develop a design harmonization process to model vehicles with diverse powertrains in order to assess the life cycle energy and GHG reduction potential of using lightweight materials in the vehicle design. This process will then be applied in Part 2 of this work to determine life cycle results for baseline and lightweight vehicles. The approach for the current work is to define the vehicle mass, powertrain specifications and material composition of a generic baseline and lightweight internal combustion vehicle (ICV), HEV, and PHEV with a 10-mile all-electric range,

PHEV-10. First, equivalency requirements are defined for all baseline and lightweight vehicles such that the vehicles are comparable for the purpose of the LCA. Then, the masses of baseline vehicles are determined from regression analysis, components are sized according to performance requirements, and materials are assigned according to vehicle teardown data. Lastly, lightweight vehicles are designed with primary and secondary mass reductions, powertrain downsizing, and a new material composition that is adjusted to reflect the design changes.

2.3 Methods

2.3.1 Defining equivalent vehicles

The functional equivalence criteria for the ICV, HEV, and PHEV-10 (hereafter referred to simply as "PHEV") are shown in Table 5. To maintain consistency, the vehicles should be of the same class (e.g. compact sedan), have the same plan view area (i.e. front track width and wheelbase) and be marketable in the US. Based on industry input, we have included the following parameters that are highly valued by US consumers: 5 passenger seating design, good vehicle "roominess", a minimum cargo volume, and acceptable vehicle performance. Vehicle "roominess" relates to the distance between the front seats and can be evaluated by the vehicle front track width (FTW), the distance between the front tires. It is assumed that the HEV and PHEV battery is located in the tunnel (and trunk if necessary) and that all other powertrain components may be packaged under the hood, similar to the GM Volt. Thus, if the powertrain required for the electric vehicles becomes very large, cargo volume will decrease.

Table 5: Functional equivalence criteria for the generic ICV, HEV, and PHEV

Functional Equivalence Criteria

• Compact sedan (FTW – see Appendix for details)
• Same plan view area
• Can seat 5 passengers (FTW – see Appendix for details)
• Same FTW
• Cargo minimum volume
• Performance requirements:
  ○ 0-60 mph in 9 seconds
  ○ Gradeability: 6% grade at 65 mph at gross vehicle weight

As shown in Figure 2, the overall vehicle design process consists of modeling the vehicle mass and materials, included in the scope of this work, as well as the fuel economy and life cycle impacts, which will be incorporated in future work (Chapter 3). While the methods for powertrain sizing, fuel economy, materials and life cycle modeling are equivalent for baseline and lightweight vehicles, the vehicle mass design process is different. For instance, the masses of baseline vehicles are determined with a regression analysis using FTW and powertrain mass as predictor variables. On the other hand, the mass of lightweight vehicles is determined by subtracting an initial mass reduction from the baseline vehicles and computing simple secondary mass reductions (including powertrain re-sizing) until the vehicle mass converges.

After the vehicle mass and powertrain specifications are determined for baseline and lightweight vehicles, this information is input to the fuel economy and material models. Fuel economy is determined with drive cycle vehicle simulation using Autonomie, a vehicle simulation software developed by ANL [17]. The material composition of each vehicle is found using mass and materials from teardown data as well as GREET 2, a vehicle life cycle modeling tool [18]. Lastly, the life cycle impact for each vehicle is determined with the fuel economy and material composition inputs and the energy/emissions intensity of the fuel and materials, found from GREET 1, a life cycle modeling tool for fuels, and GREET 2 [18], [19].

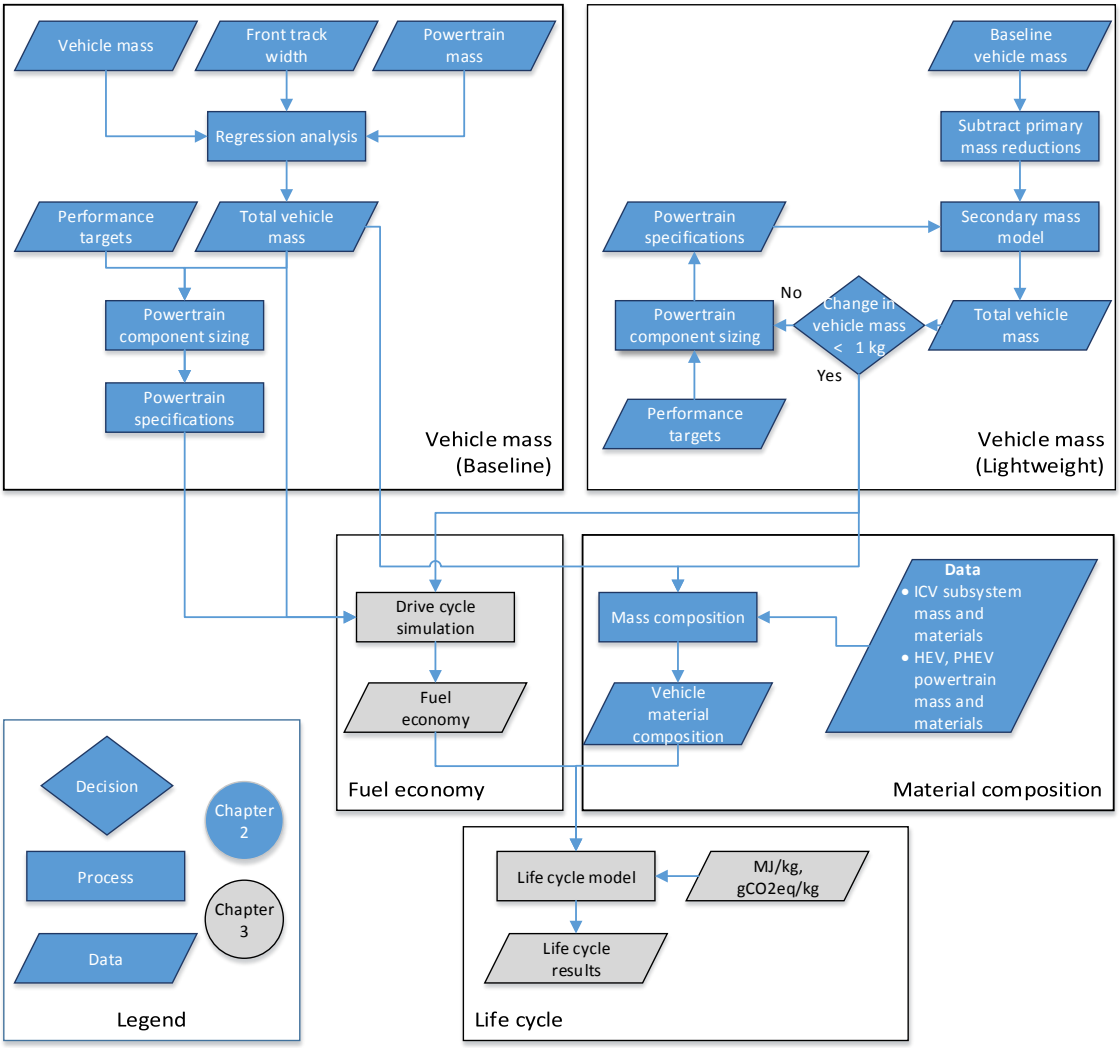

Figure 2: Design harmonization algorithm

2.3.2 Baseline vehicle models

Vehicle mass

A method is developed to account for the extra vehicle weight (e.g. structural support) required for the HEV and PHEV powertrains. Using a linear regression analysis, vehicle mass is characterized as a function of powertrain mass and FTW. Powertrain mass is a good indicator for vehicle mass because vehicles are designed to support the heaviest powertrain that will be used in that line of vehicles. FTW is chosen as a predictor variable due to its high statistical correlation with vehicle mass, as compared to wheelbase or plan view area. For this work, the FTW of the proposed vehicle design is chosen to be the average of the top three consumer rated vehicles for 2012-2013 models,

60", as this indicates a consumer-approved vehicle "roominess" [20]. Powertrain masses for the generic ICV, HEV, and PHEV are chosen based on representative vehicles designed by the same automotive manufacturer and are 188 kg, 283 kg and 327 kg, respectively.

The regression analysis is performed using vehicle teardown data from a vehicle benchmarking company [21]. To maintain consistency for the analysis, the sedans/hatchbacks included in the analysis are chosen to be similarly designed steel-bodied vehicles defined by the following attributes: steel bodies, body-frame-integral, McPherson struts and transverse front wheel drive engines [13]. Note that these vehicles are not expected to meet the functional equivalency requirements as listed in Table 5 for the generic vehicles because these are defined in the vehicle model by FTW, battery size and performance. (Ideally, the ICVs included in the analysis would be limited to only include vehicles with the heaviest powertrain for that line of vehicles, but due to data limitations only 12 ICVs have this quality.) The resulting dataset includes a total of 29 vehicles, comprised of 25 ICVs, 2 HEVs, and 2 PHEVs, as shown in Figure 3 according to marker symbol.

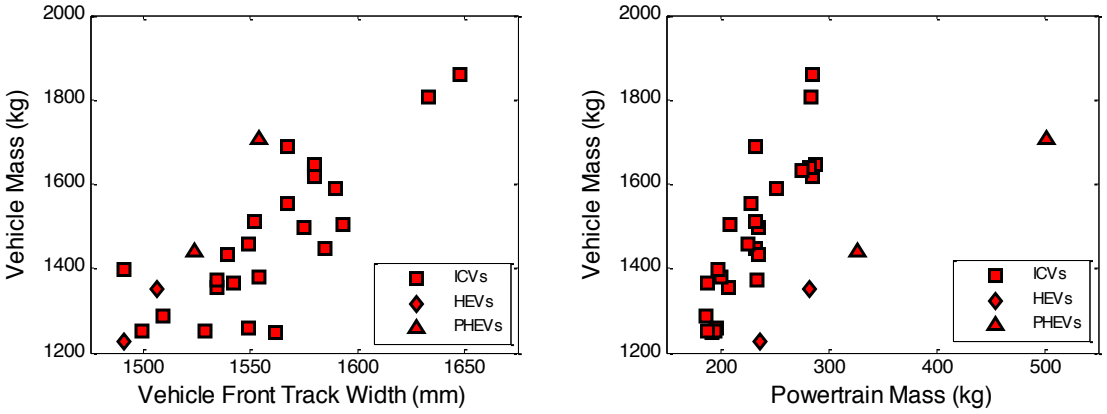

Figure 3: Vehicle teardown data used in the regression analysis [21]

In evaluating the vehicle and powertrain mass data, it is apparent that two unique trends could exist for conventional and hybrid vehicles. In general, the ICVs have a higher vehicle mass as compared to hybrids for the same powertrain mass. This could be due to the fact that some of the hybrids in the dataset use high strength steels more aggressively than the conventional vehicles, thus providing the required structural support but without the additional mass. Also, it is possible that the noted trend is due to

the powertrain characteristics of hybrid versus conventional vehicles, as hybrids are able to achieve the same 0-60 MPH acceleration time with a lower power to weight ratio [22]. While the vehicles in the dataset do not have the exact same acceleration time, it is reasonable to expect that they are designed for very similar targets (e.g. 8.5-9 seconds).Thus, as powertrain mass and power decrease, the mass of conventional vehicles decreases significantly in order to maintain the same power to weight ratio, while hybrid vehicles do not require such significant mass reductions. Also, it is evident that for a certain FTW, the vehicle mass of hybrid vehicles is higher than conventional vehicles. This is likely due to the increased mass per unit volume of the powertrain, particularly due to the battery weight.

However, an argument could also be made for characterizing all of the vehicles with one correlation. According to industry advice, all vehicles, regardless of powertrain type, must be designed to manage the mass of the powertrain in a crash. Thus, assuming no change in the materials used for these structural elements, the mass of structural components that protect the powertrain must increase with powertrain mass. Accordingly, since the precise composition of mild and high strength steel is not known for the vehicles in the dataset, there should be no distinction made between powertrain types when correlating vehicle mass with powertrain mass. In regards to the trend of FTW with vehicle mass, the lower FTW to mass ratio could be explained by the fact that two of the hybrid vehicles are hatchbacks. Thus, based on limited information for hybrid sedans, it is difficult to reach a conclusion regarding the trend of FTW and mass for hybrid vehicles.

Since reasonable arguments may be made for either a one or two correlation fit, this work evaluates the life cycle impacts from both methods. However, since one of the objectives of this work is to assess possible life cycle implications caused by higher structural mass requirements for hybrid vehicles, particular focus is given to the 1 correlation method. Accordingly, regression analysis results and resulting vehicle and subsystem masses are presented for both methods while material composition results are shown only for the 1 correlation method. A comparison of fuel economy and life cycle results is provided in Chapter 3.

The regression analysis results using the 1 and 2 correlation methods are shown in Figure 4 and Equation 7-Equation 9, where vehicle and powertrain mass, *VM* and *PWT*, respectively, are in kg, and *FTW* is in mm. As expected, the coefficient of determination (R^2-square) values are higher for the 2 correlation method (0.82 and 0.99 for the conventional and hybrid vehicles, respectively) since powertrain-specific trends are captured in individual models. However, the R^2-square value for the 1 correlation method, 0.78, is also indicative of a well-fit model and will result in reasonable estimates of vehicle mass. Lastly, the p-value from the 1 correlation analysis, 9.4E-10, indicates that the predictor variables, powertrain mass and FTW, are significant for the regression.

$$VM = -3731 + 3.2FTW + 1.2PWT$$

Equation 7: 1 correlation method – ICV, HEV, PHEV

$$VM = -1927 + 1.7FTW + 3.0PWT$$

Equation 8: 2 correlation method - ICV

$$VM = -5213 + 4.2FTW + 0.8PWT$$

Equation 9: 2 correlation method – HEV, PHEV

As shown in Figure 4, the 1 correlation method results in a best-fit solution plane that falls between the ICV and hybrid planes found with the 2 correlation method. The solution planes reflect the previously noted trends: conventional vehicle mass is most sensitive to a change in powertrain mass, while hybrid vehicle mass is most affected by a change in FTW.

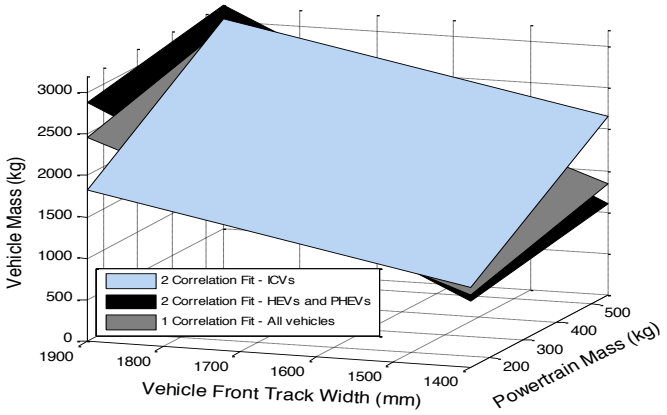

Figure 4: Regression results using the 1 and 2 correlation methods

Results of using both methods are shown in Figure 5, where vehicle mass is evaluated using Equation 7-Equation 9 and compared against the measured vehicle mass.

Since the sample size of ICVs is significantly larger than the HEV and PHEV data, the linear regression for the 1 correlation method is a better fit for conventional as compared to hybrid vehicles. Thus, the predicted vehicle mass of the HEVs and PHEVs is higher using the 1 correlation method as compared to the 2 correlation method.

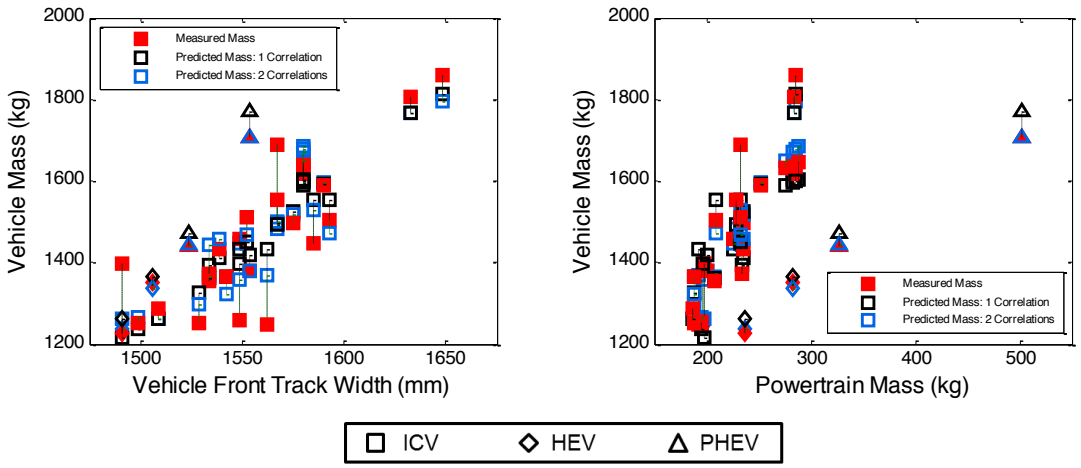

Figure 5: Results of the regression analysis

Once the total vehicle mass is determined for each vehicle, it is necessary to determine the mass of each vehicle subsystem in order to quantify the baseline vehicle material composition and determine the lightweight vehicle subsystem masses. First, ICV subsystem masses are found with the subsystem mass fractions from a representative conventional sedan, as shown in Figure 6. These values agree well with previous work (within 4%) that has calculated subsystem mass fractions for 35 conventional sedans [10]. Then, HEV and PHEV subsystem masses are determined with three assumptions: 1) subsystems that are not dependent on the powertrain have the same mass as their ICV counter-part (e.g. the interior is same for all vehicles), 2) the powertrain mass for each vehicle is equal to the powertrain used to determine the generic ICV, HEV, and PHEV vehicle mass and 3) the non-powertrain change in vehicle mass is distributed proportionally among powertrain-dependent subsystems. Thus, the increase in vehicle mass for the HEV and PHEV, as compared to the ICV, is attributed to both heavier powertrains and powertrain-dependent subsystems.

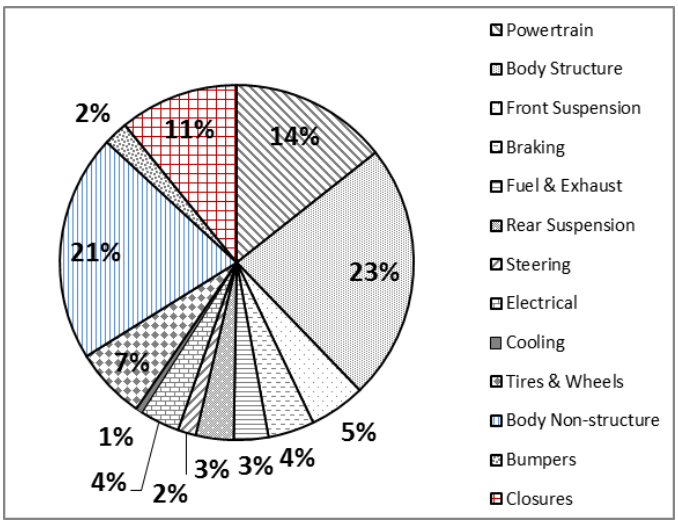

Figure 6: ICV Subsystem mass fraction of curb weight

Powertrain-dependent subsystems are determined according to previous work that has evaluated the design changes necessary for hybridization. For instance, it is assumed that the body structure and front suspension must increase in order to maintain an acceptable crash test performance with the additional weight in the powertrain and that the fuel and exhaust systems may decrease due to engine downsizing [13], [15], [23], [24]. Also, the mass of the braking system is equivalent for all vehicles because the regenerative braking system is integrated with the existing infrastructure and requires only controls modifications [23]. Thus, the powertrain-dependent subsystems include the body structure, front suspension and fuel and exhaust subsystems.

The mass of each powertrain-dependent subsystem is found for the HEV and PHEV with the assumption that the non-powertrain subsystems increase or decrease by the same percentage, x_{EV}. This simplification allows the change in subsystem mass to be modeled without detailed subsystem models, which are beyond the scope of this work. Accordingly, the change in vehicle mass due to non-powertrain subsystems, ΔVM_{nonpwt}, is calculated by subtracting the change in powertrain mass from the total vehicle change in mass. Then, according to Equation 10, values for x_{EV} are found for the HEV and PHEV by assuming that the mass of the ICV body structure, $m_{bodystruc}$, and front suspension, $m_{frontsusp}$, increase, while the fuel and exhaust mass, $m_{fuelexh}$, decreases. Lastly, $x_{EV}$is used to find the final mass for the body structure, front suspension and fuel and exhaust system in the HEV and PHEV.

$$x_{EV}(m_{bodystruc} + m_{frontsusp} - m_{fuelexh}) = \Delta VM_{nonpwt}$$

Equation 10: Powertrain-dependent subsystem mass

Component Sizing

Powertrain components are sized for the ICV, HEV, and PHEV such that the vehicle achieves the following acceleration and gradeability requirements: 0-60 mph in 9 seconds and 65 mph at a 6% grade, respectively [25]. Additionally, the PHEV must have a 10 mile all-electric range (AER) while operating on the US06 cycle when starting with a fully charged battery with a 80% state of charge (SOC) range [11], [26], [27]. The US06 cycle is chosen as a representative drive cycle because it simulates aggressive city driving and will provide a conservative estimate of the necessary components. Since each vehicle has a unique powertrain configuration, the method to achieve the performance requirements is different for each vehicle, as shown in Table 6. For instance, the ICV must meet performance targets with engine power alone, while the HEV uses a combination of engine and motor power. Similar to previous work, the ratio of engine to motor peak power for the HEV is assumed to be the same as representative Toyota and Ford power-split hybrids, 1.2 [28], [29], [30]. Once the motor power is known, the HEV battery is sized by dividing the peak power of the motor by the motor efficiency, 88% [31]. The PHEV motor and battery are sized to supply the power required for driving the US06 cycle in all-electric mode. Additionally, the battery must deliver by the energy required for a 10-mile all-electric range. After the motor and battery sizes are known, the engine is sized to meet both performance requirements. Additional information on vehicle model parameters is located in Table 12 in the Appendix.

Table 6: Performance requirements used to size powertrain components

	Engine	Motor	Battery
ICV	1) Acceleration / Gradeability ***(Velocity < 0.1% of target)***		
HEV	1) Acceleration / Gradeability ***(Velocity < 0.1% of target)*** 2) Engine power = 1.2*(Motor power)		1) Motor peak power
PHEV	1) Acceleration / Gradeability ***(Velocity < 0.1% of target)***	Peak power on US06 cycle ***(Does not miss drive cycle velocity < 2 mph)***	1) Motor peak power 2) 10 miles on US06 cycle ***(Distance < 1% of target)***

Components are sized in an iterative scaling process in Autonomie according to the velocity and distance tolerances specified in Table 6. The engine and motor performance maps and weights are scaled linearly by peak power while the battery characteristics are determined with a method proposed by Kim et al. [31], [32]. Accordingly, the resistance, power, current and mass of the battery is scaled by the ratio of the original and desired battery capacity [32]. This method ensures that the battery terminal voltage is maintained at an acceptable value since the number of battery cells does not change during the scaling process [32].

Once the mass of the engine, motor and battery are known, the mass of the remaining powertrain components are determined in order to facilitate a more accurate material analysis. Components considered in this analysis include an automatic transmission for the ICV, a continuously variable transmission (CVT), power inverter, hybrid cooling system and electrical accessories for the HEV and PHEV, and a plug-in charger cable and outlet for the PHEV. For each vehicle, the mass of these components are determined by first subtracting the mass of the engine, motor, and battery (as applicable) from the total powertrain mass and allocating the remaining mass using mass fractions from representative ICV and hybrid vehicles. For instance, the ICV powertrain is only composed of the engine and transmission so 100% of the non-engine powertrain mass is allocated to the transmission. However, since the HEV powertrain includes a power inverter, hybrid cooling system and electrical accessories in addition to the transmission, the mass fraction of each is determined from teardown data of a representative HEV. Accordingly, the CVT, power inverter, hybrid cooling system and electrical accessories are 65%, 17%, 6% and 12% of the remaining powertrain mass for the HEV. Mass fractions for the PHEV powertrain are similar to the HEV but slightly lower, as 3% of the mass is allocated for plug-in charging components.

Material Selection

The material composition of the baseline ICV is determined with teardown data from a representative sedan-sized vehicle [21]. Materials from this vehicle are classified into categories synonymous with GREET 2 and the mass fractions of materials in each subsystem is computed [18], [21]. Then, the material composition of the generic ICV is determined based on the material mass fractions and the mass of each subsystem.

Materials for the HEV and PHEV are found for each subsystem using the same material mass fractions for the ICV, with the exception of the powertrain. To capture the impact of powertrain component downsizing, powertrain materials are determined in a disaggregated method by individually defining the material composition of the engine, motor, battery, automatic transmission, CVT, power inverter, cooling system, electrical accessories, and plug-in components. While the material composition of most of these systems are determined from teardown data, GREET 2 provides more detailed information for the motor, power invertor and Li-ion battery [23].

2.3.3 Lightweight vehicle models

Vehicle mass and component sizing

Lightweight vehicles are designed in an iterative process that incorporates primary mass reduction from material substitution, secondary mass reductions in non-powertrain systems and powertrain re-sizing to maintain vehicle performance requirements. As an initial step, primary mass reductions are determined with substitution ratios in a method developed by Ashby [7]. Accordingly, material indices are calculated for each part and material and the substitution ratio is found with the ratio of material indices for baseline and lightweight materials. For instance, the material index, *M*, of a high crown panel (e.g. vehicle hood) is found from the equation:

$$M = \frac{E}{\rho^{1/2}}$$

Equation 11: Material index for high crown panel

where E is the elastic modulus and ρ is the density. Using this equation, the material index ratio of steel to aluminum yields a substitution ratio of 1:0.6, which is consistent with previous studies [33], [34]. Similarly, substitution ratios may be found for any other vehicle part, assuming that their classification (e.g. high crown panel) and function is known.

After an initial amount of mass is removed from the vehicle, secondary mass reductions for non-powertrain systems are determined with subsystem mass influence coefficients, γ_i, defined as the change in mass of subsystem *i* per unit change in gross vehicle mass [10]. Subsystem mass influence coefficients are adopted from previous work by Malen et al. that performed a regression analysis for sedans with the same

defining characteristics as used in this work (shown in to Table 13 in the Appendix) [10], [13]. Malen et al. found that mass compounding most strongly influences the body structure and has no effect on the electric, cooling, and body non-structure subsystems [13]. The new mass of each non-powertrain subsystem is found with a simple secondary mass change, assuming that only one resizing iteration takes place. Accordingly, the new vehicle mass is defined by

$$\boldsymbol{M_{RS} = M_0 + \Delta + \Delta\gamma_V}$$

Equation 12: Mass compounding calculation for all vehicle subsystems

where M_{RS} is the vehicle mass after re-sizing, M_0 is the initial vehicle mass, Δ is the primary mass change, and γ_V is the mass influence coefficient for the vehicle, found from the sum of γ_i for all subsystems.

Once the new vehicle mass is known, the powertrain is re-sized based on the component sizing criteria, as specified in Table 6. Then, the change in powertrain mass is determined and input as a primary mass reduction to the secondary mass model. The second iteration of secondary mass reductions for non-powertrain subsystems results in a second updated vehicle mass and the new vehicle mass is compared to the previous result. If the change in vehicle mass is greater than 1 kg, the process continues. However, if the change in vehicle mass is less than 1 kg, the sizing routine is complete and the powertrain specifications and vehicle mass are input to the fuel economy and material models.

Material selection

The lightweight vehicle material composition is determined by incorporating the material substitution and subsystem downsizing into the baseline material model. It is assumed that during the secondary mass savings procedure, all components in a subsystem are downsized proportionally. Thus, the material composition of the lightweight vehicle subsystems is determined with the same subsystem material mass fraction used for the baseline vehicles.

2.4 Results

2.4.1 Baseline vehicles

Vehicle masses

As shown in Figure 7 and Table 7, the total vehicle mass for the generic ICV, HEV, and PHEV are found with the 1 and 2 correlation methods with powertrain mass and FTW inputs previously discussed. Due to the bias in the 1 correlation model towards ICVs, the generic HEV and PHEV masses found with this method are higher than those found with the 2 correlation method. Also, the ICV mass determined with 1 correlation is higher since the model must also characterize hybrid vehicles with higher powertrain to vehicle mass ratios. However, since vehicle mass differs by only 0.7%-1.5% when using the two methods, it is expected that the final impact on life cycle results will be negligible. Overall, the masses of the generic vehicles are in good agreement with production sedans, as using the 1 correlation analysis results in vehicle masses only 2-5% higher than the Toyota Corolla, Toyota Prius and Toyota Prius PHEV.

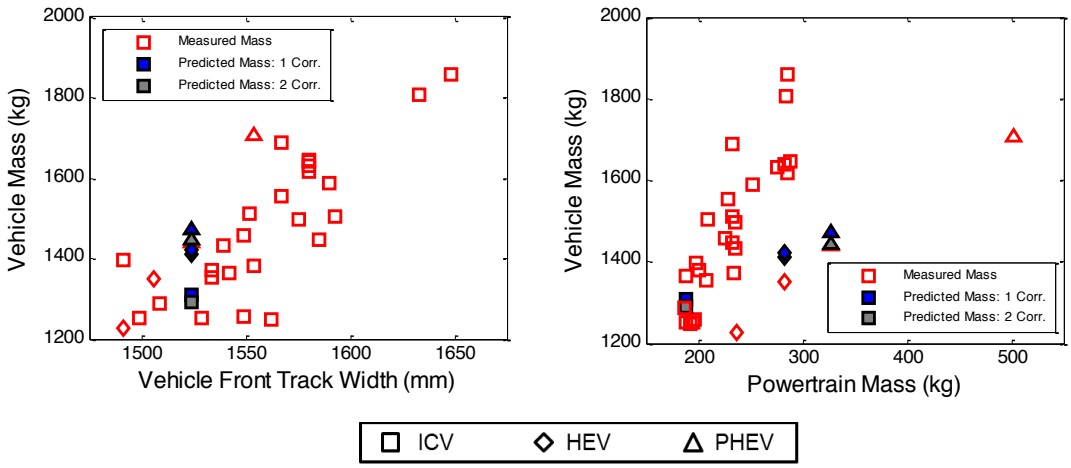

Figure 7: Vehicle mass results for the generic ICV, HEV and PHV

The additional mass for the HEV and PHEV is attributed to a mass increase in the powertrain, body structure and front suspension, and a mass decrease in the fuel and exhaust subsystem, according to Equation 10. Corresponding results for the 1 and 2 correlation methods are shown in Table 7 and Figure 8. While the majority of the mass increase for the HEV and PHEV is due to heavier powertrains, the total mass of the powertrain-dependent subsystems increases by 17-24 kg with the 1 correlation method

and 24-26 kg using the 2 correlation method. Due to the assumption that the change in mass is proportional the original subsystem mass, the impact of downsizing the fuel and exhaust subsystem is least significant (2-3 kg), while the body structure contributes over 90% of the powertrain-dependent mass increase for all vehicles.

As compared to the ICV, the increase in structural mass for the HEV is greatest when using the 2 correlation method. For a 1 kg increase in HEV powertrain mass, structural mass (i.e. body structure and front suspension) increases 0.2 kg with the 1 correlation method and 0.3 kg with the 2 correlation method. For the PHEV, results from both methods indicate that 0.2 kg of structural support is required per 1 kg increase in powertrain mass. It is important to note that this structural support value is highly dependent on the powertrain masses that we used to characterize generic vehicles and results could have a large variation due to the range of powertrain masses for ICVs, HEVs and PHEVs.

While the 1 correlation method shows that increased structure is required for the PHEV as compared to the HEV, results from using the 2 correlation methods indicate the opposite trend (i.e. structural mass actually decreases by 2 kg). This is due to the lower sensitivity of vehicle mass to powertrain mass in the hybrid vehicle regression analysis. Overall, each correlation offers unique insight to possible hybrid vehicle design trends, but both methods produce similar ratios of structural to powertrain mass. Thus, the remaining analyses in this work employ the 1 correlation method (and the life cycle sensitivity of each method is assessed in Chapter 3).

Table 7: Total vehicle and powertrain-dependent subsystem masses determined using 1 correlation (2 correlations)

	ICV	HEV	PHEV
Total vehicle mass (kg)	1309 (1290)	1421 (1411)	1472 (1451)
Powertrain mass (kg)	188	283	327
ΔVM_{nonpwt} (kg)	NA	17 (26)	24 (22)
x_{EV}	NA	5% (8%)	7% (7%)
Body Structure (kg)	307 (301)	322 (325)	329 (322)
Front Suspension (kg)	67 (66)	70 (71)	72 (70)
Fuel and Exhaust (kg)	41 (41)	39 (37)	38 (38)

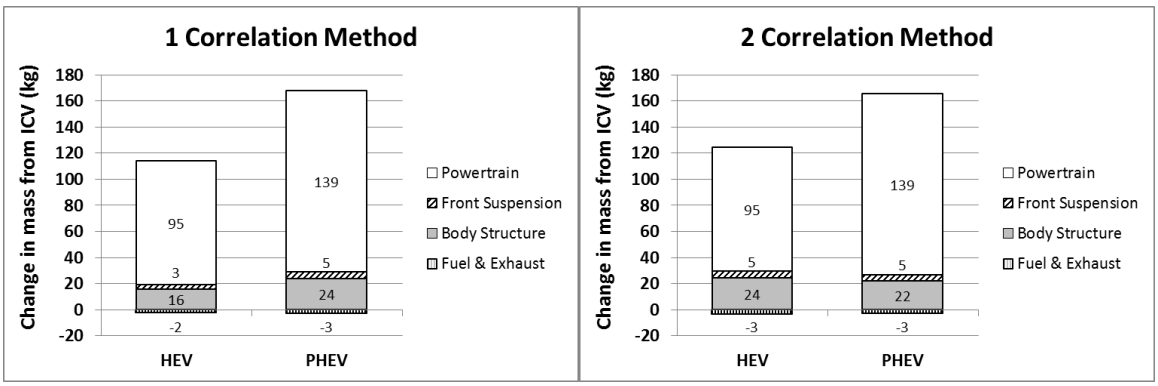

Figure 8: HEV and PHEV powertrain-dependent subsystem mass change

While the method of using a constant percentage mass increase/reduction for each powertrain-dependent subsystem is a simplified approach, this assumption will not have a significant impact on the total vehicle material composition since steel is the dominant material in each subsystem. For instance, if instead the total non-powertrain mass increase was due to increase in body structure alone, the total mass of steel and other materials in the vehicle would change less than 1%. Plastic and wrought aluminum would increase slightly due to the increase in the fuel and exhaust system mass, while rubber would decrease due to a smaller front suspension. The mass of steel would remain relatively unchanged because the increase in steel in the body structure and fuel and exhaust systems would compensate for the decrease in steel in the front suspension. Thus, the error in using x_{EV} to allocate the change in mass for the generic HEV and PHEV will have negligible impacts on life cycle results.

Component sizing

Results from sizing the powertrain components with performance requirements are shown in Table 4. For each vehicle, the acceleration requirement is more stringent than gradeability and each vehicle reaches 0-60 mph in 9 seconds exactly. The powertrain sizing method proposed in this work results in reasonable results as compared to production vehicles. For instance, the ICV engine power is within 10 kW of the Madza3 engine and the HEV engine and motor sizes are very similar to the Toyota Prius. However, the HEV battery is oversized as compared to current HEVs (e.g. Toyota Prius battery has a total capacity of 1.8 kWh and 40% SOC range) [35]. This is due to the requirement that the battery provide the peak motor power, which is not a cost effective

design constraint in production vehicles. With regards to the PHEV battery size, it is expected that the battery will be slightly oversized since the US06 cycle represents more aggressive driving [36]. However, the 5.0 kWh battery capacity is comparable to the Toyota Plug-in Prius battery, which is 4.4 kWh and results in an EPA rated 11-mile all electric range in blended mode.

Once the battery sizes are known, the cargo capacity may be calculated to determine if the functional equivalence requirements are met for the generic HEV and PHEV. Assuming that the energy density is representative of current lithium-ion technology (200 Wh/L) and the vehicle tunnel volume is equivalent to that of the GM Volt (6.8 cu ft), the HEV and PHEV batteries may be located entirely in the tunnel [37], [38]. Thus, the functional equivalence requirement of a minimum cargo volume is maintained for each vehicle.

Table 8: Powertrain specifications for the baseline vehicles

	ICV	HEV	PHEV
Engine Power (kW)	117 kW	73.3 kW	75.7 kW
Motor Power (kW)		61.1 kW	63.1 kW
Battery Power (kW)		69.4 kW	80.4 kW
Battery Capacity (kWh)		4.4 kWh (1.7 kWh useable)†	5.0 kWh (4.0 kWh useable)‡

†SOC range of 40% [35]
‡SOC range of 80% [27]

Materials

Based on the powertrain component specifications, the material composition for each powertrain is determined, as shown in Figure 9. The most significant material difference between the ICV and hybrid vehicles is due to the addition of the Li-ion battery, which is primarily composed of Lithium Manganese Oxide (LiMn2O4), wrought aluminum, copper, and graphite/carbon. The increase in copper for the hybrid vehicles is also due to the addition of the motor and generator, which are 24% copper by weight. These components, as well as the power inverter, also contribute to increased cast aluminum and steel in the powertrain. However, the overall content of steel is less for the hybrid vehicles due to the fact that the engines are almost half the size as the engines in the ICV. Also, while the automatic transmission is 70% steel by weight, the CVT replaces much of this steel with cast aluminum, resulting in a further increase in cast

aluminum for the hybrid vehicles. Lastly, the amount of plastic is increased in the hybrid vehicles due to parts required in the hybrid cooling system, electrical accessories, and in the case of the PHEV, plug-in components.

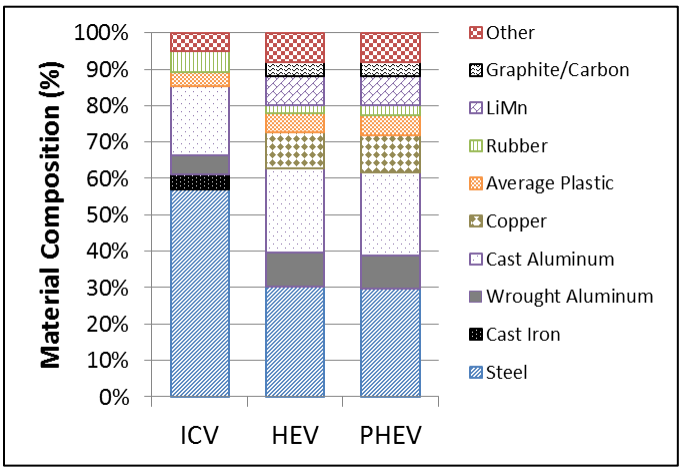

Figure 9: Powertrain percent material composition by weight

The material composition of the ICV, HEV and PHEV is shown in Figure 10. As compared to the ICV, the differences in material composition for the HEV and PHEV are due to changes in the powertrain, body structure, front suspension and fuel and exhaust subsystems. Most notably, copper and cast aluminum increase as the vehicle is electrified due to the addition of two motor/generators, a power inverter, and a battery. To a smaller extent, the amount of plastic and wrought aluminum increases for the HEV and PHEV due to modifications in the powertrain. As compared to the ICV, steel decreases by 5 kg for the HEV and increases by 15 kg for the PHEV. This is due to the tradeoff between an increase in steel in the body and front suspension and a reduction in steel in the powertrain and fuel and exhaust subsystems. For instance, while the HEV body structure and front suspension increase steel by 17 kg of steel, the change in powertrain composition reduces the mass of steel by 21 kg and the downsized fuel and exhaust eliminates 1kg. This results in a net decrease in steel for the HEV as compared to the ICV. On the other hand, the steel content in the PHEV is increased as compared to the ICV because the body structure and front suspension increase more than for the HEV due to the heavier powertrain. Also, the reduction of steel in the powertrain is less severe for the PHEV due to the increased mass of the CVT, cooling, and electrical accessories.

Since it is assumed that the wheels and non-structural part of the vehicle body remains the same for the ICV, HEV and PHEV, the mass of stainless steel, glass, and fluids are the same for each vehicle. The material category "Other" is comprised mainly of sensors, materials in the lead acid and Li-ion batteries, wiring harnesses and interior components, such as carpeting and lighting. Since the amount of materials in this category increase as the vehicle is electrified, the uncertainty of vehicle production energy and GHG emissions is greatest for the generic PHEV.

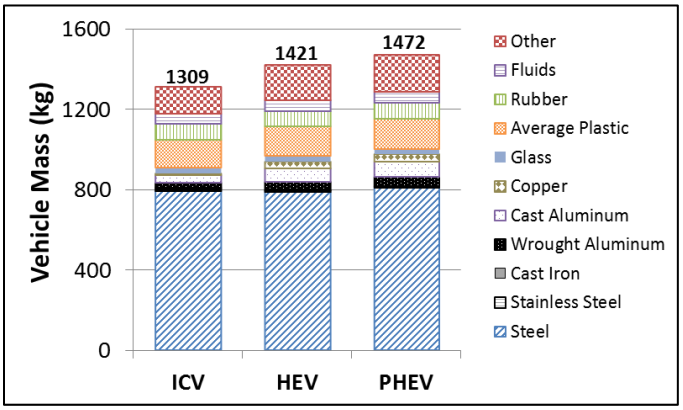

Figure 10: Material composition for the baseline vehicles

2.4.2 Lightweight vehicles

Vehicle masses and component sizing

As a demonstration of the lightweight vehicle design methodology, we assume that primary mass reductions are made in the closures and bumpers and that secondary mass reductions and powertrain re-sizing occurs until convergence criteria are met. The closures and bumpers are identified as areas where mass savings are likely to occur since material substitution in these subsystems is a relatively simple and affordable option for automobile manufacturers [39]. It should be noted that secondary mass reductions are only achieved if the decision to reduce mass is made early in the design process, which may not always be the case. However, this work assumes that the decision to lightweight the closures and bumpers is made with enough time to reap the benefits of secondary mass savings.

Similar to previous work that has assessed the potential of mass reduction in closures and bumper subsystems, we assume that steel parts can be replaced with

aluminum due to the higher strength to weight ratio of aluminum [39]. The mass of the steel parts is determined with mass fractions from teardown data of a representative ICV sedan. Specifically, the mass of steel parts in the closures and bumpers are found as a fraction of the total subsystem mass and applied to the generic ICV subsystem mass to determine the mass of the baseline steel parts. Since it is assumed that the closures are the same for the ICV, HEV and PHEV, the mass of these parts are equivalent for all vehicles.

The substitution ratio of steel to aluminum is found for each part based on its material index, which is dependent on E, ρ, or the tensile strength, σ_Y, as shown in Table 9. According to the calculated substitution ratios, it is evident that material substitution for the window frame is not beneficial because it would require an increase in mass to perform the same function with aluminum. Thus, the window frame is not included in the material substitutions considered in this work.

Table 9: Material indices and substitution ratios by part [40]

Subsystem	Part	Geometry	Design constraints	Material Index†	Substitution ratio (Steel:Aluminum)
Closures	Window frame	Beam in bending	Stiffness, Size	E/ρ	1:1.03
	Door beam		Yield strength, Size	σ_Y/ρ	1:0.25
	Hood	High crown panel	Stiffness, Size	$E^{1/2}/\rho$	1:0.6
	Trunk				
	Outer panel				
	Fenders				
	Inner/side panels	Flat panel		$E^{1/3}/\rho$	1:0.5
Bumpers	Bumper beams	Beam in bending	Buckling stiffness, strength	$E^{5/9}/\rho$	1:0.63

†Material properties are as follows [40]:
Steel: E = 200 GPa, σ_Y = 220 MPa, ρ = 7860 kg/m^3
Aluminum: E = 70 GPa, σ_Y = 260 MPa, ρ = 2710 kg/m^3

As shown in Figure 11, aluminum displaces a total of 37.5 kg of steel in the closures and bumpers, with the most significant reductions in the door beam. The mass of the closures and bumpers are reduced by 48% and 37%, respectively, which is consistent with previous work that has performed detailed modeling and crash test simulations to determine the maximum mass savings in these subsystems [39], [41].

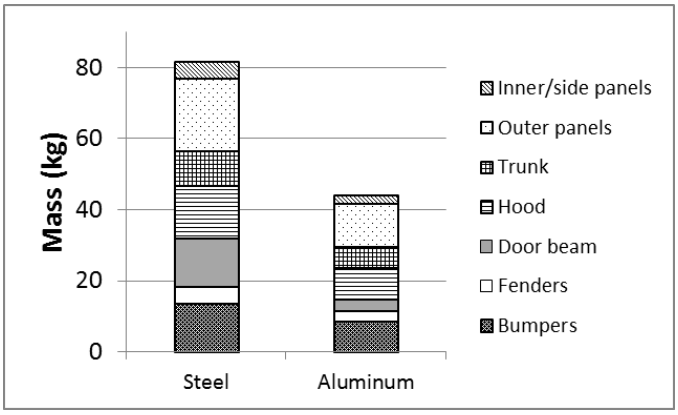

Figure 11: Mass of steel and aluminum parts in the closures and bumpers

Once the primary mass reduction is known, secondary mass reductions are considered with the secondary mass model and powertrain re-sizing routine, as shown in Table 10 and Figure 12. The initial mass reduction for each vehicle is 51 kg, based on the primary mass change and Equation 10. Subsequent mass reductions are unique for each vehicle due to the distinct powertrain characteristics and component sizing requirements. For instance, the ICV has the least potential for powertrain downsizing due to the limitations of the fixed gear ratios in the transmission and the fact that no mass savings can be yielded from downsizing a battery. On the other hand, the hybrid vehicles have the most powertrain reductions due to the potential to downsize the battery. Due to these trends, secondary mass reductions contribute 34% to the total mass reduced for the ICV and 40-41% for the HEV and PHEV.

Table 10: Secondary mass reductions and the final lightweight vehicle masses

Vehicle mass with non-powertrain secondary reductions (kg)	Reduction in powertrain mass (kg)	Vehicle mass with non-powertrain secondary reductions (kg)	Reduction in powertrain mass (kg)	Vehicle mass with non-powertrain secondary reductions (kg)	Reduction in powertrain mass (kg)
ICV Baseline Vehicle Mass: 1309 kg		**HEV Baseline Vehicle Mass: 1421 kg**		**PHEV Baseline Vehicle Mass: 1472 kg**	
1258	3.8	1370	6.7	1421	6.3
1253	0.4	1360	1.3	1412	1.1
1252	NA	1358	0.3	1410	0.3
		1358	NA	1410	NA
ICV Lightweight Vehicle Mass: 1252 kg		**HEV Lightweight Vehicle Mass: 1358 kg**		**PHEV Lightweight Vehicle Mass: 1410 kg**	

Table 11: Powertrain specifications for the lightweight vehicles

	ICV	HEV	PHEV
Engine Power (kW)	113 kW	70.3 kW	72.7 kW
Motor Power (kW)		58.6 kW	60.6 kW
Battery Power (kW)		66.6 kW	78.6 kW
Battery Capacity (kWh)		4.2 kWh (1.7 kWh useable)†	4.9 kWh (3.9 kWh useable)‡

†SOC range of 40% [35]
‡SOC range of 80% [27]

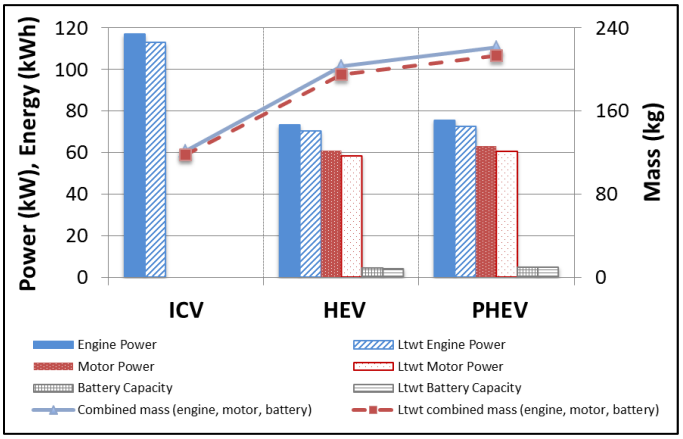

Figure 12: Powertrain specifications for the baseline and lightweight vehicles

Materials

The material composition of the lightweight vehicles is shown in Figure 13. The most significant changes in materials are due to primary reductions, as shown by the decrease in steel and increase in aluminum. In fact, at least 80% of the reductions in steel are due to material substitution, while 5-7% is due to secondary mass reductions in the body structure. Stainless steel, cast iron, aluminum, copper, plastic, and rubber are reduced by 5% or less for all vehicles due to secondary mass reductions. However, there is no change in glass and fluids because the body non-structure is equivalent to the baseline vehicles.

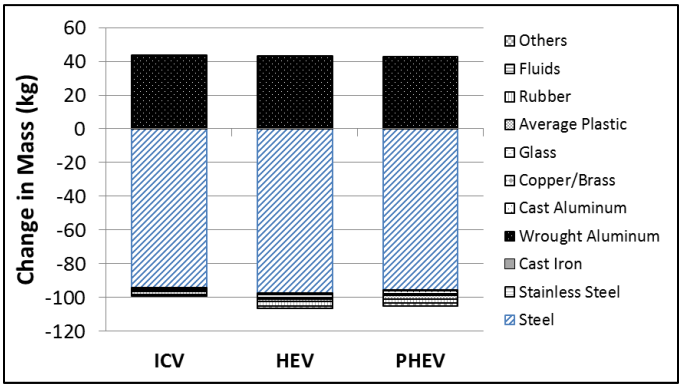

Figure 13: Change in materials for lightweight vs. baseline vehicles

2.5 Conclusions

This work provides design harmonization techniques to incorporate design changes necessary for electrified vehicles in an easily understood, systematic process, suitable for the scope of a LCA. First, vehicle mass is determined based on regression analysis of vehicle teardown data using FTW and powertrain mass as predictor variables. Then, the change in mass due to non-powertrain subsystems is determined and allocated to the body structure, front suspension, and fuel and exhaust systems. Lastly, the material composition for each subsystem is scaled according to the change in subsystem mass.

Two approaches for the regression analysis are compared in order to assess the design implications of including all vehicles in the analysis, regardless of powertrain-type, or developing unique correlations for conventional and hybrid vehicles. The 1 correlation approach assumes that conventional and hybrid vehicles are designed with the same structural materials and requirements regarding powertrain mass. However, the 2 correlation method assumes that hybrid vehicles could use increased high strength steels in the structural components and that the design criteria is powertrain-specific, depending on the power to weight characteristics of the vehicle. While results from both methods show that vehicle mass increases with electrification, the increase in structural support per increase in powertrain mass required for the HEV is more significant with the 2 correlation approach due to the lower ICV mass predicted with this method. For instance, results from using 2 correlation method indicates that 0.3 kg of structural mass is required per increase in powertrain mass for the HEV, while the 1 correlation method yields 0.2 kg. However, both methods result in 0.2 kg increase in structural mass per powertrain

mass for the PHEV. While these results provide insight to possible trends in vehicle design, the impact on vehicle mass trends is negligible for the scope of a LCA and the 1 correlation method is used for subsequent analyses.

The lightweight vehicle design process outlined in this work incorporates methods from previous authors into a streamlined process that can be used in future LCAs. Lightweight vehicles are designed using a combination of primary and secondary mass reductions, including powertrain re-sizing to maintain performance. Primary reductions from material substitutions are input to a secondary mass model which accounts for simple mass compounding in non-powertrain systems. Once an updated vehicle mass is determined, the powertrain is re-sized in Autonomie. The change in powertrain mass is input to the secondary mass model and the process continues until convergence criteria are met.

To demonstrate the utility of the vehicle design methodology, a lightweight scenario is considered where steel is replaced with aluminum in the closures and bumpers. To ensure that secondary mass reductions may be incorporated in the vehicle design, it is assumed that the decision to lightweight the vehicle is made early in the design process. As a result, the mass of the ICV, HEV, and PHEV is reduced by 57 kg, 63 kg, and 62 kg, respectively, with 34-41% of these secondary mass reductions. Overall, the most significant mass reductions occur for the hybrid vehicles due to the greater potential for powertrain downsizing. As a result of vehicle lightweighting, steel decreases by 13-14%, wrought aluminum increases by 52-64%, and all other materials decrease by 5% or less.

Part 2 of this work (presented in Chapter 3) will apply the design harmonization process to assess the life cycle energy and GHG reduction potential of lightweight materials and vehicle electrification. While the lightweight vehicle models in Chapter 2 are a useful demonstration of the design methodology, more significant primary mass reduction scenarios are considered in Chapter 3, along with fuel economy and life cycle results, according to the process shown in Figure 2. Accordingly, material substitution scenarios will include body-in-white materials replacements of conventional steel with aluminum and advanced / high strength steel. As done in the present work (Chapter 2), secondary reductions, including powertrain re-sizing, will be used to determine the final

vehicle mass and powertrain specifications. Through drive cycle simulations for the baseline and lightweight vehicles, the potential of each vehicle-type to reduce fuel consumption per unit mass reduced (known as the mass elasticity of fuel consumption) will be included in the LCA. Thus, life cycle results shown in Chapter 3 will include the fuel economy differences due to powertrain architecture as well as the design harmonization techniques presented in Chapter 2.

2.6 References

[1] Paramount Research, "WardsAuto/ DuPont Survey of Auto Industry Challenges," www.paramoundresearch.com, 2011.

[2] S. C. Davis, S. W. Diegel, and R. G. Boundy, *Transportation Energy Data Book, Edition 31*. 2012, pp. 6–7.

[3] A. Elgowainy, J. Han, L. Poch, A. Wang, M. Mahalik, and A. Rousseau, "Well-to-Wheels Analysis of Energy Use and Greenhouse Gas Emissions of Plug-In Hybrid Electric Vehicles," *Argonne National Laboratory*, 2010.

[4] H.-J. Kim, C. McMillan, G. A. Keoleian, and S. J. Skerlos, "Greenhouse Gas Emissions Payback for Lightweighted Vehicles Using Aluminum and High-Strength Steel," *Journal of Industrial Ecology*, vol. 14, no. 6, pp. 929–946, Dec. 2010.

[5] ISO, *ISO 14040 Environmental management - Life cycle assessment - Principles and framework*. 1997.

[6] I. J. Wohlecker, R., Wallentowitz, H., Johannaber, M., Espig, M., Leyers, "Determination of Weight Elasticity of Fuel Economy for Conventional ICE Vehicles, Hybrid Vehicles and Fuel Cell Vehicles," *FKA*, Report 555.

[7] M. F. Ashby, *Materials Selection, Second Edititon*. 1999.

[8] D. E. Malen, R. Gobbels, and R. Wohlecker, "Estimation of Secondary Mass Changes in Vehicle Design," SAE Paper 2013–01–0655, 2013.

[9] C. Bjelkengren, "The Impact of Mass Decompounding on Assessing the Value of Vehicle Lightweighting," MIT, Doctoral Dissertation, 2006.

[10] K. D. Malen, E, K., Reddy, "Preliminary Vehicle Mass Estimation Using Empirical Subsystem Influence Coefficients," Auto-Steel Partnership, http://www.a-sp.org/en/LightweightPrograms.aspx, 2007.

[11] A. Moawad, P. Sharer, and A. Rousseau, "Light-Duty Vehicle Fuel Consumption Displacement Potential up to 2045," *Argonne National Laboratory,* 2011.

[12] A. Bandivadekar, K. Bodek, L. Cheah, C. Evans, T. Groode, J. Heywood, E. Kasseris, M. Kromer, and M. Weiss, "On the Road in 2035," 2008.

[13] D. Malen, Design Advisor User Guide, WorldAutoSteel, http://www.worldautosteel.org/projects/, 2012.

[14] T. R. Hawkins, B. Singh, G. Majeau-Bettez, and A. H. Strømman, "Comparative Environmental Life Cycle Assessment of Conventional and Electric Vehicles," *Journal of Industrial Ecology*, vol. 17, no. 1, pp. 53–64, Feb. 2013.

[15] FKA, "Investigation of the Trade-off Between Lightweight and Battery Cost for an Aluminium-Intensive Electric Vehicle," Project No, 2012.

[16] C.-S. N. Shiau, C. Samaras, R. Hauffe, and J. J. Michalek, "Impact of battery weight and charging patterns on the economic and environmental benefits of plug-in hybrid vehicles," *Energy Policy*, vol. 37, no. 7, pp. 2653–2663, Jul. 2009.

[17] Argonne National Laboratory, "Autonomie." UChicago Argonne, LLC, 2009.

[18] Argonne National Laboratory, "GREET 2 rev1." UChicago Argonne, LLC, 2012.

[19] Argonne National Laboratory, "GREET 1 rev2." UChicago Argonne, LLC, 2012.

[20] *Consumer Report*. 2013, pp. 146–150.

[21] www.A2Mac1.com, Automotive Benchmarking, Yipsilanti, MI, 2013.

[22] S. Pagerit, P. Sharer, and A. Rousseau, "Fuel economy sensitivity to Vehicle Mass for Advanced Vehicle Powertrains," SAE Paper 2006–01–0665, 2006.

[23] A. Burnham, M. Wang, and Y. Wu, "Development and Applications of GREET 2 . 7 — The Transportation Vehicle-Cycle Model," *Argonne National Laboratory*, 2006.

[24] I. Husain, *Electric and Hybrid Vehicles Design Fundamentals, Second Edition*, CRC Press, 2011.

[25] J. Kwon, J. Kim, E. Fallas, S. Pagerit, and A. Rousseau, "Impact of Drive Cycles on PHEV Component Requirements," SAE Paper 2008–01–1337.

[26] N. Shidore and S. C. Avenue, "PHEV 'All electric range' and fuel economy in charge sustaining mode for low SOC operation of the JCS VL41M Li-ion battery using Battery HIL," *Argonne National Laboratory*.

[27] A. Pesaran and T. M. Nrel, "Battery Requirements and Cost-Benefit Analysis for Plug-In Hybrid Vehicles (Presentation)," *National Renewable Energy Laboratory*, 2007.

[28] Y. Mizuno, R. Ibaraki, K. Kondo, K. Odaka, H. Watanabe, T. Mizutani, K. Kaneshige, and D. Kitada, "Development of New Hybrid Transmission for Compact-Class Vehicles," SAE Paper 2009–01–0726.

[29] R. Teraya and M. Nakamura, “Development of the New THS-II Powertrain for Compact Vehicles,” SAE Paper 2012–01–1017, 2012.

[30] Ford, “2013 Ford c-max technical specifications.” 2013.

[31] Argonne National Laboratory, “Autonomie.” UChicago Argonne, LLC, 2009.

[32] M.-J. Kim and H. Peng, “Power management and design optimization of fuel cell/battery hybrid vehicles,” *Journal of Power Sources*, vol. 165, pp. 819–832, 2007.

[33] J. Wohlecker, R., Hallentowitz, H., Henn, R., Leyers, “FKA Final Report on Mass Reduction,” *Forschungsgesellschaft Kraftfahrwesen mbH Aachen*, Project no. 56690, 2006.

[34] M. Bertram, K. Buxmann, and P. Furrer, “Analysis of greenhouse gas emissions related to aluminium transport applications,” *The International Journal of Life Cycle Assessment*, vol. 14, no. S1, pp. 62–69, 2009.

[35] K. J. Kelly, M. Mihalic, and M. Zolot, “Battery Usage and Thermal Performance of the Toyota Prius and Honda Insight for Various Chassis Dynamometer Test Procedures Preprint,” in *17th Annual Battery Conference on Applications and Advances*, 2002, November 2001.

[36] T. Markel and A. Simpson, “Plug-In Hybrid Electric Vehicle Energy Storage System Design,” in *Preprint, Advanced Automotive Battery Conference*, 2006, no. May, pp. NREL/CP–540–39614.

[37] D. Howell, “Battery Status and Cost Reduction Prospects,” Department of Energy, 2012.

[38] M. LeGault, “Chevy Volt battery pack: Rugged but precise,” *CompositesWorld*, 2013.

[39] EPA, “Light-Duty Vehicle Mass Reduction and Cost Analysis — Midsize Crossover Utility Vehicle,” *U.S. Environmental Protection Agency*, EPA-420-R-12-026, 2012.

[40] D. E. Malen, Fundamentals of Automobile Body Structure Design, SAE International, 2011.

[41] H. Singh, “Mass Reduction for Light-Duty Vehicles for Model Years 2017-2025,” *Report No. DOT HS 811 666*, Program Reference: DOT, 2012.

[42] www.fueleconomy.gov, U.S. Environmental Protection Agency, 2013. [Online]. Available: www.fueleconomy.gov/feg/info.shtml. [Accessed: 18-Jul-2013].

[43] A. Moawad, A, Sharer, P, Rousseau, “Light-Duty Vehicle Fuel Consumption Displacement Potential up to 2045,” *Argonne National Laboratory*, 2011.

2.7 Appendix

Correlation of FTW to vehicle class and occupancy

Vehicle classes are defined by the EPA according to interior volume, defined as the sum of cargo and passenger volume [42]. As shown in Figure 14, EPA Interior Volume is reasonably well correlated to FTW for a variety of different sized sedan vehicles, chosen from the 2012-2013 Consumer Report for automobiles [20]. Similarly, as each of these vehicles have a 5 person occupancy, it is reasonable to assume that FTW in the range of 57-63" is suitable to meet this requirement.

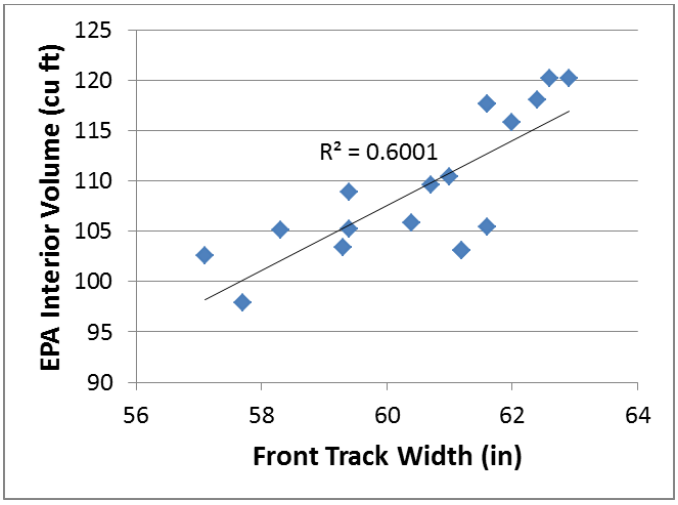

Figure 14: EPA Interior Volume (cargo + passenger volume) vs. FTW for subcompact, compact, and mid-size sedans

Vehicle model parameters

Table 12: Vehicle model parameters used in Autonomie

	ICV	HEV	PHEV
C_D	0.3		
Front area	2.58 m2		
Rolling resistance coefficients	F1 = 0.008 F2 = 0.00012		
Transmission	5 speed automatic	CVT	
Final drive ratio	3.5	4.113	
SOC range	NA	40%-80% [35]	20%-100% [26], [27], [43]
SOC target	NA	56% [35]	25% [27]

Subsystem mass influence coefficients

Table 13: Subsystem mass influence coefficients to determine secondary mass reductions (found with regression analysis of teardown data) [13]

Subsystem	Subsystem mass influence coefficient
Body non-structure	0
Body Structure	0.127
Front Suspension	0.027
Rear Suspension	0.028
Braking	0.024
Fuel and Exhaust	0.061
Steering	0.009
Tires and Wheels	0.050
Bumpers	0.035
Electrical	0
Cooling	0
Powertrain	(Not included for this work)
Closures	0

Chapter 3: Vehicle lightweighting vs. electrification: Part 2 – Life cycle energy and GHG emissions results for diverse powertrain vehicles

3.1 Introduction

Lightweight materials and vehicle electrification are gaining popularity in the US light-duty vehicle fleet and have the potential to reduce life cycle energy and greenhouse gas (GHG) emissions from the transportation sector [1], [2]. However, some lightweight materials, such as aluminum and carbon fiber, require more energy to produce than conventional materials and vehicle electrification requires electricity from the grid, which varies based on energy source [3], [4], [5], [6], [7], [8], [9], [10]. Life cycle assessment (LCA) is a useful tool to determine the impact of these technologies since it not only evaluates the vehicle use phase, but also the processes required for producing vehicle materials and fuels and the end-of-life vehicle management [11].

Since automotive trends indicate that aluminum and advanced / high strength steels (A/HSS) are steadily increasing as part of the vehicle fleet composition, the impact of these lightweight materials on life cycle energy and GHG emissions should be assessed [12]. Previous work has determined that the energy and GHG emissions of primary aluminum are significantly higher than steel, primarily due to the energy intensive process of reducing alumina to aluminum [3], [5]. However, by recycling aluminum, this process is eliminated and the energy required in production is much more similar to steel [5]. The GHG emissions intensity of aluminum has a large variability according to the fuel mix of the electricity grid and the electricity allocation protocol [5], [13]. On the other hand, the production of A/HSS is less dependent on electricity and requires little to no additional energy as compared to conventional steel. This is because steel is strengthened mainly by alloying elements or thermally treating the metal, which are reported by the steel industry to be less than 5% of the overall production impacts [14], [15].

Much of the previous work relating to mass reduction potentials of aluminum and A/HSS have focused on possible reductions in the body-in-white (BIW), as the body is generally the heaviest part of the vehicle [16]. In particular, recent studies sponsored by the National Highway Traffic Safety Administration (NHTSA), The Aluminum Association and WorldAutoSteel have contracted EDAG, an independent engineering firm, to assess the potential mass reductions possible with aluminum and/or AHSS according to specified constraints [17], [18], [19]. For instance, NHTSA evaluated the maximum mass reductions possible for the Honda Accord with the requirements that the design should not increase cost more than 10% and should be commercially feasible for high volume production by 2020 [17]. Using computer aided engineering (CAE) optimization, they found that the baseline BIW mass, which is already 48% HSS, could be reduced by 22% with AHSS and 35% with an aluminum-intensive design [17]. On the other hand, The Aluminum Association found that the BIW mass of the Toyota Venza could be reduced by 42% from the baseline BIW, comprised of HSS and AHSS [18]. However, this was only a structural feasibility study and manufacturing techniques were not taken into consideration [18]. Also, WorldAutoSteel used topology optimization in their FutureSteelVehicle design and found that the mass of a baseline HSS and AHSS BIW could be reduced by 35% if higher strength steels were used [19]. However, the AHSS steels used in this assessment are not expected to be commercially available until 2015-2020 [19]. While the studies sponsored by the aluminum and steel industries likely reflect their respective business interests, they provide insight regarding the projected capabilities of the materials based on optimistic assumptions [18], [19].

The fuel economy improvements that result from vehicle mass reductions have been shown to be a function of the powertrain architecture [20], [21], [22], [23]. For instance, a study by An et al. found that the benefit of mass reduction is less for a hybrid electric vehicle (HEV) as compared to an internal combustion vehicle (ICV) [20]. This is due to the fact that HEVs are able to capture kinetic energy through regenerative braking and eliminate engine idling, a significant source of efficiency losses for ICVs [20]. Recent work by Carlson et al. has validated these modeling results through on-road vehicle testing of an ICV, HEV and battery electric vehicle (BEV) [21]. Their results indicate that for the same change in mass, the absolute change in energy consumption is

greatest for the ICV and least for the BEV [21]. Previous work has also shown that powertrain re-sizing has a significant impact on the amount of fuel economy improvements, particularly for ICVs [22], [23]. While powertrain efficiency for HEVs is largely a function of regenerative braking and controls strategy, the efficiency of ICVs relies on the engine efficiency and therefore, the operating regime [22], [23]. Since smaller engines increase efficiency, powertrain downsizing is required for ICVs to achieve significant fuel economy improvements from vehicle mass reduction [22], [23].

Previous vehicle LCAs have demonstrated the tradeoffs between increased emissions during the material production phase and decreased emissions during vehicle use for aluminum and HSS lightweight vehicles [3], [4], [5]. For instance, Kim et al. compared aluminum and HSS in a life cycle model, assuming various levels of vehicle mass reduction using each material (11-23% with aluminum and 6-11% with HSS) [3]. For the range of mass reduction scenarios considered, the GHG emissions payback period is 4-10 years for aluminum and 1-4 years with HSS. However, if secondary aluminum is used in a low carbon grid region, the payback period is reduced to 1-2 years. Results by Das show similar results, as the higher production energy and emissions of primary aluminum outweighs the lower energy consumption during vehicle use [4]. Ultimately, the life cycle benefits of using aluminum as a lightweight vehicle material are highly dependent on the amount of aluminum that is recycled, while the impact of HSS relies primarily on the amount of mass it is able to reduce from the vehicle [3], [4].

In addition to evaluating the impact of mass reduction, previous LCAs have compared the impact of conventional versus electrified vehicles and found that results are highly dependent on assumptions regarding the source of electricity and vehicle lifetime [6], [7], [8], [9]. For example, a study by Argonne National Laboratory (ANL) assessed life cycle GHG emissions of an ICV and various types of plug-in hybrid electric vehicles (PHEVs) for different grid regions. They found that the emissions for the PHEV ranged from 90% lower than the baseline ICV in the lowest fossil fuel region to 10% higher in the region dominated by coal [6]. Similarly, Bandivadekar et al. found that life cycle GHG emissions of a BEV would increase by 72% if coal was used instead of natural gas to produce electricity [7]. MacPherson et al. also demonstrated the sensitivity of GHG emissions for plug-in electric vehicles by evaluating the impact of electric grid region.

They found that life cycle GHG emissions could change by more than 100 gCO_2/mi-eq for a PHEV and 150 gCO_2/mi-eq for a BEV depending on the GHG intensity of the grid [24]. In addition to evaluating the impact of fuel source on life cycle impacts, recent work by Hawkins et al. has demonstrated the importance of vehicle lifetime assumptions when comparing a conventional and electrified vehicle [8]. Since vehicle production GHG emissions are higher for a BEV as compared to an ICV (due to increased electric components), reducing the lifetime vehicle miles traveled (VMT) decreases the GHG reduction benefit of a BEV [8].

While previous LCAs provide valuable insight to the life cycle impacts of lightweight materials and electrification, the vehicle models used have assumed either a constant glider for all powertrains or a fixed increase in structural mass per increase in powertrain weight [6], [7], [8]. Since previous work has not developed equivalent vehicle models for diverse powertrains, comparisons between the vehicles may have a bias towards one powertrain technology over another. The objective of this work is to assess the potential of aluminum and A/HSS to reduce life cycle energy and GHG emissions from conventional and electrified vehicles with the vehicle design harmonization techniques described in Part 1. Accordingly, the life cycle impacts of a baseline ICV, HEV, and PHEV with a 10-mile all-electric range (AER), PHEV-10, are evaluated in a LCA and evaluated against lightweight versions of these vehicles. Baseline vehicles are designed according to Part 1 (using the 1 correlation method) and lightweight vehicles are modeled assuming that the baseline BIW can be re-designed using aluminum or A/HSS. Also, it is assumed that secondary mass reductions, including powertrain downsizing, are implemented to the vehicle design in an early stage and can provide further mass reductions. The impact of mass reduction on fuel economy is determined individually for each vehicle, thereby capturing the differences due to powertrain architecture. Lastly, vehicle-cycle energy and GHG emissions are determined and scenario analyses are used to determine the impact of a range of material production and electricity energy and GHG intensities, including a closed-loop recycling scenario. To assess the impact of using the design harmonization method as compared to previous approaches, life cycle results are also obtained using the constant glider and structural mass multiplier methods and evaluated against the current method.

3.2 Method

Consistent with Part 1, the life cycle evaluation of vehicles with diverse powertrains is conducted according to the design harmonization algorithm shown in Figure 15. Similar to the work in Part 1, the current work evaluates vehicle mass, powertrain component sizes and the material composition of a baseline and lightweight ICV, HEV and PHEV-10 (hereafter referred to simply as "PHEV"). In addition, drive cycle fuel economy results are obtained using Autonomie, a forward facing (drive-to-wheels) vehicle simulation software developed by ANL [25]. Life cycle energy and GHG emissions are determined with fuel economy results, material composition of the vehicle and the energy and GHG emissions intensity of materials and fuels. The energy and GHG emissions intensity of materials are determined for mild steel, A/HSS and aluminum based on previous literature, while the production data for all other materials are adopted from GREET 2, a vehicle life cycle modeling tool [26]. Fuel cycle impacts are obtained for liquid fuels with GREET 1, a life cycle modeling tool for fuels, and for electricity with eGRID, the environmental database on the electric power sector provided by the U.S. Environmental Protection Agency (EPA) [27], [28].

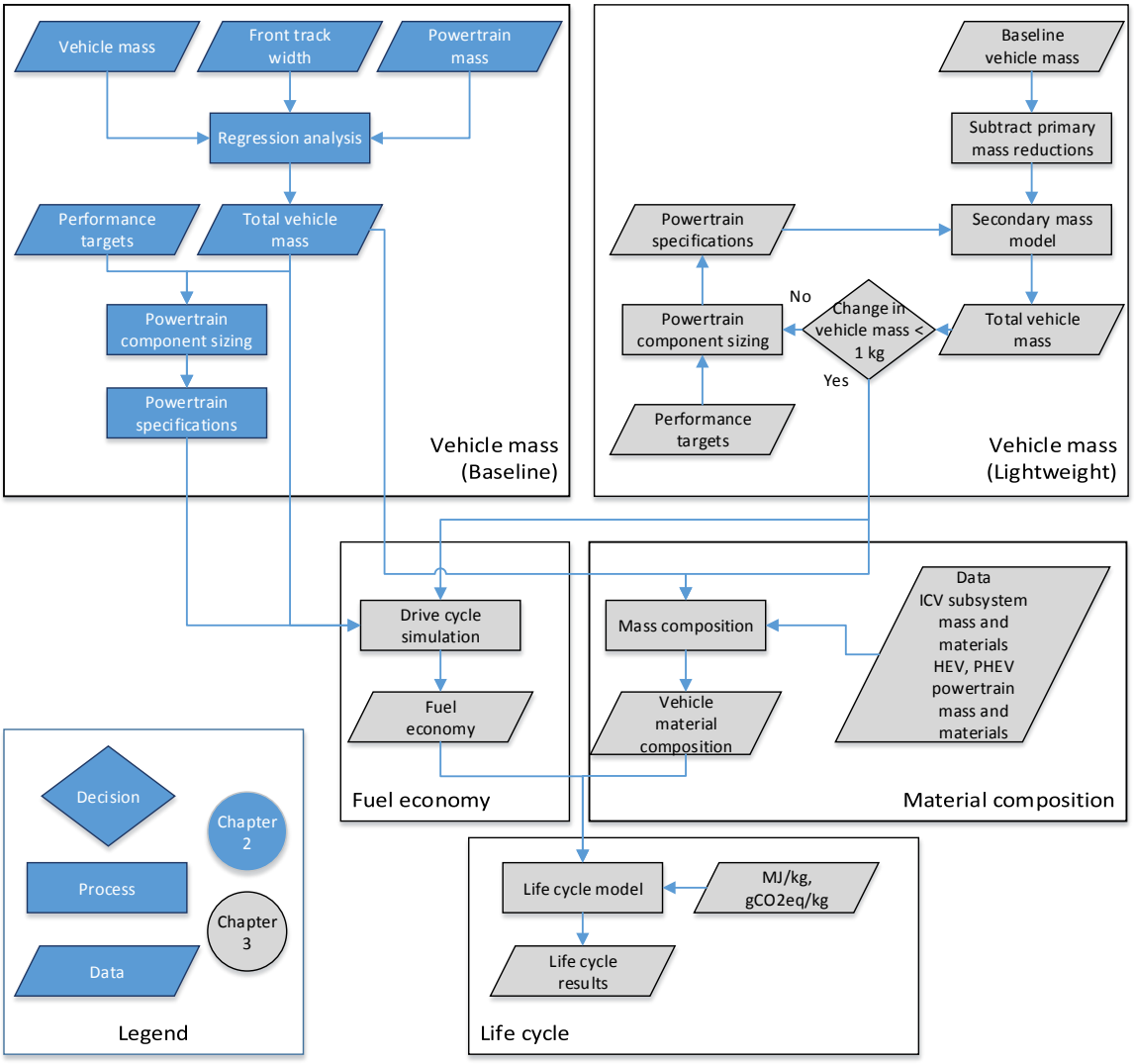

Figure 15: Design harmonization algorithm

3.2.1 Baseline vehicle models

The methods described in Part 1 are used to develop baseline vehicle models for this work. Accordingly, vehicle mass is determined with regression analysis of vehicle teardown data using front track width (FTW) and powertrain mass as predictor variables for vehicle mass. Then, component sizes are determined based on performance criteria, such as acceleration time, gradeability and AER. Lastly, the material composition of the vehicle is found based on vehicle teardown data of a representative ICV and powertrain-specific components for a HEV and PHEV. (Refer to Part 1 for more detailed descriptions on the method and results for baseline vehicle models.)

3.2.2 Lightweight vehicle models

Similar to the baseline vehicle models, lightweight vehicles are designed using the process described in Part 1. However, while the work in Part 1 evaluated a material substitution scenario to demonstrate the lightweight vehicle design method, this work assesses increased mass reduction scenarios with both aluminum and A/HSS to show the potential of each to reduce life cycle energy and GHG emissions. Since current vehicle design trends indicate that A/HSS is increasing as part of the BIW composition, it is assumed that the BIW of the baseline vehicle is comprised of a combination of mild and high strength steels [12]. Accordingly, the following maximum BIW reduction values for AHSS and aluminum are adopted from NHTSA: 22% with A/HSS, 35% with an aluminum space frame. Thus, this work evaluates the two materials in an apples-to-apples comparison for a baseline vehicle that already has a significant amount of A/HSS in the design. Consistent with results from NHTSA, the following BIW mass reduction scenarios are considered: 15% and 20% with A/HSS and 15%, 20%, 25% and 35% with the aluminum-intensive design. As described by NHTSA, the aluminum space frame design is comprised of 92% aluminum (22% extrusions, 35% sheet, 35% castings) and 8% steel. While the reduction scenarios considered in this work represent a range of possible mass reductions that could occur, the amount of mass reduction is largely dependent on the exact composition of the baseline vehicle body and other design constraints, such as the cost of implementation.

3.2.3 Energy and GHG emissions models

The life cycle energy and GHG emissions for each vehicle are determined with vehicle cycle models that account for processes spanning from raw material extraction to vehicle disposal/recycling, and fuel cycle models that include everything from mining of materials to vehicle fuel consumption. GHG emissions are calculated using 100-year global warming potentials from the IPCC Fourth Assessment Report and include CO_2, CO, VOC, CH_4, N_2O, CF_4, and C_2F_6 [29].

Vehicle-cycle

Vehicle production energy and GHG emissions are determined based on the material composition of each vehicle and the energy and GHG emissions intensity for each material. For most materials, energy and emission intensities are found using GREET 1, which calculates the energy and emissions from raw material recovery and extraction through vehicle disposal and recycling [27]. However, since steel, A/HSS and aluminum are the focus of this work, energy and GHG emissions for these materials are adopted from the most recent publications from the aluminum and steel industries, as shown in Table 14 [30], [31], [32]. Since the energy and GHG emissions intensities of conventional and advanced steels are very similar, it is assumed that no additional energy is required for A/HSS as compared to mild steel [15]. However, due to the energy-intensive process of alumina reduction, the energy required to produce 1 kg of primary aluminum is up to seven times more than steel, based on the values shown in Table 14. The alumina reduction process also is a significant source of GHG emissions because two species with very high global warming potentials (7,390 and 12,200), CF_4 and C_2F_6, are produced in addition to the GHGs that results from combustion (i.e. CO_2, CO, VOC, CH_4 and N_2O).

By recycling steel and aluminum, energy consumption is reduced by 50% for steel and up to 92% for aluminum, as shown in Table 14. Similarly, the GHG emissions intensity of the materials is lowered by 63% and 92%, respectively. As compared to steel, aluminum has a greater potential for energy and GHG emissions reductions through recycling because it eliminates the need for alumina reduction. Thus, the ratio of secondary to primary aluminum in the vehicle composition has a significant impact on the vehicle-cycle energy and GHG emissions results. Unless otherwise noted, this work assumes that the vehicles have 11% secondary aluminum in wrought products and 85% recycled aluminum in cast products [32]. Also, it is assumed that 26% of the steel content in the vehicles is made from recycled materials [26].

Table 14. Energy and GHG emissions intensities

		MJ/kg	kgGHG/kg
Primary steel/AHSS		26.10 [31]	2.36 [31]
Secondary steel/AHSS		13.06 [31]	0.88 [31]
Primary wrought aluminum	Extruded	147 [30]	10.74 [30]
	Cold rolled sheet	218 [30]	15.94 [30]
Primary cast aluminum		168 [30]	12.22 [30]
Secondary wrought aluminum	Extruded	11.56 [32]	0.84 [32]
	Cold rolled sheet	28.26 [32]	2.08 [32]
Secondary cast aluminum		19.06 [32]	1.37 [32]

Since the final impact of an aluminum-intensive vehicle is strongly dependent on the electricity sources for primary aluminum production and the percentage of secondary aluminum in the vehicle, two sensitivity analyses are performed to evaluate the sensitivity of the baseline assumptions. As shown in Table 15, a range of GHG emission factors for primary aluminum ingot production is evaluated based on previous work by Colett et al. that assessed the impact of assigning electricity sources to aluminum producers in increasing levels of localization [13]. Collet et al. found that with the most localized method of power plant aggregation, GHG emission intensities could range from 4.28 to 29.99 kgGHG/kg if main fuel source for the region was based on hydroelectric power or coal [13]. Thus, these values for primary aluminum ingot production are considered in the first sensitivity analysis. In a second sensitivity analysis, the impact of increasing the ratio of secondary to primary aluminum in the vehicle is evaluated. Accordingly, it is assumed that closed-loop recycling is feasible and the percentage of secondary aluminum in the vehicle is increased from 11% to 50%.

Table 15. Sensitivity analyses

	Design parameter	Baseline value	Alternative values
Vehicle Cycle	Aluminum ingot GHG intensity	10.33 kgGHg/kg [30]	4.28-29.99 kgGHG/kg [13]
	Wrought aluminum recycled content	11% [32]	50%
Fuel Cycle	PHEV charging location	Average US	Lowest and highest NERC grid region [28]

Fuel-cycle

The energy and GHG emissions associated with liquid fuels and electricity are a combination of two phases: well-to-tank (WTT), which includes all processes upstream of vehicle use, and tank-to-wheel (TTW), consisting of fuel consumption on-board the vehicle. The WTT impacts of gasoline are calculated for the extraction, refining, and distribution processes using GREET 1 [27]. In accordance with GREET 1 model assumptions, 92% of the gasoline is from conventional oil while 8% is from oil sands (4% surface mining, 4% in situ extraction) [27]. To account for the regional variation in the electric grid, energy and emission rates are determined according to the affiliation of power plants with a North American Electric Reliability Corporation (NERC) sub-region [28]. Energy and emissions rates for electricity generation are determined using the eGrid database, as described in MacPherson et al., and upstream fuel-cycle impacts are evaluated with GREET 1 according to fuel type for each NERC sub-region [24], [27], [28]. Baseline results are calculated with eGRID data for the average US grid and the variation in carbon intensities for different NERC sub-region locations is explored in a sensitivity analysis using the lowest and highest carbon dependent regions on the US, as shown in Table 15. Specifically, the NYCC Upstate New York and WECC Rockies regions are identified as having the lowest and the highest annual GHG/kWh emissions, as the NYCC region is largely dependent on hydroelectric and nuclear power while the WECC region is dominated by coal.

The TTW energy and GHG emissions for each vehicle are determined with city and highway drive cycle vehicle simulations in Autonomie.[1] In accordance with EPA guidelines for adjusted fuel economy, the combined CAFE fuel economy is determined with a harmonic average of the city (UDDS) and highway (HWFET) drive cycle with weights of 47% city and 53%, respectively [33]. Also, aggressive driving is simulated by 1.25*CAFE (i.e. velocity profiles for the UDDS and HWFET drive cycles are multiplied by 1.25 and these are used to calculated the combined fuel economy) to capture the impacts of heavy accelerations and increased vehicle speeds beyond the standard city and highway drive cycles [20]. The fuel economy of hybrid and plug-in hybrid vehicles is

[1] Drive cycle simulations use the engine map developed in Chapter 4 for a naturally aspirated spark-ignited gasoline engine.

measured considering charge sustaining (CS) and charge depleting (CD) modes of operation [34]. CS mode is measured for the HEV and PHEV by ensuring that the state of charge (SOC) at the end of the drive cycle test is equal to the initial SOC [34]. CD mode for the PHEV is measured assuming that the battery is fully charged to the allowable SOC at the beginning of the drive cycle test [34]. Consistent with previous work that has addressed SOC ranges and targets, the HEV is assumed to have a SOC window of 40% while the PHEV has a range of 80% [35], [36], [37], [38]. Please refer to the Appendix of Chapter 2 for a complete list of vehicle parameters.

Total vehicle life cycle

The total vehicle life cycle (TVLC) energy and GHG emissions are found on a per mile basis by adding the vehicle and fuel cycle impacts and dividing by the VMT during the lifetime of the vehicle. Since the PHEV may be driven in all-electric mode, the TVLC impacts are determined with the weighted sum of energy and GHG emissions from gasoline and electricity. This is done using a utility factor (UF) that indicates the amount of driving done in CS versus CD mode [39]. The UF of a vehicle is defined based on the vehicle's AER [39]. For instance, a 10-mile range is equivalent to a UF of 0.271 indicating that 27.1% of the drive miles are driven in CD mode while 72.9% are driven in CS mode [39]. Consistent with assumptions in GREET, this work assumes that the lifetime VMT for each vehicle is 160,000 miles [26].

3.3 Results

3.3.1 Lightweight mass and powertrain sizing

The final mass of each lightweight vehicle is determined with the powertrain sizing routine and secondary mass reduction model. After the BIW mass is reduced through material substitution, secondary mass reductions in non-powertrain and powertrain subsystems are determined in an iterative procedure until the vehicle mass is reduced less than 1 kg. This convergence criterion is met after 4 iterations for the ICV and PHEV and 5 iterations for the HEV. Results for the 35% mass reduction scenario are shown in Table 16, while the results for the other levels of mass reduction are included in the Appendix. For all mass reduction scenarios and vehicles, secondary mass reductions

contribute 35-41% of total mass reductions, with the most reductions occurring for the HEV and PHEV due to the potential for battery downsizing. Of these reductions, 79% to 88% occur in the first downsizing iteration due to the relative magnitude of the mass reduction that initiates further downsizing. For instance, during the first iteration of downsizing the ICV for the 35% scenario, the BIW mass is reduced by 108 kg, non-powertrain subsystems are reduced by 39 kg and the powertrain is reduced by 11 kg, resulting in a 12% reduction in vehicle mass. All subsequent secondary mass reductions reduce another 7 kg, only 12% of the total secondary mass reductions.

Table 16. Lightweight design process for 35% BIW mass reduction

Vehicle mass with non-powertrain secondary reductions (kg)	Reduction in powertrain mass (kg)	Vehicle mass with non-powertrain secondary reductions (kg)	Reduction in powertrain mass (kg)	Vehicle mass with non-powertrain secondary reductions (kg)	Reduction in powertrain mass (kg)
ICV Baseline Vehicle Mass: 1309 kg		**HEV Baseline Vehicle Mass: 1421 kg**		**PHEV Baseline Vehicle Mass: 1472 kg**	
1163	11	1268	20.4	1315	18.7
1147	1.2	1238	4.0	1288	3.2
1145	0.3	1232	0.8	1284	0.5
1145	NA	1231	0.1	1283	NA
ICV Lightweight Vehicle Mass: 1145 kg		**HEV Lightweight Vehicle Mass: 1231 kg**		**PHEV Lightweight Vehicle Mass: 1283 kg**	

The final engine, motor and battery specifications for each BIW reduction scenario and vehicle are shown in Figure 16. Overall, powertrain components are downsized by 5-8% for the lightest A/HSS vehicle and by 10-14% for the lightest aluminum-intensive vehicle. Due to the fact that the hybrid vehicles achieve the performance targets using a combination of energy and motor power, the HEV and PHEV engine size is about 42% lower than the ICV engine for a similar vehicle mass. Also, the PHEV battery must have a 13% higher energy capacity than that of the HEV battery to meet the 10-mile AER requirement.

Due to the fact that the acceleration requirement requires a higher torque at the wheels than the gradeability requirement, all vehicles meet the 9 second acceleration time exactly and exceed the gradeability target. Accordingly, the size of powertrain components increase linearly with vehicle mass, as the power to weight ratio of the

vehicles must be constant for each type of vehicle to maintain the same acceleration time. However, the change in component size per change in vehicle mass (i.e. the slope of the line in Figure 16) is not always equivalent for each vehicle, as this is dependent on the powertrain design and component sizing process. For instance, as compared to the HEV and PHEV engines, the ICV engine decreases more per unit decrease in vehicle mass. This is due to the fact that the ICV relies entirely on the engine for propulsion power, unlike the hybrid vehicles that utilize the motor for the majority of initial acceleration power. Also, as compared to the PHEV battery, the HEV battery is downsized more per change in vehicle mass due to the requirement that it provide the motor with peak power (instead of the 10-mile all-electric range). Thus, a greater reduction in battery mass occurs for every kg of primary mass reductions. Since the battery mass is a significant portion of the total powertrain mass, the HEV has a slightly higher potential for secondary mass reductions as compared to the PHEV.

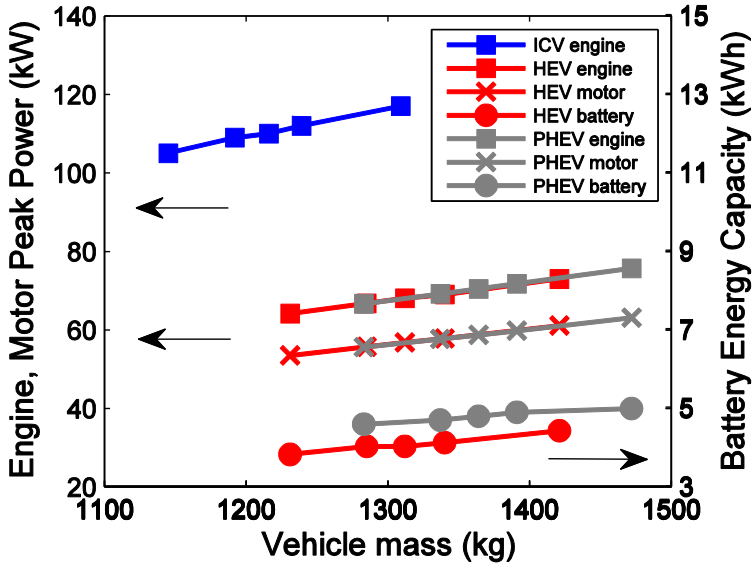

Figure 16. Powertrain downsizing potential for each vehicle

The final lightweight vehicle mass for each vehicle is shown in Figure 17. For reference, the potential vehicle mass with only BIW mass reductions (i.e. no secondary mass reductions) is also included. As the fraction of BIW mass reduction increases, secondary mass reductions become more significant due to the nature of the mass compounding effects. With both primary and secondary mass reductions included in the vehicle design for the lightest aluminum-intensive vehicle, mass is reduced by 164 kg for

the ICV (a 14% reduction), 190 for the HEV (a 15.4% reduction) and 189 for the PHEV (a 14.7% reduction). The maximum reduction for the A/HSS material substitution scenario decreases vehicle mass by 93-109 kg (a 7.7-8.3% reduction).

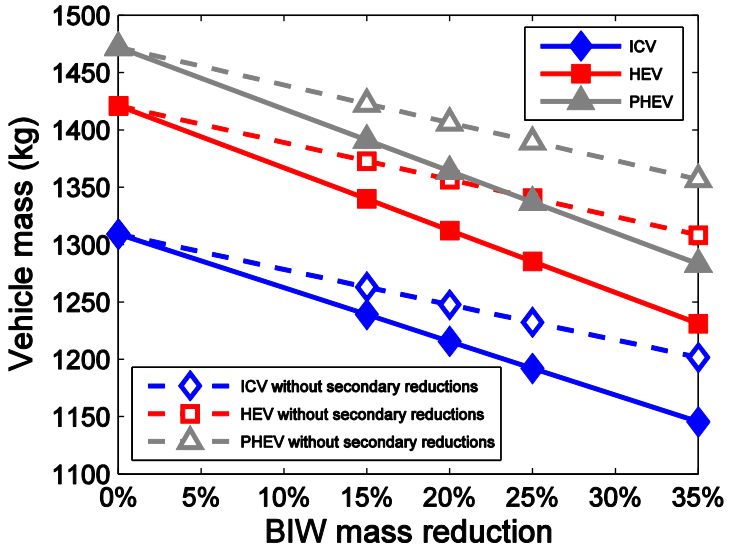

Figure 17: Lightweight vehicle mass results with and without secondary mass reductions

3.3.2 Lightweight vehicle material composition

The material composition for each lightweight vehicle is determined based on the mass of the lightweight subsystems and material mass fractions of the baseline vehicle models. The material composition of the lightest aluminum-intensive and A/HSS vehicles are shown in Figure 18. The maximum steel reductions (340 kg) occur for the aluminum-intensive PHEV with 35% BIW mass reductions. Of these, 8% are the result of secondary mass reductions, which also reduce aluminum, copper, rubber, plastic, and stainless steel by 4-8%. Trends for the ICV and HEV are similar, as 7-8% of the steel reductions are due to secondary mass reductions. Since secondary mass reductions have less of an impact for the A/HSS vehicle due to the lower amount of primary mass removed, the mass of non-steel materials is only reduced by 5% at most. As compared to the baseline vehicles, 90 kg of steel is removed at most for the PHEV, with 27% of these reductions due to subsystem downsizing.

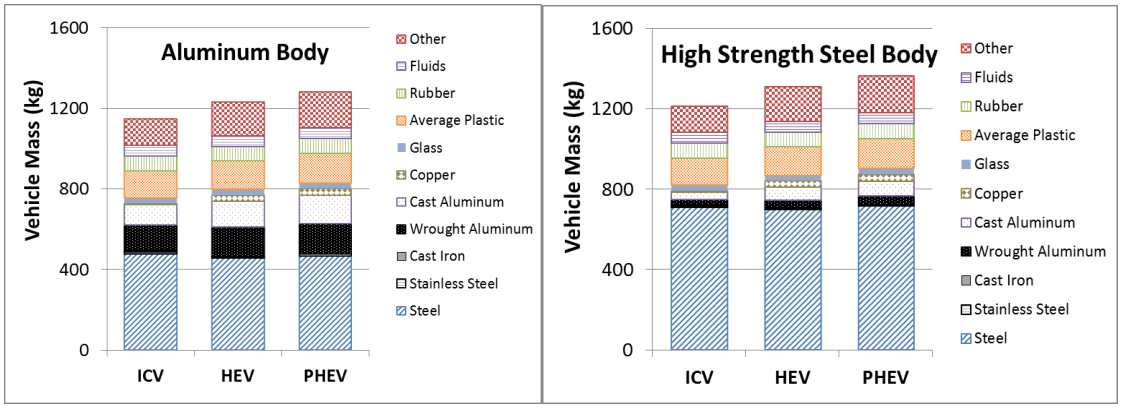

Figure 18: Material composition of the lightest aluminum-intensive (35% BIW mass reductions) and A/HSS vehicle (20% BIW mass reductions)

3.3.3 Fuel economy

As shown in Figure 19, the fuel economy for each vehicle is determined using Autonomie (see Figure 27 in the Appendix for aggressive drive cycle results). Due to increased vehicle efficiency for hybrid vehicles, fuel economy in charge sustaining mode is 49-50% higher for the HEV and PHEV as compared to the ICV. The MPGe for the PHEV is higher than the HEV due to the high efficiency during charge depleting mode (221 Wh/mi to 205 Wh/mi for the baseline and lightweight PHEVs) and the method of calculating MPGe based on the EPA's conversion of 33.6 kWh to 1 gallon of gasoline. Consequently, fuel economy is increased by 56% for the PHEV as compared to the HEV.

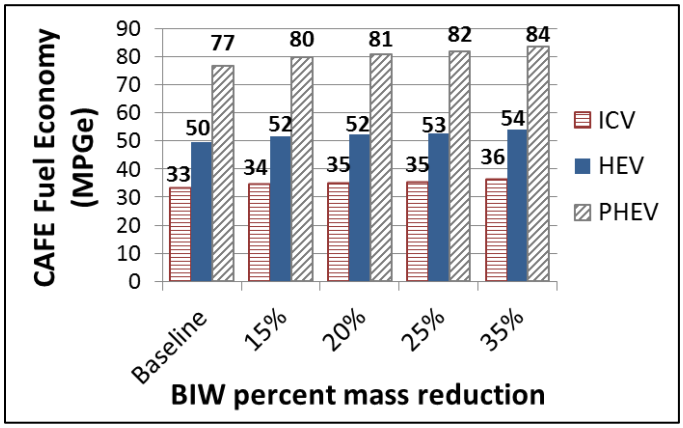

Figure 19: Fuel economy results for baseline and lightweight ICVs, HEVs and PHEVs[2]

The impact of mass reduction on fuel economy is determined for each vehicle, as shown for the UDDS cycle in Figure 20(a) with the mass elasticity of fuel economy and

[2] Calculated with gasoline density of 745 kg/m^3 [27]

in Figure 20(b) with the absolute change in fuel consumption per change in mass. Also, mass elasticity results for the CAFE cycle are included in Table 21 in the Appendix. Similar to results found in previous literature, the PHEV and HEV have the lowest mass elasticity of fuel consumption due to their regenerative braking capabilities and increased powertrain efficiency. While the HWFET drive cycle results follow the same trends, results from the UDDS cycle most clearly demonstrate the difference between different powertrains due to the increased regenerative braking that occurs during city driving. For instance, when the mass of the HEV decreases by 10%, the total braking energy at the wheels during the UDDS drive cycle also decreases by 10% and the recovered energy at the battery decreases by 8%. Thus, as mass is reduced from the vehicle, some of the fuel economy gains from the lower vehicle inertia are offset by the loss of regenerative braking energy. As compared to the HEV, the PHEV has a lower sensitivity to vehicle mass due to the increased efficiency during all-electric operation.

Mass elasticity of fuel consumption results determined in this work agree well with previous simulation results, as CAFE fuel consumption is decreased by 6.8% for a 10% decrease in vehicle mass for the ICV [20], [22], [23]. Similarly, the HEV and PHEV fuel consumption is reduced by 6.2% and 6.5% for a 10% decrease in vehicle mass. Due to the higher baseline fuel economy of the PHEV, the percent reduction in fuel consumption is higher as compared to the HEV even though the absolute fuel consumption reduction is lower. A complete list of fuel economy and fuel consumption mass elasticity results from this work is included in Table 21 in the Appendix, along with results from previous literature.

The impact of powertrain re-sizing on fuel economy, also shown in Figure 20, is much more significant for the ICV as compared to the HEV. If the mass of an ICV is decreased without powertrain downsizing, the engine operates at a lower torque that has a lower efficiency. By downsizing the engine, the operating regime is shifted to higher torques and efficiency is increased (e.g. by 3.5% for the case shown in Figure 20). However, if the mass of a hybrid vehicle is reduced without modifying the powertrain, the impact on vehicle efficiency is much less pronounced. This is due to the fact that the efficiency of the motor is less sensitive to downsizing than the engine. For instance, a 14% decrease in weight results in a 2% increase in efficiency for the ICV engine but only

a 0.3% efficiency increase for the motor. Since this is the case, the hybrid control strategy has an important role in determining the final impact on vehicle efficiency, as the engine will be utilized for a shorter duration of the drive cycle and operated at higher, more efficient torque levels.

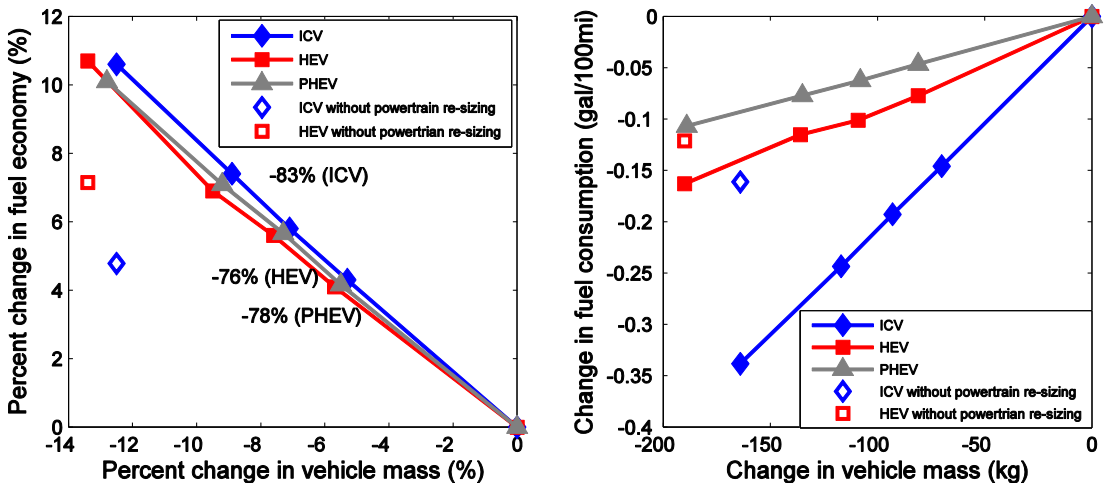

Figure 20: UDDS drive cycle results for all baseline and lightweight vehicles (a) mass elasticity of fuel economy (elasticity results shown for each vehicle), (b) absolute change in fuel consumption per absolute change in vehicle mass

3.3.4 Total life cycle energy and GHG emissions

As shown in Figure 21, the total life cycle results for the baseline ICV, HEV and PHEV demonstrate the benefit of vehicle hybridization as a means to reduce life cycle energy and GHG emissions. Total life cycle results are largely dependent on the vehicle use phase, as 84-91% of the total life cycle results are attributed to the fuel-cycle. Accordingly, vehicle efficiency and upstream fueling sources play a key role in determining the total life cycle performance. For instance, even though the vehicle production energy and emissions are slightly higher for the HEV as compared to the ICV, the fuel consumption of the HEV is 34% lower and total life cycle energy and GHG emissions are reduced by 29%. While a similar trend is noted for the PHEV, the fuel consumption reduction is much more significant due to the method of converting kWh to an equivalent gallon of gasoline (e.g. MPGe fuel consumption is 57% lower for the PHEV as compared to the ICV, but life cycle results are only 35% lower). Since the electricity to gasoline conversion is based on the energy content of the fuel and does not account for the combustion processes required to create electricity, life cycle results yield a more accurate basis on which to compare the PHEV to the non-plug in vehicles than by

simply evaluating MPGe results. When considering the upstream fuel cycle and power plant combustion processes for the average US grid, it is evident that the PHEV reduces energy and GHG emissions by only 8% as compared to the HEV and 35% as compared to the ICV.

As vehicle electrification increases, vehicle-cycle energy and GHG emissions are increased due to changes in the powertrain and powertrain-dependent subsystems (i.e. body structure, front suspension, and fuel and exhaust). The most significant impact is the addition of a Li-ion battery to the powertrain, as this increases vehicle production GHG emissions by 2.5 gGHG/mi (78% of the total increase) for the HEV as compared to the ICV. Of the remaining increase (0.7 gGHG/mi), 40% is due to other changes in the powertrain and 60% is due to increased structural support. Thus, the design harmonization techniques employed in this work result in a 1% increase in vehicle production energy and GHG emissions for the HEV and PHEV.

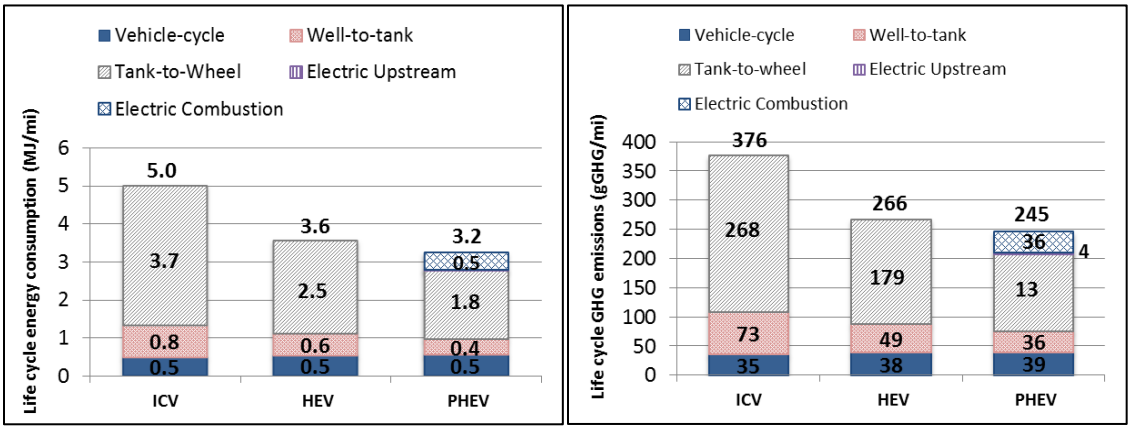

Figure 21: Baseline vehicle life cycle energy and GHG emissions

Vehicle cycle, fuel cycle and total life cycle results are shown in Figure 22-Figure 24, respectively, for all of the baseline and lightweight vehicles. Since energy and GHG emissions follow the same trends, GHG emissions data is shown here and the corresponding energy consumption figures are included in the Appendix. As shown in Figure 22, the aluminum-intensive vehicles produce more GHG emissions (and consume more energy) during the vehicle production phase as compared to the A/HSS and baseline vehicles. Since the energy and emission intensities of mild and A/HSS steel are assumed to be equivalent, the baseline and A/HSS vehicles follow the same linear trend according to powertrain type. However, due to component and material differences

between the hybrid and conventional powertrains, the A/HSS hybrid vehicles are more energy and GHG intensive to produce than the baseline or A/HSS ICVs of an equivalent mass. On the other hand, vehicle production energy and GHG emissions for aluminum-intensive HEVs are higher than for PHEVs with the same vehicle mass, despite the fact that the powertrain is more energy intensive to produce for the PHEV. This trend is due to the fact that for a given vehicle mass, the mass of the body structure is higher for the HEV and therefore the content of aluminum in the vehicle is significantly increased. Since the average energy and emissions intensity of primary aluminum is at least five times that of steel, the differences in the body weight are amplified as compared to the A/HSS vehicles. However, in the context of the total vehicle life cycle, the vehicle-cycle contributes only 20% at most to total GHG emissions. Thus, the differences in vehicle production due to powertrain type are less than 1% of the total vehicle life cycle results.

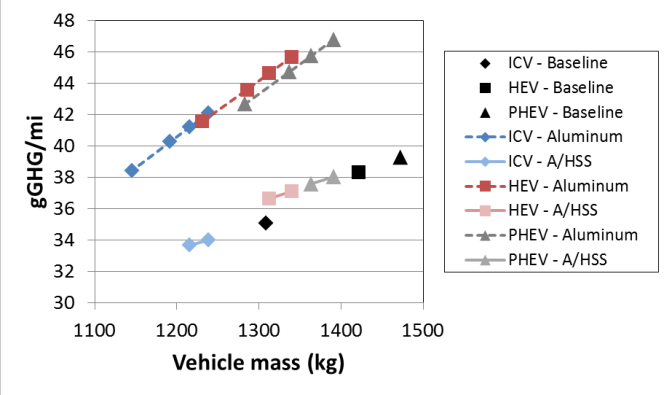

Figure 22: Vehicle-cycle gGHG/mi for each vehicle

Fuel cycle results for the lightweight and baseline vehicles, shown in Figure 23, include combustion and upstream processes for gasoline and electricity, which are combined for the PHEV using the UF for a 10-mile all-electric range. Since the upstream energy and GHG emissions correspond to the tank-to-wheel fueling demand, the fuel cycle results are consistent with the previously reported fuel consumption. That is to say, the ICV has the lowest efficiency while the PHEV has the highest efficiency due to regenerative braking capabilities and all-electric operation. Also, the mass elasticity of fuel consumption is shown for each vehicle, as GHG emissions decrease at an increased rate for the ICV than the HEV or PHEV as vehicle mass is decreased.

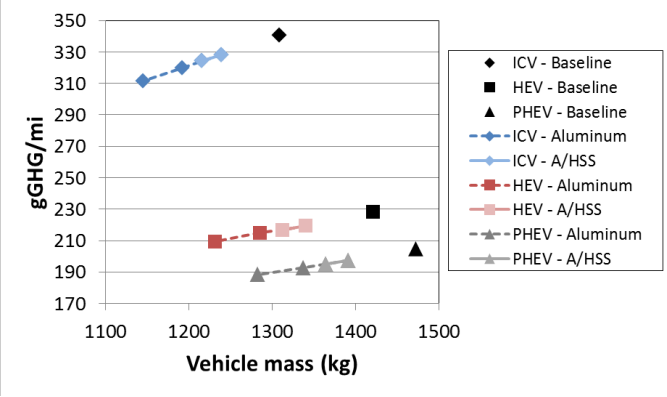

Figure 23: Fuel-cycle gGHG/mi for each vehicle

Combining the vehicle and fuel cycle results, total vehicle life cycle results are shown in Figure 24. Accordingly, A/HSS lightweight vehicles have a lower energy and GHG emissions impact for each powertrain-type vehicle. In fact, results show that the A/HSS ICV with 15% BIW mass reductions achieves 87% of the life cycle GHG reductions possible as the 25% BIW mass reduction scenario with aluminum. Also, the total life cycle results reflect the trends due to the distinct mass elasticity of fuel economy for each vehicle. For instance, a 100 kg reduction in vehicle mass reduces ICV life cycle GHG emissions by 6% but only by 5% for the HEV and PHEV. Thus, results indicate that applying lightweight materials to the ICV results in the greatest impact per unit of mass reduction.

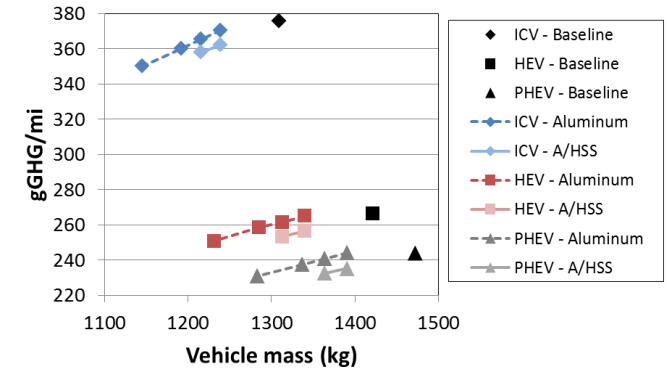

Figure 24: Total life cycle gGHG/mi for each vehicle

Overall, the trend of life cycle results for the conventional lightweight vehicle with aluminum and A/HSS is consistent with previous work, as both materials result in a

reduction of life cycle energy and GHG emissions [3], [4], [40], [41]. For instance, work by Kim et al. found that by reducing ICV mass by 6% using either aluminum or A/HSS, life cycle GHG emissions are reduced by 5-8% [3]. Similarly, this work shows a 5-6% reduction in GHG emissions per 6% ICV mass reduction with both lightweight materials [3]. However, as compared to Kim et al., the input emissions intensity of A/HSS is lower, leading to a greater reduction in life cycle impacts for A/HSS vehicles [3]. Life cycle results are largely dependent on the assumptions regarding aluminum and A/HSS emissions, as Kim et al. found that GHG emissions could change by 100 gGHG/mi when considering high and low emissions factors for both materials [3].

While this work has included detailed powertrain re-sizing and secondary mass savings models, life cycle results are similar to previous work [40]. This is due to the large variability of life cycle results in the literature and the fact that life cycle results are most correlated to fuel consumption reductions, regardless of how these reductions are achieved [4], [40]. As evaluated by Kim et al., LCA results regarding lightweight materials and vehicles have a great variability, depending on the vehicle modeling method, input assumptions on energy and GHG emissions of materials, and a number of other value judgments [40]. Ultimately, since life cycle results are most dependent on fuel consumption reductions, the powertrain re-sizing and secondary mass models in this work provides more confidence in the results but does not show surprising differences from previous work. However, the modeling detail in this work does have a significant impact on the trend of life cycle impacts for hybrid vehicles, as discussed in the "Impact of design harmonization techniques" section of this work.

3.4 Sensitivity Analysis

The life cycle variation of recycling aluminum and electricity allocation protocols is shown for the aluminum-intensive PHEVs in Figure 25. Since the PHEVs contain the highest mass fraction of aluminum for a given BIW mass reduction scenario (e.g. 12-14%), the energy and GHG reductions due to modifying the aluminum production processes represent the best-case scenario for the vehicles considered in this work. By recycling 50% of the wrought aluminum in the closed loop recycling scenario, the average energy and emissions required to produce 1 kg of aluminum is reduced by 40%

for the PHEV. As a result, vehicle production energy and emissions are reduced by 9%-11% and life cycle results decrease by 2%.

The variation of primary aluminum ingot GHG emissions due to electricity allocation protocol is also evaluated for the aluminum-intensive PHEV and shown in Figure 25. Consistent with the baseline scenario, 11% of wrought aluminum and 85% of cast aluminum in the vehicle is secondary aluminum (and the corresponding GHG emissions do not vary with electricity allocation protocol). Depending on if the electricity is allocated to coal or hydroelectric power, vehicle cycle GHG emissions could increase by 44% or decrease by 14%, resulting in a life cycle sensitivity of +14% to -3%. Since the electricity allocation protocol for wrought aluminum has a significant impact on life cycle results for aluminum-intensive vehicles, it is essential to clearly define the level of localization for electricity allocation within the LCA framework.

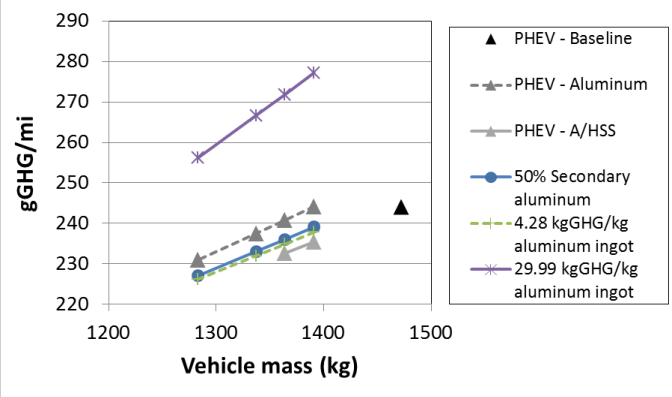

Figure 25: Variation of aluminum due to recycling and production allocation for the aluminum-intensive PHEVs

The range of energy and GHG emissions due to PHEV charging location is evaluated with the NERC regions that have the greatest and least carbon intensity. Accordingly, the WECC Rockies region represents a high carbon grid, as 68% of the grid is dominated by coal, while the NPCC Upstate New York grid region represents a low carbon grid, since it uses a significant amount of hydroelectric and nuclear power. As shown in Figure 26, the life cycle impact ranges from -9% to 7% gGHG/mi depending on if the vehicle is charged in a low or high carbon grid region. As this range of life cycle results is more significant than the previous analysis with sourcing aluminum production, the results emphasize the necessity to consider the charging region (i.e. electricity fuel

sources) when evaluating life cycle performance of a PHEV. Furthermore, since these results are only for a 10-mile range PHEV, a PHEV with a larger range would have a greater variability due to charging location.

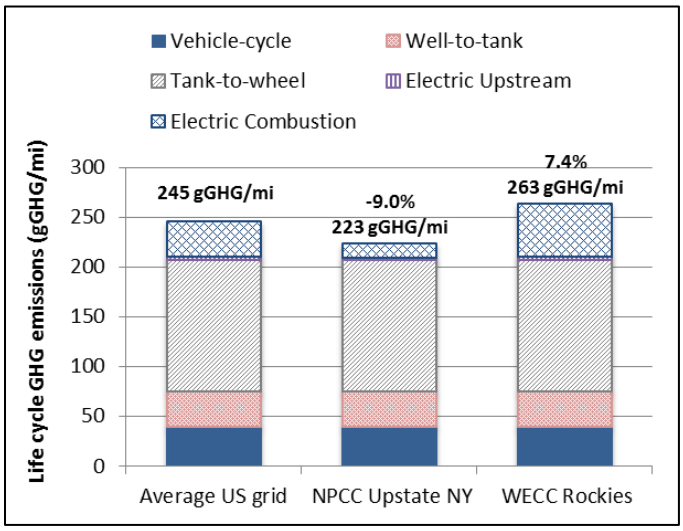

Figure 26: Life cycle sensitivity to charging location for the baseline PHEV

3.5 Impact of design harmonization techniques

The design harmonization techniques developed in this work provide an alternative approach to the constant glider or structural mass multiplier vehicle modeling methods. A comparison of results from using the current harmonized method, constant glider approach and structural mass multiplier method (using the ratio of 0.5:1 structural mass to powertrain mass increase) is shown in Table 17. Since results from the single correlation harmonized design method indicate that only 0.2 kg of structural mass is required per unit increase in powertrain mass, the vehicle mass determined with the current method is less than the structural multiplier method, but greater than the constant glider approach. Accordingly, the proposed harmonized method offers a middle-of-the-road approach to determine life cycle impacts of electrified vehicles. For instance, this approach results in life cycle GHG emissions that are up to 2.0% lower as compared to the structural mass multiplier method, and 1.1% higher as compared to the constant glider approach. Thus, the current method validates previous methods and provides an alternative approach that more accurately captures trends in current vehicle design.

Within the design harmonization framework, single and combined correlation methods are evaluated to determine the impact of including conventional and hybrid

vehicle designs together or separately. As discussed in Part 1, the 1 correlation method shows that more structural support is required as electrification increases, while the 2 correlation method indicates that the relationship between structural mass and powertrain mass is less significant. However, the difference in life cycle results is mainly due to the fact that the 2 correlation method predicts lower vehicle masses for all vehicles, leading to increased fuel economy. Thus, fuel consumption and life cycle GHG emissions are reduced by 1% when the 2 correlation method is used instead of the single fit. Note that results for the 2 correlation method in Table 17 should not be directly compared to the glider and structural mass multiplier results, as these are based on the ICV model determined with the 1 correlation method.

Lightweight vehicle models developed using the design harmonization method include fuel economy simulation for each powertrain-type vehicle, thus incorporating the mass elasticity of fuel economy trends of conventional and electrified vehicles in the LCA. If a constant fuel reduction value (FRV) was used instead, as is often done in lightweight vehicle LCAs, the hybrid vehicle life cycle reductions would have been inflated [40]. For instance, if the FRV that was determined for the ICV was used for the HEV, fuel consumption for each vehicle would be reduced by 0.21 gal/100mi (0.49 L/100km) per 100 kg mass reduction. As a result, HEV fuel economy would increase from 50 to 62 MPG (instead of 50 to 54 MPG) for the baseline and 35% BIW mass reduction scenario, resulting in a life cycle GHG emissions reduction of 16% (instead of 6%). Thus, by including the powertrain-specific FRVs with the design harmonization approach, life cycle impacts for a HEV with 15.4% mass reduction are 12% lower than they would be otherwise. Since there has not been much literature published concerning the life cycle comparison of mass reduction for conventional and electrified vehicles, future work should ensure that powertrain-specific fuel economy trends are included in the LCA, as these have been shown to have a significant impact on life cycle results.

Table 17: Comparison of results using current and previous vehicle modeling methods

	ICV		HEV			PHEV		
	Harmonized method - 1 Corr. (2 Corr.)	**Glider / Structural mass mult.**	**1 Corr. (2 Corr.)**	**Glider**	**Structural mass mult.**	**1 Corr. (2 Corr.)**	**Glider**	**Structural mass mult.**
Vehicle mass (kg)	1309 (1290)	1309	1421 (1411)	1404	1452	1472 (1451)	1448	1518
Body structure (kg)	307 (301)	307	322 (325)	307	355	329 (322)	307	377
Front suspension (kg)	67 (66)	67	70 (71)	67	67	72 (70)	67	67
Fuel and exhaust (kg)	41 (41)	41	39 (37)	41	41	38 (38)	41	41
Fuel economy (MPG)	33.2 (33.6)	33.2	49.6 (49.9)	50.0	48.9	77.1 (77.9)	78.0	75.5
Life cycle GHGs (g/mi)	471 (466)	471	330 (329)	328	335	292 (289)	289	298
% difference in LC results	0% (-1.1%)	0%	0% (-0.5%)	-0.8%	1.4%	0% (-1.0%)	-1.1%	2.0%

3.6 Conclusions

This work evaluated the life cycle energy and GHG emissions of baseline and lightweight ICVs, HEVs and PHEVs with aluminum and A/HSS. Using the design harmonization technique described in Part 1, lightweight aluminum vehicles were designed for 15%, 20%, 25% and 35% BIW mass reduction scenarios and lightweight A/HSS vehicles were designed for 15% and 20% BIW mass reduction scenarios. Results show that with secondary mass reductions, including powertrain downsizing, lightweight vehicles are 16% lighter than baseline vehicles, with 35-41% of these reductions due to secondary mass reductions.

The mass elasticity of fuel economy was assessed for each vehicle by simulating the drive cycle performance of each powertrain-type vehicle with Autonomie. Consistent with results from previous literature, results showed that the fuel economy of the ICV is more sensitive to a change in vehicle mass than the hybrid vehicles. Since the use phase

is the most significant portion of the total vehicle life cycle, the mass elasticity of fuel economy is evident in the life cycle results. Thus, results of this work indicate that it is more beneficial to lightweight an ICV than a hybrid vehicle because for one unit of mass reduction there is a greater decrease in life cycle energy and GHG emissions.

Life cycle results show that it is possible to achieve more life cycle energy and GHG emissions reductions with A/HSS than with aluminum per unit mass reduced for the vehicle. However, due to the greater potential of aluminum to reduce vehicle mass, maximum life cycle reductions are achieved with the aluminum-intensive 35% BIW mass reduction scenario. However, for all powertrain-type vehicles, a similar reduction in energy and GHG emissions is achieved with either the 25% BIW mass reduction scenario with aluminum or 15% BIW mass reduction scenario with A/HSS. Thus, depending on practical constraints such as cost and manufacturing, lightweight vehicle designs using A/HSS or aluminum may achieve equivalent life cycle goals. Overall, results from this work demonstrate the life cycle benefits of applying lightweight materials to electrified vehicles, as the lightest aluminum-intensive PHEV reduces life cycle energy and GHG emissions by 39% as compared to a baseline ICV.

The design harmonization techniques used for the life cycle analysis enable a comparison between different powertrain-type vehicles that accounts for the structural mass required to support heavier, electrified powertrains. As compared to a constant glider or structural mass multiplier approach (assuming 0.5 kg of structural mass is required per kg powertrain mass increase), the current design method offers an alternative approach, as 0.2-0.3 kg of structural support is required per unit increase in powertrain mass. Consequently, vehicle production impacts are increased by up to 1.6% as compared to the constant glider approach and CAFE fuel economy decreases up to 1.2%, resulting in only a 1% change in life cycle results. Conversely, life cycle results are 2% lower as compared to the structural mass multiplier method. Overall, since life cycle results obtained with the harmonized design method are only 1-2% different than results determined with previous methods, it is recommended that the design harmonization method should only be used if vehicle design and electric powertrains are the focus of the work. Otherwise a glider approach may provide a less computationally intensive method to obtain similar results. Also, as more information becomes available regarding hybrid

vehicle design, this framework should be re-applied to determine if electric vehicle design modifications have become more significant and should be included for future vehicle LCAs.

3.7 References

[1] Paramount Research, "WardsAuto / DuPont Survey of Auto Industry Challenges," www.paramountresearch.com, 2011.

[2] S. C. Davis, S. W. Diegel, and R. G. Boundy, *Transportation Energy Data Book, Edition 31*. 2012, pp. 6–7.

[3] H.-J. Kim, C. McMillan, G. A. Keoleian, and S. J. Skerlos, "Greenhouse Gas Emissions Payback for Lightweighted Vehicles Using Aluminum and High-Strength Steel," *Journal of Industrial Ecology*, vol. 14, no. 6, pp. 929–946, 2010.

[4] S. Das, "The life-cycle impacts of aluminum body-in-white automotive material," *Jom*, vol. 52, no. 8, pp. 41–44, 2000.

[5] F. Stodolsky, A. Vyas, R. Cuenca, and L. Gaines, "Life-Cycle Energy Savings Potential from Aluminum-Intensive Vehicles," in *1995 Total Life Cycle Conference & Exposition*, 1995.

[6] A. Elgowainy, J. Han, L. Poch, A. Wang, M. Mahalik, and A. Rousseau, "Well-to-Wheels Analysis of Energy Use and Greenhouse Gas Emissions of Plug-In Hybrid Electric Vehicles," *Argonne National Laboratory*, 2010.

[7] A. Bandivadekar, K. Bodek, L. Cheah, C. Evans, T. Groode, J. Heywood, E. Kasseris, M. Kromer, and M. Weiss, "On the Road in 2035," MIT, 2008.

[8] T. R. Hawkins, B. Singh, G. Majeau-Bettez, and A. H. Strømman, "Comparative Environmental Life Cycle Assessment of Conventional and Electric Vehicles," *Journal of Industrial Ecology*, vol. 17, no. 1, pp. 53–64, 2013.

[9] A. Lewis, J. Kelly, and G. Keoleian, "Evaluating the life cycle greenhouse gas emissions from a lightweight plug-in hybrid electric vehicle in a regional context," *2012 IEEE International Symposium on Sustainable Systems and Technology (ISSST)*, pp. 1–6, May 2012.

[10] S. Das, "Life cycle assessment of carbon fiber-reinforced polymer composites," *The International Journal of Life Cycle Assessment*, vol. 16, no. 3, pp. 268–282, 2011.

[11] ISO, *ISO 14040 Environmental management - Life cycle assessment - Principles and framework*. 1997.

[12] A. I. Taub, P. E. Krajewski, A. A. Luo, and J. N. Owens, "The Evolution of Technology for Materials Processing over the Last 50 Years : The Automotive Example," *JOM*, vol. 59, no. 2, pp. 48–57, 2007.

[13] J. S. Colett, J. C. Kelly, and G. A. Keoleian, “Impacts of regional variation and electricity allocation protocol on aluminum production GHG emissions,” *Draft submitted to Environmental Science & Technology*, 2013.

[14] C. Tamarelli, “AHSS 101: The evolving use of advanced high-strength steels for automotive applications,” 2011.

[15] WorldSteel, “GHG emissions of high strength steels versus conventional steels,” http://old.worldsteel.org/pictures/storyfiles/GHGemissionsandAHSS.pdf, 2010.

[16] N. Lutsey, “Review of technical literature and trends related to automobile mass-reduction technology,” *California Air Resources Board*, 2010.

[17] H. Singh, “Mass Reduction for Light-Duty Vehicles for Model Years 2017-2025,” *Report No. DOT HS 811 666*, Program Reference: DOT, 2012.

[18] EDAG, “Venza aluminum BIW concept study,” 2013.

[19] H. Shaw, J., Singh, “Overview Report - FutureSteelVehicle Phase 2,” World Auto Steel, 2011.

[20] F. An and D. J. Santini, “Mass Impacts on Fuel Economies of Conventional vs . Hybrid Electric Vehicles,” SAE Paper 2004–01–0572.

[21] R. B. Carlson, J. Diez, and J. Gibbs, “The Measured Impact of Vehicle Mass on Road Load Forces and Energy Consumption for a BEV, HEV, and ICE Vehicle,” *SAE Paper No.*, vol. 2013–01–14, 2013.

[22] R. Wohlecker, M. Johannaber, and M. Espig, “Determination of Weight Elasticity of Fuel Economy for ICE , Hybrid and Fuel Cell Vehicles,” SAE Paper 2007–01–0343, 2007.

[23] S. Pagerit, P. Sharer, and A. Rousseau, “Fuel economy sensitivity to Vehicle Mass for Advanced Vehicle Powertrains,” SAE Paper 2006–01–0665, 2006.

[24] N. D. MacPherson, G. a. Keoleian, and J. C. Kelly, “Fuel Economy and Greenhouse Gas Emissions Labeling for Plug-In Hybrid Vehicles from a Life Cycle Perspective,” *Journal of Industrial Ecology*, vol. 16, no. 5, pp. 761–773, 2012.

[25] Argonne National Laboratory, “Autonomie.” UChicago Argonne, LLC, 2009.

[26] Argonne National Laboratory, “GREET 2 rev1.” UChicago Argonne, LLC, 2012.

[27] Argonne National Laboratory, “GREET 1 rev2.” UChicago Argonne, LLC, 2012.

[28] US Environmental Protection Agency, “eGRID2012 year 2009 Summary Tables,” 2012.

[29] P. Forster, V. Ramaswamy, P. Artaxo, T. Berntsen, R. Betts, D. W. Fahey, J. Haywood, J. Lean, D. C. Lowe, G. Myhre, J. Nganga, R. Prinn, G. Raga, M. Schulz, and R. Van Dorland, “Changes in Atmospheric Constituents and in Radiative Forcing. In: Climate Change 2007: The Physical Science Basis. Contribution of Working Group I to the Fourth Assessment Report of the Intergovernmental Panel on Climate Change,” *Cambridge University Press*, pp. 589–662, 2007.

[30] P. Americas, “Final Report Life Cycle Impact Assessment of Aluminum Beverage Cans, for Aluminum Association, Inc.,” 2010.

[31] R. Geyer, “Life Cycle Energy and Greenhouse Gas (GHG) Assessments of Automotive Material Substitution: WorldAutoSteel Energy and GHG Model,” 2012.

[32] I. Roy F. Weston, “Life cycle inventory report for the North American aluminum industry,” 1998.

[33] U. S. E. P. Agency, “Light-Duty Automotive Technology , Carbon Dioxide Emissions , and Fuel Economy Trends : 1975 Through 2012 Appendix A Database Details and Calculation Methods,” 2012.

[34] “Recommended practice for measuring the exhaust emissions and fuel economy of hybrid-electric vehicles, including plug-in hybrid vehicles", SAE Standard SAE_J1711_201006,” 2010.

[35] K. J. Kelly, M. Mihalic, and M. Zolot, “Battery Usage and Thermal Performance of the Toyota Prius and Honda Insight for Various Chassis Dynamometer Test Procedures Preprint,” in *17th Annual Battery Conference on Applications and Advances*, 2002, 2001.

[36] N. Shidore and S. C. Avenue, “PHEV ‘All electric range’ and fuel economy in charge sustaining mode for low SOC operation of the JCS VL41M Li-ion battery using Battery HIL,” *Argonne National Laboratory*.

[37] A. Moawad, A, Sharer, P, Rousseau, “Light-Duty Vehicle Fuel Consumption Displacement Potential up to 2045,” *Argonne National Laboratory*, 2011.

[38] A. Pesaran and T. M. Nrel, “Battery Requirements and Cost-Benefit Analysis for Plug-In Hybrid Vehicles (Presentation),” *National Renewable Energy Laboratory*, 2007.

[39] "Utility factor definitions for plug-in hybrid electric vehicles using travel survey data", SAE Standard J2841, 2010.

[40] H. C. Kim and T. J. Wallington, "Life-Cycle Energy and Greenhouse Gas Emission Bene fits of Lightweighting in Automobile : Review and Harmonization," *Environmental Science & Technology*, vol. 47, no. 12, pp. 6089–6097, 2013.

[41] J. Sullivan, J.L., Hu, "Lifecycle Energy Analysis of Automobiles," SAE Paper 951829, 1995.

[42] L. W. Cheah, "Cars on a Diet : The Material and Energy Impacts of Passenger Vehicle Weight Reduction in the U.S.," MIT, Doctoral Dissertation, 2010.

[43] I. J. Wohlecker, R., Wallentowitz, H., Johannaber, M., Espig, M., Leyers, "Determination of Weight Elasticity of Fuel Economy for Conventional ICE Vehicles, Hybrid Vehicles and Fuel Cell Vehicles," *FKA*, Report 555.

[44] A. Casadei and R. Broda, "Impact of Vehicle Weight Reduction on Fuel Economy for Various Vehicle Architectures," Ricardo Project FB769, 2010.

3.8 Appendix

Table 18. Lightweight design process for 25% BIW mass reduction

Vehicle mass with non-powertrain secondary reductions (kg)	Reduction in powertrain mass (kg)	Vehicle mass with non-powertrain secondary reductions (kg)	Reduction in powertrain mass (kg)	Vehicle mass with non-powertrain secondary reductions (kg)	Reduction in powertrain mass (kg)
ICV Baseline Vehicle Mass: 1309 kg		**HEV Baseline Vehicle Mass: 1421 kg**		**PHEV Baseline Vehicle Mass: 1472 kg**	
1205	7.9	1311	14.6	1360	13.4
1193	0.9	1290	2.8	1341	2.3
1192	0.1	1286	0.5	1337	.5
	NA	1285		1337	NA
ICV Lightweight Vehicle Mass: 1192 kg		**HEV Lightweight Vehicle Mass: 1285 kg**		**PHEV Lightweight Vehicle Mass: 1337 kg**	

Table 19. Lightweight design process for 20% BIW mass reduction

Vehicle mass with non-powertrain secondary reductions (kg)	Reduction in powertrain mass (kg)	Vehicle mass with non-powertrain secondary reductions (kg)	Reduction in powertrain mass (kg)	Vehicle mass with non-powertrain secondary reductions (kg)	Reduction in powertrain mass (kg)
ICV Baseline Vehicle Mass: 1309 kg		**HEV Baseline Vehicle Mass: 1421 kg**		**PHEV Baseline Vehicle Mass: 1472 kg**	
1226	6.3	1333	11.7	1383	10.7
1217	0.7	1316	2.3	1367	1.2
1216	.02	1313	0.4	1364	0.3
	NA	1312		1364	NA
ICV Lightweight Vehicle Mass: 1216 kg		**HEV Lightweight Vehicle Mass: 1312 kg**		**PHEV Lightweight Vehicle Mass: 1364 kg**	

Table 20. Lightweight design process for 15% BIW mass reduction

Vehicle mass with non-powertrain secondary reductions (kg)	Reduction in powertrain mass (kg)	Vehicle mass with non-powertrain secondary reductions (kg)	Reduction in powertrain mass (kg)	Vehicle mass with non-powertrain secondary reductions (kg)	Reduction in powertrain mass (kg)
ICV Baseline Vehicle Mass: 1309 kg		**HEV Baseline Vehicle Mass: 1421 kg**		**PHEV Baseline Vehicle Mass: 1472 kg**	
1247	4.7	1355	8.8	1405	8.1
1240	0.5	1342	1.7	1393	1.4
1239		1340	0.3	1391	0.2
	NA	1340		1391	NA
ICV Lightweight Vehicle Mass: 1239 kg		**HEV Lightweight Vehicle Mass: 1340 kg**		**PHEV Lightweight Vehicle Mass: 1391 kg**	

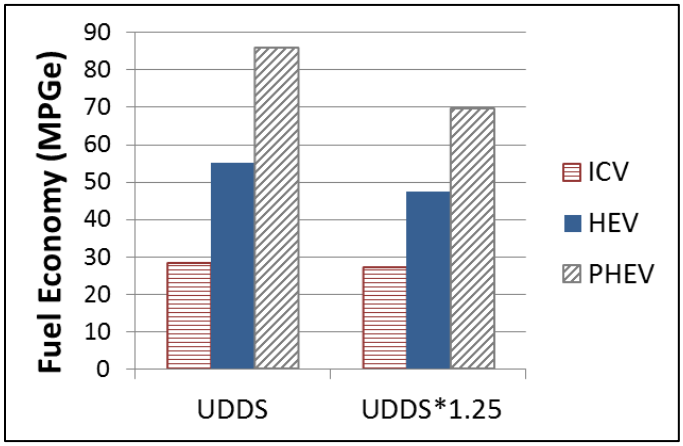

Figure 27: Aggressive drive cycle results for the baseline vehicles

Table 21: Elasticity of fuel consumption and fuel economy for a 10% mass reduction and comparison with previous literature that included powertrain re-sizing for the combined drive cycles (CAFE)

	Results from this work		Previous Literature	
	FC % decrease	**MPGe % increase**	**FC % decrease**	**MPG % increase**
ICV	6.8% (0.21 gal/100mi)	7.3%	6.9% [42], 6.8% (NEDC) / 5.5% (HYZEM) [43]	6.4% [44]*, 8.2% [20], 8.3% [23]**
HEV	6.2% (0.13 gal/100mi)	6.7%	5.7% (NEDC) / 4.9% (HYZEM)† [43]	6.9% [20]‡, 8.2%[23]** †
PHEV	6.5% (0.08 gal-eq/100mi)	7.0%	-	-

*This was based on the FTP-75 which is a variant of the UDDS city drive cycle
**Reported results interpolated for 10% mass reduction
†Parallel hybrid
‡Power-split, FWD

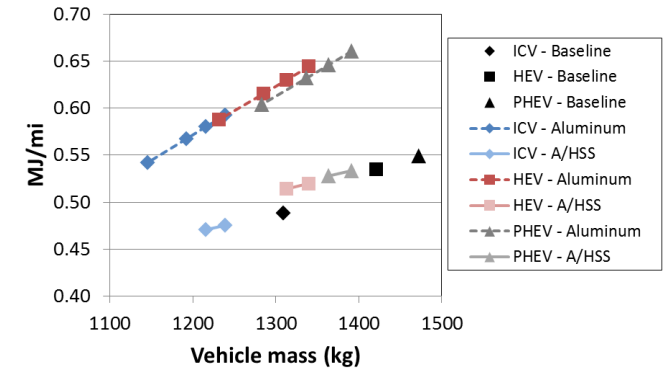

Figure 28: Vehicle-cycle MJ/mi for each vehicle

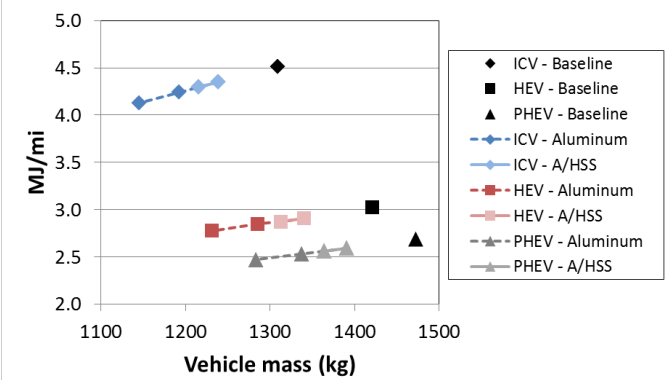

Figure 29: Fuel-cycle MJ/mi for each vehicle

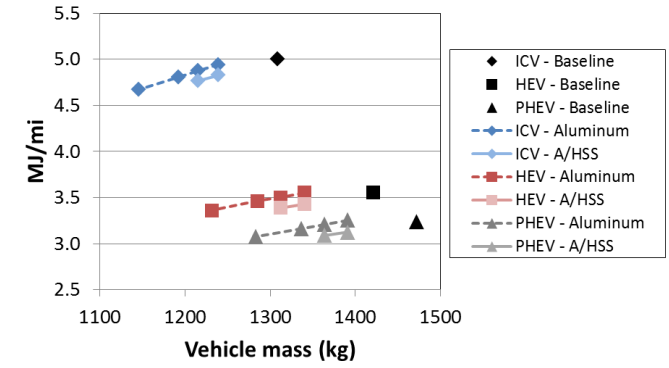

Figure 30: Total vehicle life cycle MJ/mi for each vehicle

Chapter 4: Scaling and dimensional methods to incorporate knock and flammability limits in models of high efficiency gasoline and ethanol engines

4.1 Abstract

Recent work has shown the utility of using simplified models with prescribed burn rates to assess the potential of advanced combustion strategies to increase engine efficiency. However, this approach could be improved by incorporating knock and flammability limits in such models. This work incorporates such limits using a combination of conceptual models that are based on theoretical understanding of knock and flame phenomenon and experimental results that have identified knock and flammability limits for SI engines. Using this method, the ideal and feasible potential of a high efficiency gasoline and E85 engine are compared against a baseline naturally aspirated gasoline engine. Turbocharging, dilution with EGR, and higher compression ratios are used to increase the efficiency potential of the high efficiency gasoline and E85 engines. Results demonstrate the benefit of using this simplified approach to modeling high efficiency engines, as the expected trends occur: the high efficiency gasoline engine is most limited by knock while the E85 engine permits spark timings closer to maximum brake torque (MBT); and increased EGR can be used for the E85 engine due to the higher flame speeds of ethanol. Fuel economy maps are created for each engine/fuel strategy and evaluated in a vehicle model to obtain fuel economy results. Results show that peak brake thermal efficiency (BTE) is increased by 13.7% for the high efficiency gasoline engine and 17.7% for the E85 engine, as compared to the baseline gasoline engine.

4.2 Introduction

Downsizing and turbocharging is one of the most effective technologies for gasoline engines to maintain performance while increasing efficiency [1]. By lowering the engine displacement, the engine operates in a higher load regime where it is more efficient [1], [2], [3], [4]. At these high load, boosted conditions, thermal efficiency increases due to reductions in pumping and friction losses. As load increases, absolute friction increases but the relative impact of friction decreases [5]. In addition, downsized engines reduce absolute friction for all speeds and loads due to the lower surface area traversed by the piston [5].

The main challenge to downsized and turbocharged gasoline engines is reducing knock while maintaining optimal performance. One solution could be to reduce the compression ratio, thus lowering the peak cylinder pressure and temperature. However, this is not desirable because a lower compression ratio decreases thermal efficiency. Other strategies include enriching the fuel-air mixture with excess fuel, thus lowering combustion temperatures, or retarding spark timing away from maximum brake torque (MBT) timing until knock does not occur. These methods are clearly undesirable from an efficiency standpoint. Another option is to use cooled exhaust gas recirculation (EGR) to dilute the mixture. EGR has the combined benefit of lowering peak temperatures and consequently increasing the ratio of specific heats, γ, for unburned and burned mixtures. A higher γ increases thermal efficiency by enabling more work to be done on the mixture during compression. This leads to an increased change in pressure during combustion and corresponding work output. The increase in efficiency due to EGR is augmented at low loads because EGR reduces pumping work by displacing intake air. At high loads, EGR may replace enrichment as a means to reduce exhaust gas temperatures because EGR enables spark timings near MBT timing and increases the specific heat capacity of the burned gases. The main disadvantage of adding EGR to a fuel-air mixture is the resulting slower burn rates, which increases the chance of misfire or partial burning [6], [7], [8]. Technologies to extend the lean limit include charge stratification and advanced ignition systems [9]. While charge stratification can be used to stabilize combustion by ensuring sufficient fuel exists around the spark, under typical overall lean operation a 3-way catalyst cannot be used to treat emissions (particularly NOx). However, a variety of

advanced ignition systems demonstrate the potential to control combustion in highly dilute homogeneous mixtures [9], [10]. For example, researchers at Southwest Research Institute (SwRI) have developed a new ignition system that emits a continuous current which is maintained at a high energy level throughout the entire discharge [9]. This is thought to increase flame kernel growth and burn rates, providing increased combustion stability [9]. Results from using this system with their high-efficiency dilute gasoline engine (HEDGE) concept show that 0-50% MFB duration decreases and combustion stability is improved for 0-25% external EGR compared to the stock ignition system [9].

An alternative method to reduce knock while maintaining efficiency is to replace or blend gasoline with a higher octane fuel, such as ethanol. Previous work has shown that ethanol-gasoline blends can be used at MBT timing without knock even when the compression ratio and peak BMEP is increased from the gasoline baseline [11], [12]. For instance, Caton et al. found that E85 may be used with a 16.5 compression ratio with only modest spark retard [13]. This is possible due to ethanol's higher octane number (ON) and higher heat of vaporization, which increases charge density and volumetric efficiency through cooling [14], [15]. This also results in lower heat losses for the same intake pressure and temperature conditions [16]. The main limitation to using ethanol in a gasoline engine is that at high loads, peak cylinder pressures can easily exceed 100 bar, typically considered the limit for most SI engines [17], [18].

Since there are many ways to increase engine efficiency, thermodynamic models have proven a useful tool to assess the thermodynamic potential of advanced lean or dilute combustion strategies [5], [19]. For example, Lavoie et al. used conceptual models to assess the benefits of HCCI, SI, and advanced combustion for conventional and downsized / turbocharged engines [5]. Since the objective was to show the thermodynamic potential of each technology, engine operating constraints (e.g. knock, flame limits) were not considered. Their results show that reductions in friction losses play an important role in increasing efficiency for downsized engines and that additive gains in efficiency are possible by using advanced combustion strategies with these engines. For example, when evaluated over the combined city and highway drive cycles, a naturally aspirated (NA) advanced combustion and downsized/turbocharged SI engine increase fuel economy 23% and 36%, respectively, while a turbocharged advanced

combustion engine results in a 58% improvement from the baseline NA engine [5]. These improvements are an upper limit on the potential of each strategy.

The objective of this work is to incorporate knock and flame limits in a thermodynamic engine model to assess the realistic, or feasible potential versus the ideal potential of highly efficient engine technologies. In particular, ideal and feasible versions of high efficiency gasoline and ethanol engines are compared against a baseline SI engine. The approach is to use an engine cycle simulation with 1-D gas dynamics to create fuel consumption maps and evaluate each engine design [20]. First, the maximum thermodynamic potential is assessed using MBT timing and optimistic EGR assumptions. Then, a method is developed to determine knock and flammability limits for each high efficiency engine. Lastly, these limits are incorporated into the drive cycle models and new fuel consumption and efficiency results are obtained.

4.3 Model

A single cylinder engine model was built in GT-Power, a commercial software platform for engine simulation, to represent a light duty gasoline direct-injection (GDI) engine. As shown in Table 22, the single cylinder model has a displacement of 0.5L and variable, fixed cam intake valve timing. To minimize pumping losses the intake timing was advanced for low speeds and retarded for high speeds.

Table 22. Single cylinder engine model specifications

Volume (L)	0.5
Bore (mm)/Stroke (mm)	87.4 / 83
Intake Valves (2) **Lift (mm)/Diameter (mm)**	10.2 / 34.5
IVO (deg ATDC gas exchange)	-44 to 25
IVC (deg ATDC gas exchange)	218 to 287
Exhaust Valves (2) **Lift (mm)/Diameter (mm)**	10.2 / 31
EVO (deg ATDC firing)	131
EVC (deg ATDC firing)	384

A turbocharger model, described in Lavoie et al., is used to apply a backpressure on the system for a given intake pressure and overall turbocharger efficiency, η_{OTC} [5]. The model is based on an energy balance equation that determines that amount of turbine work needed to operate the compressor while accounting for efficiency losses [5]. η_{OTC} is

a product of the turbine, compressor, and mechanical link efficiencies and is assumed to be 40% for this work. If η_{OTC} or exhaust temperature decrease, the backpressure and associated pumping work increase accordingly [5]. Also, it is assumed that a heat exchanger located between the compressor and engine maintains the intake temperature at a constant temperature.

Heat transfer is determined with the standard Woschni correlation [6]. Friction is modeled with the Chen-Flynn expression, where friction is a function of cylinder pressure and mean piston speed [21]. Heat release is modeled with the Wiebe function [6]. Inputs to the Wiebe function are 10-90% burn duration, CA50 (location of 50% mass fraction burned), and combustion efficiency. For maximum brake torque (MBT), the 10-90% burn duration is set to 25 deg ATDC and CA50 is determined on a case by case basis. Unless otherwise stated, MBT conditions will be used with a combustion efficiency of 98%.

Similar to previous gasoline engine modeling studies, iso-octane is used as a thermodynamic surrogate for gasoline [8]. The fuel properties of gasoline and neat ethanol (E100) are obtained from GT-Power, as shown in Table 2. Also shown are the properties of E85 (85% ethanol, 15% gasoline by volume), which are calculated with the weighted sum of the two fuels. The heat of vaporization, which is significantly higher for ethanol, is incorporated into the model during the fuel vaporization process. It is assumed that all of the fuel is vaporized immediately after injection and that the necessary energy is extracted from the surrounding gases.

Table 23. Fuel properties

	Gasoline†	E85	E100
Lower Heating Value (MJ/kg)	44.3	30.2	27.7
Heat of Vaporization (kJ/kg)	308	831	924
ON	92	107	110

†Thermodynamic properties taken from iso-octane.

4.4 Fuel and engine configurations

To assess the potential of gasoline and ethanol to increase engine efficiency, engines are designed for each fuel and compared against a baseline gasoline engine. The design parameters of the three engine/fuel strategies are shown in Table 3. All engines

operate at stoichiometry ($\phi = 1$) but differ in air handling, compression ratio, and EGR. The baseline engine is naturally aspirated and does not use any external EGR, while both high efficiency engines are turbocharged with up to 2 bar intake pressure and use up to 25% cooled EGR, maintained at 60° C in the intake manifold. A 10.5:1 compression ratio is chosen for the baseline engine [22]. Since the high efficiency gasoline engine is designed to have a higher knock resistance by using cooled EGR, its compression ratio can be increased to 12:1 [23], [24], [25]. Previous work has shown that when modifying a gasoline SI engine for ethanol, up to a 7.6 increase in ON allows 1 compression ratio increase [26], [27]. The E85 engine has a 15 ON increase, so the compression ratio can be increased from 12:1 to 14:1.

Table 24. Overview of engine/fuel model parameters

	Baseline Gasoline	**High Efficiency Gasoline**	**High Efficiency E85**
Intake Air	NA (≤ 1 bar)	TC (≤ 2 bar)	TC (≤ 2 bar)
Compression Ratio	10.5	12	14
External EGR	0%	≤ 25%	≤ 25%
Cooled EGR Temperature	60° C	60° C	60° C
Φ	1	1	1

Since the purpose of this work is to incorporate realistic limits to the thermodynamic models, ideal and feasible versions of each engine are assessed. The ideal engine/fuel strategies are not restricted by knock or flammability limits and operate at MBT timing with 25% external EGR over the entire speed and load range. Feasible engine/fuel strategies are limited by knock and flammability. Knock is eliminated by retarding spark timing and flame quench is avoided by limiting the amount of acceptable external EGR.

4.5 Knock model

Knock is a major limitation of SI engines because it leads to high cylinder pressure fluctuations which could be very damaging to the engine. In practical applications, spark timing must be delayed away from MBT to eliminate knock. Since this work uses a fixed Wiebe function with a constant burn duration, spark timing is

effectively replaced by setting the CA50 location. Knock limits are applied by first identifying knock with an autoignition correlation and then retarding CA50 until knock does not occur.

Knock is assumed to occur if the flame traversing the charge does not consume the end gas before it autoignites. The ignition delay, τ_{ID}, or the time required for the onset of knock, is dependent on the pressure, unburned temperature and mixture composition. The residence time, τ_{RES}, decreases with increasing engine speed. Short ignition delays mean that the end gas can autoignite before the flame is able to fully consume the charge. As engine speed increases and residence time decreases, there is a speed at which the ignition delay is greater than the residence time and knock does not occur.

While other more complex approaches exist for evaluating knock, such as the autoignition integral or direct integration of chemical kinetics, we have chosen a simpler approach in which knock is identified if $\tau_{ID} < \tau_{RES}$. Since previous work on HCCI combustion has shown that evaluating the ignition delay at top dead center (TDC) conditions correlates well with ignition characteristics, for the case of SI knock we calculate the relevant ignition time, τ_{ID}, with unburned temperature and pressure at the location of peak pressure, analogous to the TDC conditions for HCCI [28]. Fuel ON and EGR also have a significant impact on τ_{ID} since higher ON fuels increase the ignition delay and EGR prevents knock due to its impact on ignition chemistry. To calculated the ignition delay, this work uses an autoignition correlation that incorporates the effects of unburned temperature, pressure, ON, and EGR. The equation combines the Hoepke et al. correlation with the ON multiplier term from the Douaud and Eyzat correlation, as follows [29], [30]:

$$\tau_{ID} = \left(\frac{ON}{100}\right)^{3.402} 8.449\times10^{-5} \left(\frac{P}{T}\right)^{-1.343} (1 - x_{EGR})^{-0.8881} \exp\left(\frac{5266}{T}\right)$$

Equation 13: Ignition delay

where τ_{ID} is in ms, P in bar, and T in K. Pressure and unburned temperature are evaluated at peak pressure conditions and x_{EGR} is the total EGR mass fraction in the cylinder.

τ_{RES} is calculated with engine speed and residence period in crank angle degrees (CAD). While the speed at which knock becomes borderline is different for every engine due to engine geometry, flow and heat transfer differences, previous work has shown that

a typical SI-NA engine is not significantly knock limited for speeds equal to or greater than 3000 RPM at WOT [31]. Thus, the residence period is calibrated such that $\tau_{ID} = \tau_{RES}$ = 0.75 ms at 3000 RPM and WOT for the baseline engine, as shown in Figure 31. τ_{ID} decreases with engine speed due to decreased residual gas fraction and increased unburned temperature and pressures until 5000 RPM when the peak cylinder pressure and temperature begin to decrease. A residence period of 13.5 CAD was chosen such that $\tau_{RES} = \tau_{ID}$ at 3000 RPM. Thus τ_{RES} is defined by:

$$\tau_{RES} = 13.5 * 1000/(6 \cdot \text{RPM})$$

Equation 14: Residence time

For speeds less than 3000 RPM the ratio of τ_{ID} to τ_{RES} is less than one, indicating that knock occurs.

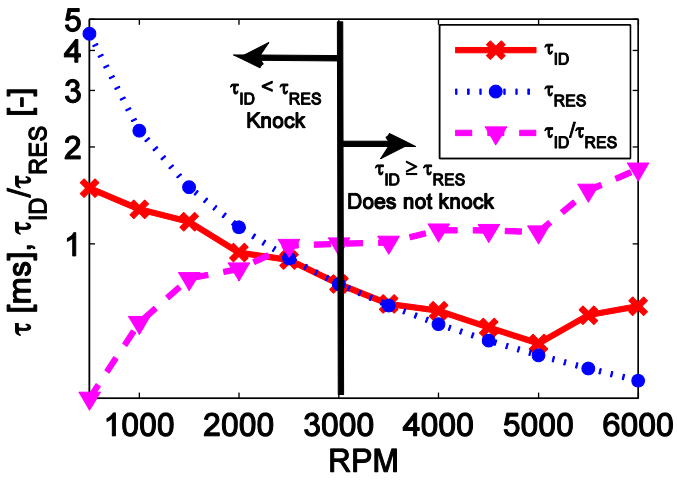

Figure 31. Baseline gasoline engine ignition delay at WOT and residence time with the constraint for knock defined by τ_{ID}/τ_{res} at 3000 RPM.

4.5.1 Baseline gasoline engine

The criteria to identify knock ($\tau_{ID}/\tau_{RES} < 1$) is applied to each engine/fuel strategy over the full range of speeds and loads using the same residence time definition. For instance, consider the baseline engine operating at 2000 RPM. Figure 32 shows that τ_{ID}/τ_{RES} decreases as load increases and knock is identified from 7.2 to 9.3 bar BMEP. As load increases, the unburned temperature and pressure of the end gas increase. This increases reaction rates and lowers τ_{ID}. Note that the results shown in Figure 32 are found

using the CA50 location that results in peak BTE, or MBT timing, for each load level (CA50 ranges from 10.5 to 9.5 deg aTDC for 1 to 9.3 bar BMEP).

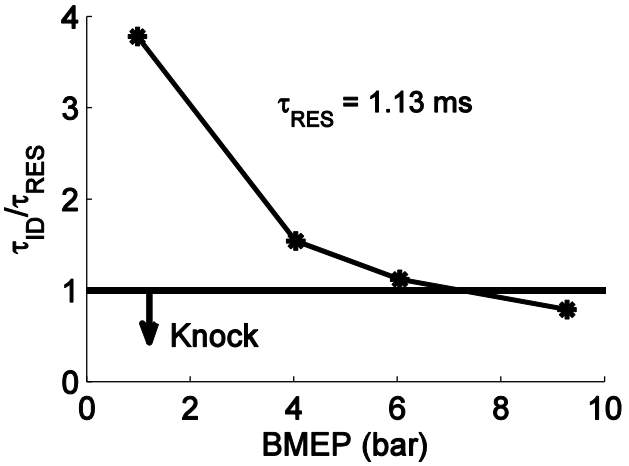

Figure 32. Knock limits for the baseline gasoline engine at 2000 RPM.

For the conditions that knock, i.e. BMEP > 7.2 bar, CA50 (spark timing) is retarded until knock does not occur (τ_{ID}/τ_{RES} = 1). As CA50 is retarded, combustion occurs later in the expansion stroke and peak cylinder pressure and unburned temperature decrease. This increases τ_{ID} and reduces the likelihood of knock. To illustrate this for a range of operating conditions at 2000 RPM, CA50 locations are identified where τ_{ID}/τ_{RES} = 1 for each desired load. Results from this method are shown in Figure 33(a-b), where Figure 33(a) shows ΔCA50, the difference between the CA50 that does not knock and CA50 for MBT timing, and Figure 33(b) shows the BTE for the non-knocking conditions. Since ΔCA50 at 2000 RPM and WOT (9.3 bar BMEP) results in only a 0.5% loss in BTE, there is no significant decrease in BTE from the ideal, MBT conditions, as shown in Figure 33(b).

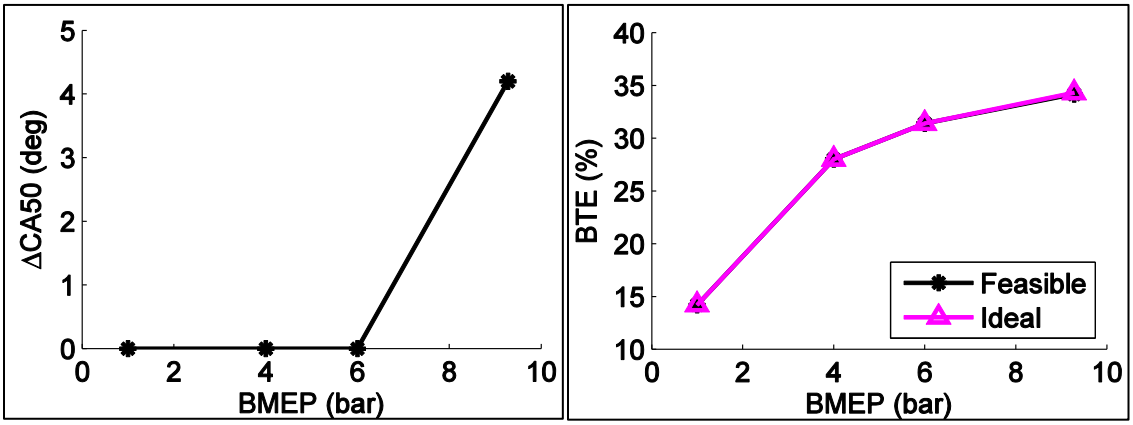

Figure 33. Baseline gasoline engine results at 2000 RPM: (a) the change in knock limited CA50 from CA50 at MBT timing (ΔCA50), (b) brake thermal efficiency comparison between ideal (CA50 at MBT timing) and knock-limited engines.

4.5.2 High efficiency gasoline engine

Knock limits for the high efficiency gasoline engine with different amounts of external EGR are determined with the same method as the baseline engine, with MBT timing and the calibrated τ_{RES}, as shown in Figure 4. Note that for the 0% EGR case, knock is predicted at 5.8 bar BMEP, which is lower than the knock limit for the baseline engine at 2000 rpm (7.2 bar BMEP), previously shown in Figure 2. This is due to the higher compression ratio of the high efficiency engine, which increases peak temperature and pressure and decreases τ_{ID}.

The benefit of EGR as a means to reduce knock is also shown in Figure 34, as 25% external, cooled EGR extends the knock limited BMEP from 5.8 to 7.7 bar BMEP. As EGR increases for a constant low to mid load BMEP level, τ_{ID} increases due to lower unburned gas temperatures, despite higher peak cylinder pressures. EGR also increases the unreactive portion of the mixture, which increases τ_{ID} through the x_{EGR} term in Equation 13. At high load conditions, the impact of EGR on τ_{ID} is much less pronounced. This is due to a combination of significantly higher boost pressures, required to maintain load during dilute operation, and a fixed burn rate that is assumed in the model. As EGR and boost pressures increase for a high load condition, it is assumed that the intake temperature is maintained at 60° C by a heat exchanger. However, peak cylinder pressures increase substantially with load, resulting in increased peak unburned temperatures. Thus, unburned temperature has an opposite trend with EGR at high loads than at low loads. Increased EGR causes both pressure and unburned temperature to

increase, resulting in a lower τ_{ID} (mitigated by the increased value of x_{EGR} used in Equation 13. However, since these results were found with a fixed burn duration, they do not account for the slower flame speeds expected with EGR dilution, which would lower peak cylinder pressure and unburned temperature, thus increasing τ_{ID} with EGR.

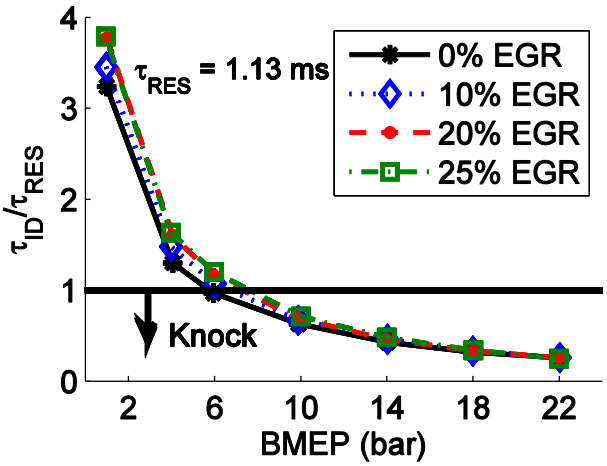

Figure 34. Knock limits for the high efficiency gasoline engine at 2000 RPM.

Results from retarding spark timing for knocking conditions are shown in Figure 5(a-b). Compared to the baseline engine, the trend of ΔCA50 with load is much more pronounced. Since the non-knocking CA50 is significantly later than the CA50 for MBT timing, less work is extracted during the expansion stroke and BTE is reduced. Adding EGR mitigates this effect and enables an earlier CA50, closer to MBT timing, without knock. In addition to enabling earlier spark timings, EGR increases BTE at low loads by reducing pumping work and across all loads through benificial thermal and composition effects. This is demonstrated for 4 bar BMEP where MBT timing is possible for all EGR levels; as EGR increases BTE increases above the 0% EGR baseline value. Due to dilution, EGR lowers combustion temperatures and therefore decreases the specific heat capacity, c_p, of the burned gas mixture. While this benefit is somewhat offset by an increased mass fraction of triatomic molecules (that increases c_p), the overall effect is that gamma increases during combustion. Thus, as EGR increases more work is done per unit of combustion heat.

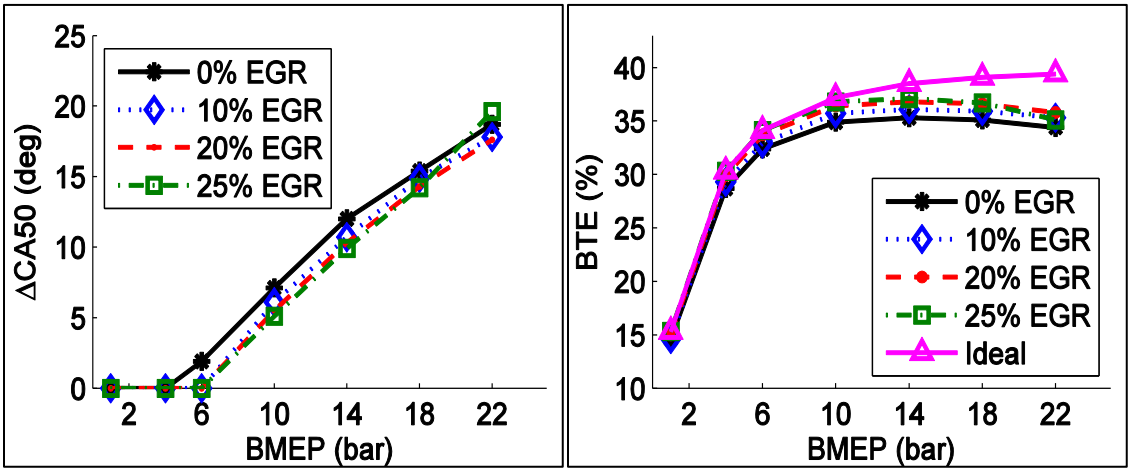

Figure 35. High efficiency gasoline engine results at 2000 RPM: (a) the change in knock limited CA50 from CA50 at MBT timing (ΔCA50), (b) brake thermal efficiency comparison between ideal (CA50 at MBT timing, 25% EGR) and knock-limited engines.

4.5.3 High efficiency E85 engine

Figure 36 shows the ignition delay results as a function of load for the E85 engine. Due to the higher ON and higher heat of vaporization of E85, which lower temperatures, τ_{ID} is significantly higher than τ_{ID} for the baseline and high efficiency gasoline engine for all load conditions. The majority of this increase (68% to 100%) is due to the higher ON, since an increase from 92 to 107 ON results in a 67% increase in τ_{ID}, according to Equation 13. However, the lower unburned temperatures of the E85 engine also increase τ_{ID}, particularly at high loads when the higher heat of vaporization of E85 has the largest impact. As more fuel is injected to meet the desired load, more energy is required to vaporize the fuel. Since the heat of vaporization for E85 is more than twice that of iso-octane, much more energy is required to vaporize the same mass of fuel. In addition, since E85 has a lower energy content than iso-octane, more grams of fuel must be injected to achieve the same load. Thus, as load increases the impact of the heat of vaporization increases and the temperature after injection and during combustion is significantly lower for the E85 engine. Even though the E85 engine has higher peak cylinder pressures due to a higher compression ratio, the peak unburned temperatures are up to 8.6% lower as compared to the high efficiency gasoline engine. For the conditions shown in Figures 4 and 6, τ_{ID} is 66% to 140% higher for the E85 engine and knock is not detected until 14 bar BMEP.

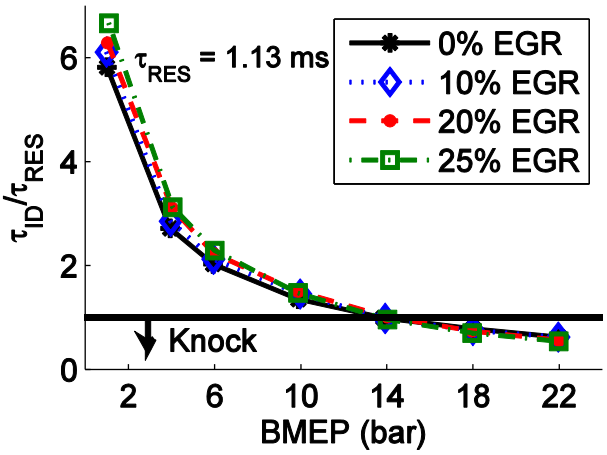

Figure 36. Knock limits for the high efficiency E85 engine at 2000 RPM.

Similar to gasoline, ΔCA50 and BTE were found for each load, shown in Figure 37. Due to the higher compression ratio of the E85 engine, heat loss increases for the same BMEP and MBT timing occurs at slightly later CA50 locations. At most, CA50 must only be delayed 7.3 CAD from MBT timing (22 bar BMEP, 22% EGR), resulting in a 2% decrease in BTE. This small decrease in efficiency demonstrates the benefit of using a high ON fuel to enable high load operation without requiring spark retard. Compared to the high efficiency gasoline engine, the maximum BTE at 2000 RPM is improved 10.2%.

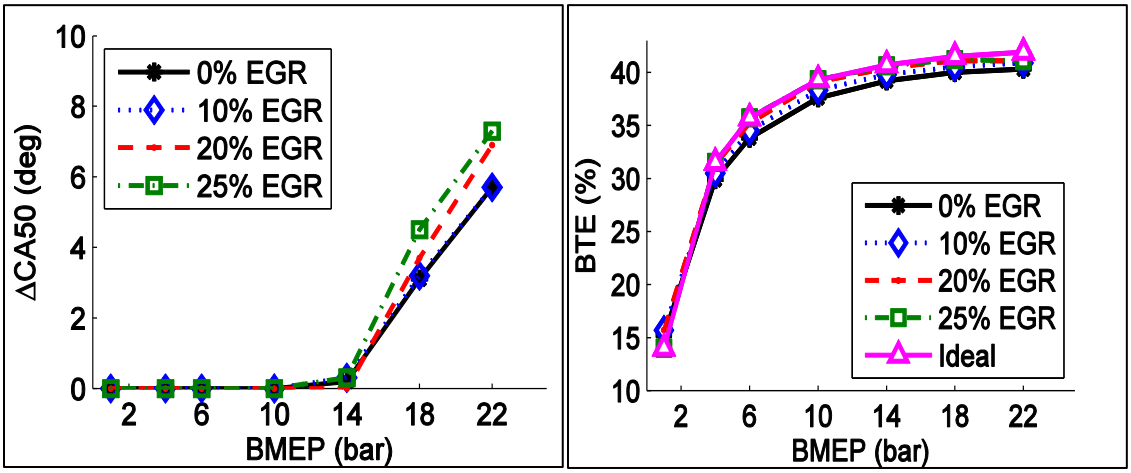

Figure 37. E85 engine results at 2000 RPM: (a) **the change in knock limited CA50 from CA50 at MBT timing (ΔCA50),** (b) **brake thermal efficiency comparison between ideal (CA50 at MBT timing, 25% EGR) and knock-limited engines.**

4.6 Flammability limits

Diluting the fuel-air mixture with air or EGR is known to increase the likelihood of abnormal combustion events, such as misfire or partial burning. Predicting such events in detail would require modeling of the turbulent flame structure, an approach beyond the scope of this work. This work uses a combination of qualitative dimensional theory with appropriate experimental calibration to estimate flammability limits and assess the feasibility of proposed external EGR levels in the engine maps considered.

Experimental results of EGR tolerance from SwRI's HEDGE engine provide insight on the amount of EGR that can be used in an advanced SI engine. As detailed in Alger et al., an EGR map was developed for a 2.4L, multi-port injection (MPI) engine with a 11.4:1 compression ratio, a similar engine to the high efficiency gasoline engine we are considering [23]. As done in this work, the compression ratio of the HEDGE engine was increased from the baseline engine to be used with a high amount of cooled, external EGR. Results from the HEDGE engine show that it is possible to incease EGR with load and that the amount of feasible EGR does not vary significantly with engine speed. Stable combustion is maintained up to almost 30% EGR, at which point flammability limits are encountered [23]. However, due to limitations of the turbocharger system, EGR is decreased at high load and low speed conditions to increase torque and achieve the desired BMEP [23].

To understand the ways in which dilute operation can be enhanced or restricted, it is helpful to review the flame development process and the related abnormal combustion phenomena. During the initial flame development period, misfire occurs if the mixture is too dilute and there is insufficient fuel for the flame to ignite. If the flame kernel survives, flame propagation will proceed in a locally laminar process. As the flame gets exposed to the turbulent flow field, the flame becomes increasingly wrinkled, thereby enhancing the burning velocity due to larger flame surface areas. If the burning rate is too low, the mixture may not completely burn by the time the exhaust valve opens, resulting in partial burning. As turbulence increases, flame straining has a dominant impact over flame wrinkling and the likelihood of flame quenching increases [7].

Conceptual turbulent flame studies have identified the key parameters that influence the combustion regimes. These are: turbulence intensity, u', turbulence integral

length scale, L, laminar flame speed, S_L, and laminar flame thickness, δ_L. These are used in nondimensional models such as the Leeds combustion diagram, shown in Figure 8. The x and y axes are defined by nondimensional ratios, L/δ_L and u'/S_L, respectively. Combustion regimes are defined by the Karlovitz stretch factor, K, the turbulent strain rate normalized by chemical rate in the flame. Following Abdel-Gayed et al., K is defined by the following expression [32]:

$$K = 0.157\left(\frac{u'}{S_L}\right)^2 Re_t^{-0.5}$$

Equation 15: Karlovitz stretch factor

where Re_t is the turbulent Reynolds number based on the integral length scale. As K increases, the flame is more likely to quench due to the increasing impact of flame strain, i.e. when the stretch time becomes low enough to interfere with the energy release time in the flame. Also, if the mixing time is not on the same order as the chemical time, the flame cannot propagate and flame quenching occurs at $KRe^{-0.5} = 0.079$, equivalent to a Damkohler number, $Da \equiv (L/u')(S_L/\delta_L)$, on the order of 1.

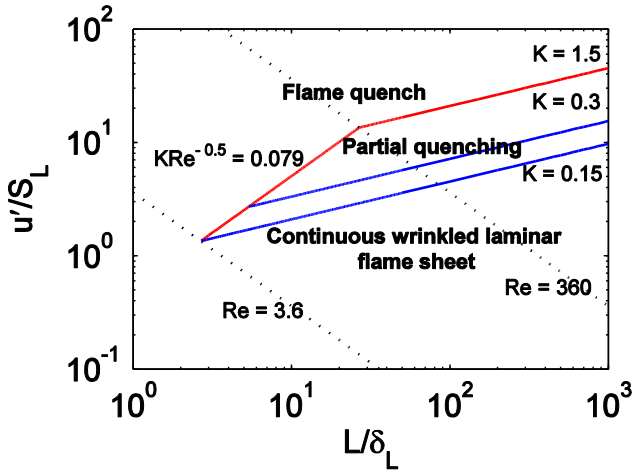

Figure 38. Modified Leeds Diagram for premixed combustion regimes.

Previous work has shown that combustion regime diagrams can be used to characterize combustion in SI engines [7]. For example, Dai et al. found that the Leeds diagram could be used to map combustion regimes and predict misfire for a 1.6L and 2.0L SI engine [7]. As the mixture became leaner, with either air or EGR dilution, the combustion regime moved closer to the flame quench limit (upwards and to the left) until

misfire was predicted at the K = 1.5 flame quench boundary. Experimental results corroborate these results, thus demonstrating that the Leeds Diagram can representatively predict misfire limits of SI engines [7].

This work also uses the Leeds diagram to predict flame quench, but with simulation results for the high efficiency gasoline and E85 engines. S_L and δ_L for gasoline are taken from iso-octane and are obtained with laminar flame speed correlations developed by Middleton et al. with the unburned temperature and pressure immediately before the start of combustion, total EGR (external and residual fraction) and equivalence ratio [8]. S_L and δ_L for E85 are also found with the Middleton correlations, but are scaled directly by the ratio of S_L for ethanol to iso-octane, β, to account for the higher flame speed and inversely by $1/\beta$ to account for the shorter flame thickness of ethanol. Based on measured iso-octane and ethanol flame speeds in the literature, β was set to 1.3 for this work [33]. To account for the fact that only 85% of the fuel by volume is ethanol, the final value for S_L and δ_L for E85 is the weighted sum of S_L and δ_L for both fuels. Consistent with previous estimates that indicate L is 20% of the clearance height, L = 0.8 mm for this work [34]. As u' may be approximated by half the piston speed at TDC, u' = 3.5 m/s at 2000 RPM [6]. These values of u' and L are held constant for the load and EGR range at 2000 RPM for the high efficiency gasoline and E85 engines.

Engine simulation results are obtained for the high efficiency gasoline and E85 engine operating at different EGR levels (0%, 10%, 20%, 25%, 30%) and loads (1, 4, 6, 10, 14, 18, 22 bar BMEP) and at 2000 RPM, shown in Figure 39(a-b). Since u' and L are constant for the conditions shown, trends with increasing EGR and load are solely due to changes in S_L and δ_L, caused primarily by changes in unburned temperature, pressure, density, total EGR, and O_2 concentration. Values for these parameters for the conditions shown in Figure 39(a-b) are included in the Appendix.

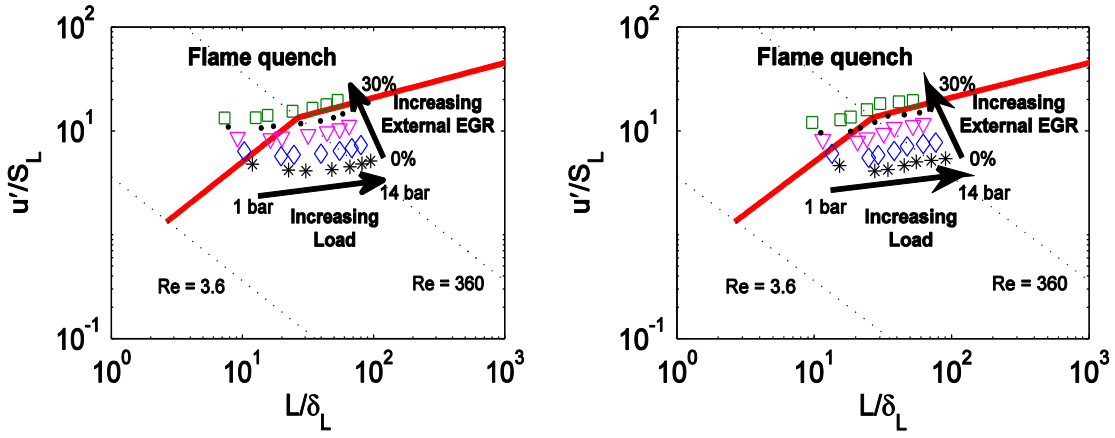

Figure 39. Simulated combustion results at 2000 RPM plotted on the Leeds Diagram (conditions just before the start of combustion) (a) high efficiency gasoline engine, (b) E85 engine.

Table 25. Feasibility of operating conditions shown in Figure 39

External EGR	BMEP (bar)			
	1	4	6	10 - 22
30%	×	×	×	×
25%	×	×	✓	✓✓
20%	×	✓	✓✓	✓✓
10%	✓	✓✓	✓✓	✓✓
0%	✓✓	✓✓	✓✓	✓✓

(✓✓ = yes for high efficiency gasoline and E85 engines, ✓ = yes for just the E85 engine, × = no for either engine/fuel).

As EGR increases along a constant load for both engine/fuel strategies, the points on the Leeds Diagram shift upwards and to the left, similar to results seen by Dai et al. [7]. The upward trend is caused by lower S_L, resulting from lower O_2 concentrations and higher pressures as EGR is increased [8]. The leftward trend on the Leeds Diagram is due to higher δ_L, consistent with lower S_L as EGR increases.

As load increases for a constant EGR level, the points on the Leeds Diagram shift slightly upward and to the right for both engine/fuel strategies. S_L decreases with increasing load because the increase in pressure and decrease in unburned temperature is more significant than the increase in O_2 concentration. The shift to the right on the combustion diagram, due to lower δ_L, is a result of increased unburned density, which outweighs the impact of a slightly lower S_L. For instance, as load increases from 1 to 22 bar BMEP with no external EGR for the high efficiency gasoline engine, unburned density increases 763% and δ_L decreases by 88% while S_L decreases by only 7%.

The high efficiency gasoline and E85 engines operate in very similar combustion regimes for the same speed, load and EGR conditions, as shown in Figure 39(a-b). This is due to a tradeoff between unburned temperatures and flame speed characteristics of the fuels based on their molecular structure. Since ethanol is a straight chain alcohol with a lower carbon content than iso-octane (a branched alkane), ethanol has a faster flame speed than iso-octane for the same temperature, pressure and EGR conditions. However, due to the higher heat of vaporization of E85 as compared to iso-octane, the unburned temperatures for E85 are significantly lower (see Appendix), resulting in slower flame speeds. This trend is augmented as load increases since a greater mass of fuel is vaporized. For the conditions shown in Figure 9(a-b), the resulting trend is that S_L is up to 8% higher for E85 at low loads and 11% lower at high loads. Since δ_L is inversely related to S_L and unburned density, which is higher for E85**,** δ_L is lower for E85 at low loads and the combustion regime is shifted to the right. At high loads, there is little difference in δ_L between the E85 and high efficiency gasoline engine.

The feasible operating conditions for both the high efficiency gasoline and E85 engines are indicated by the flame quench boundary in Figure 9(a-b) and are listed in Table 4. Any point on or above the flame quench line is considered infeasible. Since the slope of the flame quench boundaries are positive, as load increases and the combustion regime shifts to the right, higher amounts of external EGR may be used while maintaining stable combustion. Since the high efficiency gasoline engine was calibrated to exclude 30% from the feasible regime, the maximum external EGR for this engine is 25% and occurs at the highest load. Due to the tradeoff between lower unburned temperatures and the faster flame speed of ethanol, the maximum external EGR for the E85 engine is also 25%. However, since the combustion regime for the E85 engine is shifted to the right at low loads, there are three conditions that are feasible for the E85 engine that are not feasible for the high efficiency gasoline engine: 1 bar BMEP with 10% EGR, 4 bar BMEP with 20% EGR, and 6 bar BMEP with 25% EGR.

The theoretical flame limit results for the high efficiency gasoline engine are compared to the experimental results from SwRI's HEDGE engine in Figure 10. Aside from peak torque, where the HEDGE engine is limited by the turbocharger, the theoretically determined EGR limits are in good agreement with those used at SwRI.

Thus, the EGR limits for the high efficiency gasoline are chosen to be analogous to the experimental results for constant BMEP levels, but with no restrictions on EGR due to turborcharging, as shown in Figure 40. Using these same BMEP levels, EGR limits for the E85 engine are defined based on the theoretical results shown in Figure 9(b). As shown in Figure 40, the E85 engine has a higher EGR tolerance at low loads, due to the faster flame speed of ethanol at these conditions.

The variation of EGR with speeds other than 2000 RPM is not evaluated in this work, as experimental results indicate that EGR varies little with speed, particularly in the region where the engine typically operates (1000-2000 RPM, 0-5 bar BMEP). This is likely due to similar trends in u' and S_L as engine speed varies. As speed increases, higher piston speeds increase u' and higher unburned temperatures increase S_L. Thus, combustion regime results would be similar for speeds other than 2000 RPM.

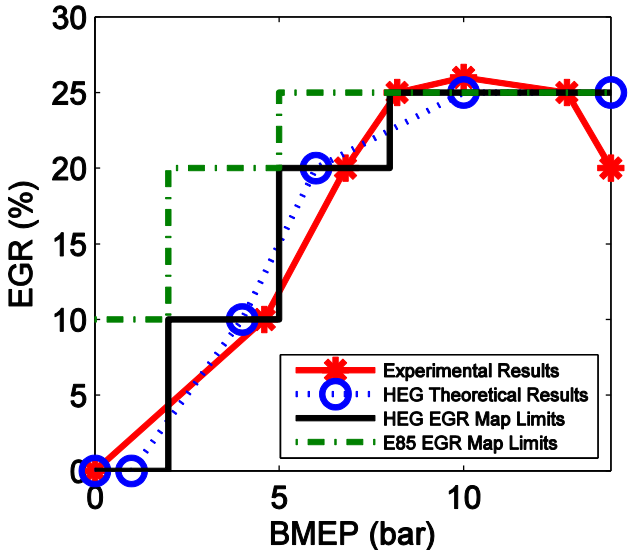

Figure 40. EGR trends with load for the SwRI HEDGE engine, theoretical results, and EGR map limits for this work.

The results of implementing EGR and knock limits to the high efficiency gasoline and E85 engine at 2000 RPM are shown in Figure 41(a-b). Also shown are the ideal and worst case scenarios, as defined by EGR level and CA50 location. With flame and knock limits taken into account, BTE is lower than the ideal case, but improved from the 0% EGR case. The impact of knock on reducing efficiency is more significant for the high efficiency gasoline engine, particularly at high loads (e.g. at 22 bar BMEP spark timing is 20 CAD after MBT and efficiency is reduced 14.5%). Since the E85 engine is less

limited by knock and flammability constraints, efficiency is increased up to 17% as compared to the high efficiency gasoline engine for the conditions shown in Figure 41.

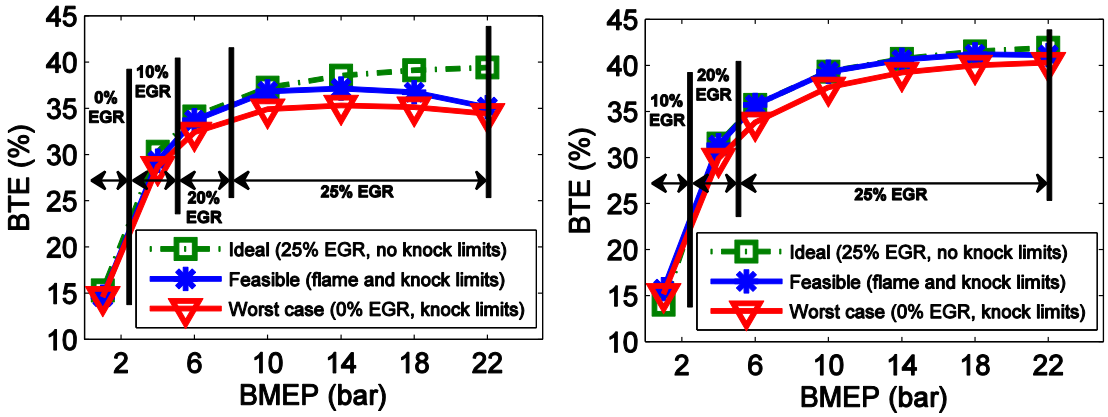

Figure 41. Brake thermal efficiency at 2000 RPM under ideal, realistic, and worst case scenarios (a) **high efficiency gasoline engine,** (b) **E85 engine.**

4.7 Feasible and ideal engine maps

To obtain ideal and feasible engine maps, the calculations for 2000 RPM are repeated over the full engine range, 800-6000 RPM. The ideal strategies assume that 25% cooled EGR may be used over the entire speed/load range with MBT timing, while feasible maps are based on the previously discussed criteria to ensure that flame quench and knock do not occur. Thus, external EGR is limited according to Figure 10 and CA50 location is determined for each speed/load/EGR level such that $\tau_{ID}/\tau_{RES} \geq 1$. If knock is identified at the MBT timing, CA50 is determined using a linear interpolation based on intake pressure at the lower knocking load limit up to the full load condition where the maximum CA50 retard is necessary. Accordingly, the maximum spark retard occurs at low engine speeds since residence time is the longest. In fact, the high efficiency gasoline requires that spark timing occur slightly after TDC to mitigate knock for high loads and speeds less than 1000 RPM. In practice, excess fuel would be used at such conditions to cool the charge and allow earlier spark timings, but these considerations are beyond the scope of this work.

Brake thermal efficiency (BTE) maps for the ideal and feasible baseline gasoline, high efficiency gasoline, and E85 engines are shown in Figure 42(a-f). A comparison of the ideal maps shown in Figure 12(a,c,e) demonstrates the benefits of using turbocharging, increased compression ratios, EGR, and ethanol to increase efficiency.

The maximum gain in efficiency results from extending the load limit of the engines, as the impact of friction and pumping losses decreases as load increases. For instance, the peak BTE for the ideal high eficiency gasoline and E85 engines occur at peak load and are 13.7% and 17.7% higher than the ideal baseline engine. At low-mid load conditions, efficiency is also increased for these engine/fuel strategies due to thermodynamic benefits of a higher compression ratio and use of 25% cooled, external EGR. For instance, from 2 to 5 bar BMEP, the median percent increase in BTE as compared to the ideal baseline engine is 7.5% for the high efficiency gasoline engine and 8.0% for the E85 engine. The ideal E85 engine has higher efficiencies than the high efficiency gasoline engine due to a higher compression ratio and higher heat of vaporization of ethanol, which increases volumetric efficiency and reduces heat losses for the same BMEP.

As shown in Figure 42(a,b), the BTE for the feasible and ideal baseline engines are very similar. This is because the feasible engine is only knock constrained from 8 bar BMEP to peak load, where knock is most severe. However, the spark retard required to eliminate knock at peak load is at most 6 CAD, resulting in an efficiency penalty of less than 1%. Thus, incorporating knock constraints for the baseline engine does not result in a significant efficiency penalty.

Shown in Figure 42(d,f), feasible engine maps for the high efficiency gasoline and E85 engines demonstrate efficiency reductions due to both flammability and knock limits, which are more significant at boosted conditions. Thus, the difference in BTE between the ideal and feasible high efficiency gasoline engines is much more pronounced as compared to the baseine engines. For instance, the maximum reduction in BTE is due to flammability limits, as BTE is reduced up to 10% at low loads where external EGR is eliminated. At high loads, knock constraints reduce BTE by up to 5%, corresponding to a spark retard of 15 CAD.

The feasible E85 engine has similar efficiency reduction trends as the feasible high efficiency gasoline engine, but to a lesser extent. For instance, the maximum reductions in BTE occur due to flammability limits at low loads, but the median reduction is only 2% for 0-2 bar BMEP, whereas the feasible high efficiency gasoline efficiency is reduced 5% at these loads. Also, since the higher octane number and higher heat of vaporization of ethanol aids in reducing knock, spark timing does not need to be

retarded from MBT as much as the gasoline engine (e.g. 8 vs. 15 CAD at peak load, 5000 RPM with 25% EGR) and efficiency at peak load decreases by less than 1% for all speeds.

The engine maps for the feasible engine/fuel strategies are similar to experimental engine results. For instance, the peak BTE for the feasible baseline engine, 34.4%, corresponds to 236 g/kWh, which is very similar to the minimum BSFC of recent low friction NA engines (240 g/kWh) [22]. The minimum BSFC for the feasible high efficiency gasoline engine is 213 g/kWh and is comparable to the minimum BSFC results from the HEDGE engine with a 11.4 compression ratio (216 g/kWh) [35]. However, results shown in Figure 42(a-f) do not show a significant BTE island that is expected due to enrichment at high loads. Thus, the miminum BSFC occurs much closer to peak BMEP, while previous results indicated that the minimum BSFC condition is around 75% peak load.

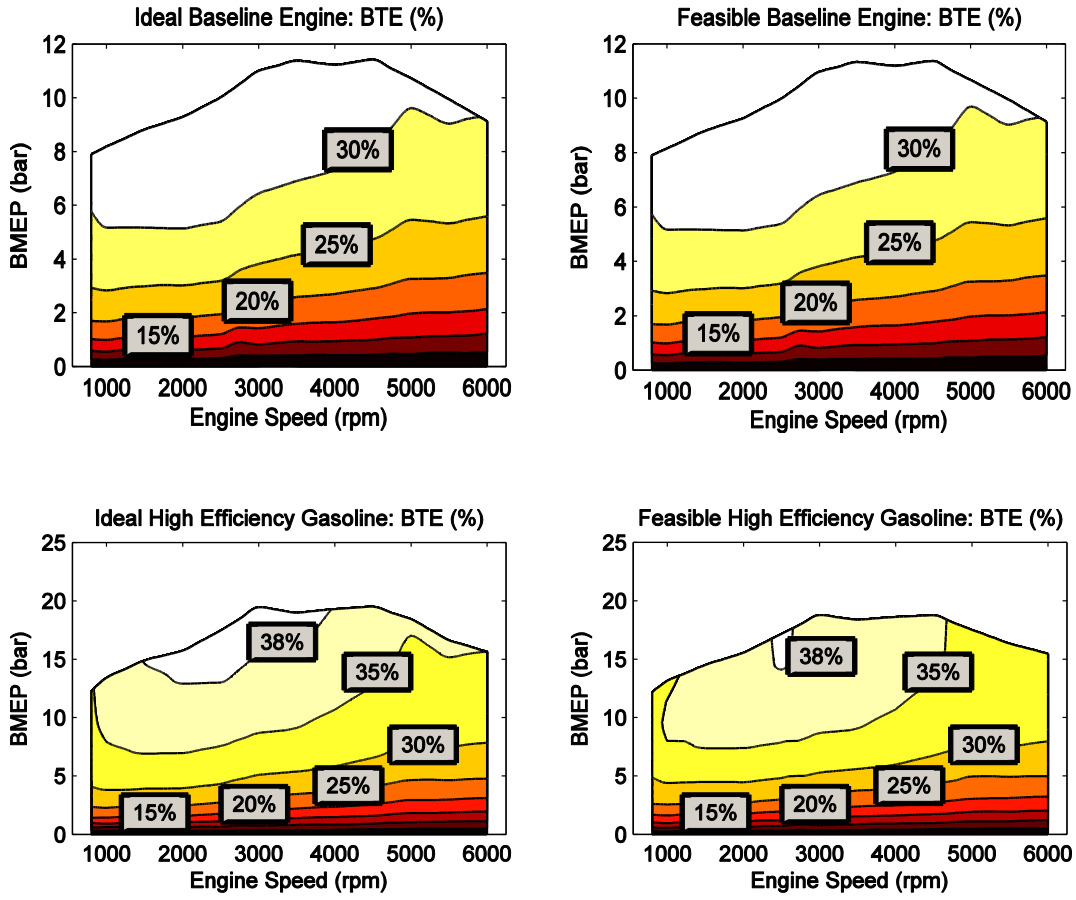

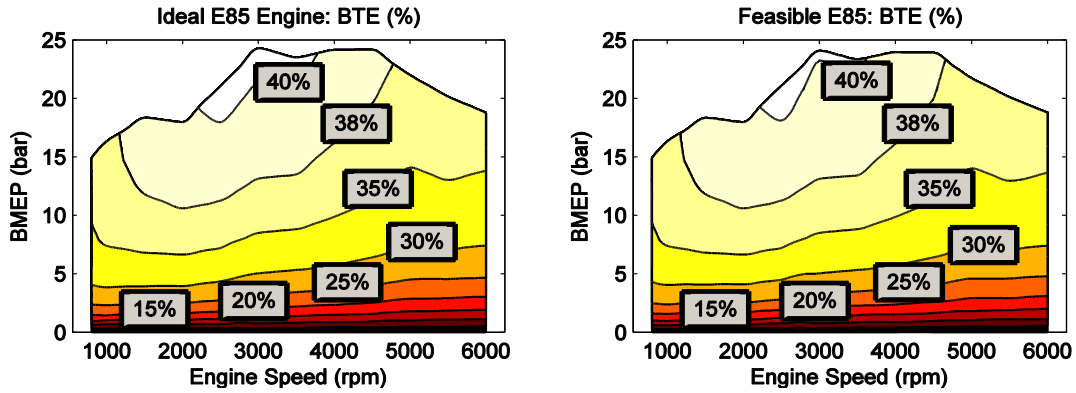

Figure 42. BTE engine maps: (a) ideal baseline engine, (b) feasible baseline engine, (c) ideal high efficiency gasoline engine, (d) feasible high efficiency gasoline engine, (e) ideal E85 engine, (f) feasible E85 engine.

4.8 Vehicle fuel economy

Each engine/fuel strategy was then evaluated in a vehicle model developed in MATLAB/Simulink, as done in Lavoie, et al. [5]. (See Lavoie et al. for more information on the vehicle model parameters [5].) A mid-size sedan is chosen as the vehicle platform and the baseline engine is assumed to be a 4 cylinder, 2.5 L engine. To ensure consistent torque and performance for all engine/fuel strategies, the high efficiency gasoline and E85 engines were sized to match the peak torque and RPM of the ideal baseline engine. Accordingly, the high efficiency gasoline engine has a displacement of 1.5 L (3 cylinders) while the E85 engine is 1.2 L (2 cylinders).

Fuel economy results are shown in Figure 43, as well as the percent MPGe improvement from the ideal baseline engine over the combined City-Highway cycle. The E85 engine offers the most fuel economy improvements (41.1% and 40.9% for the ideal and feasible, respecitvley) due to the previously discussed efficiency benefits of the fuel, compression ratio, and EGR, as well as the fact that the engine is downsized from 2.5 L to 1.2 L. The high efficiency gasoline engines are also downsized, but to a lesser extent, and also show an improvement from the baseline (33.0% and 30.1% for the ideal and feasible, respectively). Fuel economy is slightly reduced for the feasible high efficiency gasoline engine, since it operates in low load regions where flammability limits are most severe. The feasible baseline engine shows no reduction in fuel economy as compared to the ideal baseline engine because spark retard is minimal near peak load and the engine operates mainly at low to mid loads.

The increase in efficiency for the high efficiency gasoline and E85 engines is due to a variety of factors. Primarily, the relative impact of friction is reduced through downsizing and boosting the engine. Since peak torque is constant, peak BMEP scales inversely with engine size. Thus, downsizing the engine increases BMEP and therefore BTE. Secondly, increasing the compression ratio increases the thermal efficiency due to the higher amount of work produced during the expansion stroke, relative to the compression stroke. Thirdly, fuel is used to increase the efficiency for the E85 engine. By using a fuel with a higher laminar flame speed and heat of vaporization, the amount of dilution is increased even at low loads, resulting in small efficiency gains. Also, the higher heat of vaporization of ethanol increases volumetric efficiency and decreases heat transfer losses. Fourthly, the use of fuels and dilution are used to relax combustion constraints and enable engine downsizing/boosting and increased compression ratios. Thus, by manipulating the constraints due to knock and flammability limits, the engine operating space is extended and vehicle efficiency is increased.

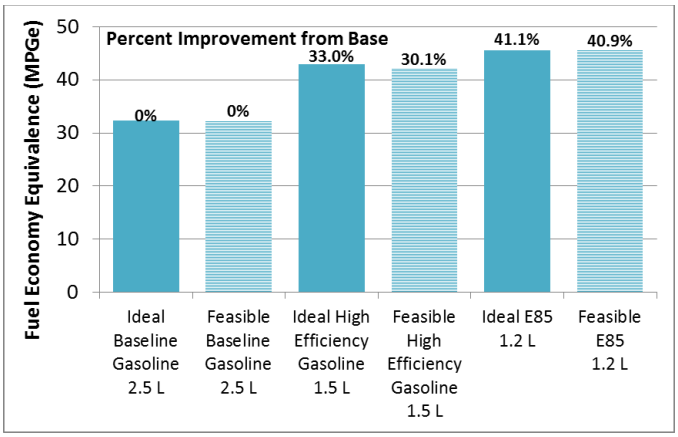

Figure 43. Combined city and highway fuel economy equivalence results for each engine/fuel strategy.[3]

4.9 Conclusions

Thermodynamic models were used to assess three SI engine/fuel strategies: a baseline gasoline engine, high efficiency gasoline engine, and high efficiency boosted ethanol engine. The ideal potential of each was assessed assuming that MBT timing and

[3] MPG is calculated with the density of gasoline (as done in Chapter 3). Miles per gallon equivalence (MPGe) is calculated with the LHV ratio of the fuels: 120 MJ/gal for gasoline and 87 MJ/gal for E85. Thus, the gallon of gasoline equivalence is 1.4.

25% EGR was possible at all operating conditions. Feasible versions of these maps were developed by incorporating knock and flammability limits. Each ideal and feasible engine/fuel strategy was then evaluated in a vehicle model with engines downsized to maintain equivalent torque and RPM to obtain drive cycle results.

The main conclusions of the advanced engine analysis are summarized as follows:

- This work provides an easily understood method of assessing knock and flammability constraints on combustion. Knock is assessed by comparing residence time, which varies with speed, to ignition delay time, calculated with a combined Hoepke et al. and Douaud and Eyzat correlation that accounts for unburned temperature, pressure, ON, and EGR [29], [30]. Flammability limits are determined by evaluating the impact of strain on the flame, using the Karlovitz number, ratio of laminar to turbulent parameters, and the Leeds Combustion Diagram.
- Results from the knock model show that as load is increased at 2000 RPM, knock is first identified at 6 bar BMEP for the high efficiency gasoline engine, but not until 14 bar BMEP for the E85 engine. The E85 engine is more resistant to knock due to the high octane of the fuel and higher heat of vaporization, which reduces unburned temperatures.
- Flame model results indicate an upper limit of 25% EGR for the high efficiency gasoline and E85 engine. For both engines, EGR may increase with load while maintaining stable combustion. However, the E85 engine may use more EGR at low loads, as compared to the high efficiency gasoline engine, due to the molecular structure of ethanol which results in a higher flame speed.
- Engine fuel economy maps were developed for each engine/fuel strategy. Compared to the ideal baseline engine, peak BTE is increased by 13.7% for the high eficiency gasoline engine and 17.7% for the E85 engine. Knock and flammability constraints reduce peak efficiency by 2.6% for the high efficiency gasoline engine but less than 1% for the E85 engine. Fuel economy results show a similar trend, as the difference between ideal and feasible fuel economy is 2.2% for the high efficiency gasoline engines but only 0.14% for the E85 engines. The

differences between the feasible and ideal baseline engines are negligible due to the minimal spark retard required to eliminate knock.

- The increase in fuel economy for the high efficiency gasoline and E85 engines is mainly due to downsizing/boosting and higher compression ratios. Also, ethanol is used to increase efficiency by increasing volumetric efficiency, lowering heat transfer losses, and enabling more dilution to be used at low loads. These efficiency benefits of downsizing and boosting are enabled by dilution and ethanol which relax combustion constraints (e.g. knock and flammability limits).

The conceptual approach developed in this work could be used to assess the knock and flammability limits of other engine/fuel strategies. For instance, the tradeoffs in efficiency and knock could be evaluated for very high compression ratios (e.g. 18:1) for gasoline and ethanol engines. Also, the potential of alcohol fuels to increase EGR tolerance could be evaluated by modeling a wider range of fuel blends in advanced engines using the framework presented in this work.

Acknowledgements
The authors would like to thank Robert Middleton for providing his flame correlation model, John Hoard for valuable discussions on engine operating constraints, and Dr. Terry Alger for sharing his insight on the knock limitations of highly dilute engines.

4.10 References

[1] S. Richard, G. Font, F. Le Berr, O. Grasset, and M. Fremovici, "On the use of system simulation to explore the potential of innovative combustion systems: methodology and application to highly downsized SI engines running with ethanol-gasoline blends," SAE Paper 2011–01–0408, 2011.

[2] N. Fraser, H. Blaxill, G. Lumsden, and M. Bassett, "Challenges for increased efficiency through gasoline engine downsizing," SAE Paper 2009–01–1053, 2009.

[3] T. V. Johnson, "Review of CO2 emissions and technologies in the road transportation sector," SAE Paper 2010–01–1276, 2010.

[4] P. Leduc, B. Dubar, A. Ranini, and G. Monier, "Downsizing of gasoline engine: an efficient way to reduce CO2 emissions," *Oil & Gas Science and Technology*, vol. 58, no. 1, pp. 115–127, 2003.

[5] G. Lavoie, E. Ortiz-Soto, A. Babajimopoulos, J. B. Martz, and D. N. Assanis, "Thermodynamic sweet spot for high-efficiency, dilute, boosted gasoline engines," *Int J of Engine Res*, pp. 1–19, Aug. 2012.

[6] J. B. Heywood, *Internal Combustion Engine Fundamentals*. New York, 1998.

[7] W. Dai, S. G. Russ, N. Trigui, and K. V Tallio, "Regimes of premixed turbulent combustion and misfire modeling in SI engines," SAE Paper 982611, 1998.

[8] R. J. Middleton, J. B. Martz, G. A. Lavoie, A. Babajimopoulos, and D. N. Assanis, "A computational study and correlation of premixed isooctane air laminar reaction fronts diluted with EGR," *Combustion and Flame*, vol. 159, no. 10, pp. 3146–3157, May 2012.

[9] T. Alger, J. Gingrich, B. Mangold, and C. Roberts, "A Continuous Discharge Ignition System for EGR Limit Extension in SI Engines," SAE Paper 2011–01–0661, 2012.

[10] J. D. Dale and M. D. Checkela, "Application of high energy ignition systems to engines," *Prog. Energy Combust. Sci.*, vol. 23, pp. 379–398, 1997.

[11] P. Grabner, H. Eichlseder, and G. Eckhard, "Potential of E85 Direct Injection for Passenger Car Application," SAE Paper 2010–01–2086, 2012.

[12] S. Utsumi, A. Ota, K. Kawatake, T. Kawai, and T. Tsunooka, "The Effect of Ethanol Fuel on a Spark Ignition Engine," SAE Paper 2006–01–3380, 2006.

[13] P. A. Caton, L. J. Hamilton, and J. S. Cowart, "Experimental and Modeling Investigation into the Comparative Knock and Performance Characteristics of E85,

Gasohol [E10] and Regular Unleaded Gasoline [87 (R+M)/2],” SAE Paper 2007–01–0473, 2007.

[14] E. Kasseris and J. Heywood, “Charge Cooling Effects on Knock Limits in SI DI Engines Using Gasoline / Ethanol Blends: Part 2-Effective Octane Numbers,” SAE Paper 2012–01–1284, 2012.

[15] J. Szybist, M. Foster, W. R. Moore, K. Confer, A. Youngquist, and R. Wagner, “Investigation of Knock Limited Compression Ratio of Ethanol Gasoline Blends,” SAE Paper 2010–01–0619, 2010.

[16] E. P. Kasseris, “Knock Limits in Spark Ignited Direct Injected Engines Using Gasoline / Ethanol Blends,” PhD Thesis, Massachusetts Institue of Technology, 2011.

[17] K. S. Hoyer, W. R. Moore, and K. Confer, “A Simulation Method to Guide DISI Engine Redesign for Increased Efficiency using Alcohol Fuel Blends,” SAE Paper 2010–01–1203, 2010.

[18] M. J. Christie, N. Fortino, and R. B. Llc, “Parameter Optimization of a Turbo Charged Direct Injection Flex Fuel SI Engine Hakan Yilmaz,” SAE Paper 2009–01–0238, 2009.

[19] J. A. Caton, “An Assessment of the Thermodynamics Associated With High-Efficiency Engines,” in *Proceedings of the ASME 2010 Internal Combustion Engine Division Fall Technical Conference*, San Antonio, Texas, 12-15 September 2010. Paper no. ICEF 2010-35037.

[20] E. Ortiz-Soto, D. Assanis, and A. Babajimopoulos, “A comprehensive engine to drive-cycle modelling framework for the fuel economy assessment of advanced engine and combustion technologies,” *Int J of Engine Res*, vol. 12, pp.1-19, 2011.

[21] S. Chen and P. Flynn, “Development of a Single Cylinder Compression Ignition Research Engine,” SAE Paper 650733, 1965.

[22] T. Tsuchiya, H. Hosoi, K. Hoshi, H. Shimamura, T. Hagiwara, Y. Ito, and F. Arai, “Newly Developed Inline 4 AR Series SI Engine,” SAE Paper 2009–01–1048, 2009.

[23] T. Alger and J. Gingrich, “Cooled EGR for Fuel Economy and Emissions Improvement in Gasoline Engines,” JSAE Paper 20105013, 2010.

[24] T. Alger, B. Mangold, C. Roberts, and J. Gingrich, “The Interaction of Fuel Anti-Knock Index and Cooled EGR on Engine Performance and Efficiency,” SAE Paper 2012–01–1149, 2012.

[25] T. Alger, S. Hanhe, C. E. Roberts, and T. W. Ryan, “The Heavy Duty Gasoline Engine – A Multi-Cylinder Study of a High Efficiency, Low Emission Technology,” SAE Paper 2005–01–1135, 2005.

[26] J. Gingrich, T. Alger, and B. Sullivan, “Ethanol flex-fuel engine improvemens with exhaust gas recirculation and hydrogen enrichment,” SAE Paper 2009–01–0140, 2009.

[27] S. Taniguchi, K. Yoshida, and Y. Tsukasaki, “Feasibility study of ethanol applications to a direct injection gasoline engine,” SAE Paper 2007–01–2037, 2007.

[28] A. Babajimopoulos, G. a. Lavoie, and D. N. Assanis, “On the Role of Top Dead Center Conditions in the Combustion Phasing of Homogeneous Charge Compression Ignition Engines,” *Combustion Science and Technology*, vol. 179, no. 9, pp. 2039–2063, Aug. 2007.

[29] B. Hoepke, S. Jannsen, E. Kasseris, and W. K. Cheng, “EGR effects on boosted SI engine operation and knock integral correlation,” SAE Paper 2012–01–0707, 2012.

[30] A. Douaud and E. P, “Four-Octane-Number Method for Predicting the Anti-Knock Behavior of Fuels and Engines,” SAE Paper 780080, 1978.

[31] S. Russ, “A review of the effect of engine operating conditions on borderline knock,” SAE Paper 960497, 1996.

[32] R. G. Abdel-Gayed and D. Bradley, “Combustion regimes and the straining of turbulent premixed flames,” *Combustion and Flame*, vol. 76, pp. 213–218, 1989.

[33] H. L. et al. Glaude, PA, Herbinet, O, Dirrenberger, P, Gall, “Laminar Flame Velocity of Gasolines with Addition of Ethanol,” in *Proceedings of the European Combustion* Meeting, Lund University, Lund, Sweden, 2011.

[34] F. V. Loye, A. O. zur, Bracco, “Two-Dimensional Visualization of Premixed-Charge Flame Structure in an IC Engine,” SAE Paper 870454.

[35] T. Alger, “SwRI’s HEDGE Technology for High Efficiency , Low Emissions Gasoline Engines,” in *DEER Conference*, Detroit, MI, USA, 29 September, 2010.

4.11 Appendix.

Parameters for data points in Figure 9:

High Efficiency Gasoline (HEG) Engine

External EGR	S_L (cm/s) - HEG						
	1	**4**	**6**	**10**	**14**	**18**	**22**
30%	26	26	25	23	21	20	18
25%	32	33	32	30	28	26	24
20%	41	42	40	38	36	34	31
10%	55	61	59	58	55	51	48
0%	73	83	85	82	78	73	69

External EGR	δ_L (cm) - HEG						
	1	**4**	**6**	**10**	**14**	**18**	**22**
30%	0.0110	0.0063	0.0051	0.0033	0.0023	0.0018	0.0015
25%	0.0102	0.0057	0.0046	0.0029	0.0020	0.0016	0.0014
20%	0.0087	0.0049	0.0040	0.0025	0.0018	0.0014	0.0012
10%	0.0078	0.0041	0.0032	0.002	0.0014	0.0012	0.0010
0%	0.0067	0.0036	0.0026	0.0017	0.0012	0.001	0.0008

External EGR	Unburned Temperature (K) - HEG						
	1	**4**	**6**	**10**	**14**	**18**	**22**
30%	873	822	797	808	826	838	839
25%	878	817	794	806	818	822	825
20%	887	825	802	805	810	809	806
10%	885	831	804	804	804	795	787
0%	888	827	819	804	799	786	775

External EGR	Pressure (bar) - HEG						
	1	**4**	**6**	**10**	**14**	**18**	**22**
30%	9	15	19	32	50	70	94
25%	9	14	17	30	46	63	80
20%	9	14	17	29	43	57	71
10%	8	13	16	27	39	50	62
0%	8	12	16	25	36	46	56

External EGR	Total EGR (%) - HEG						
	1	**4**	**6**	**10**	**14**	**18**	**22**
30%	47	39	36	35	34	34	34

25%	44	35	32	30	29	28	28
20%	41	31	28	25	24	23	22
10%	36	24	20	16	14	13	12
0%	30	17	13	8	5	3	2

External EGR	**Unburned Density (g/m^3) - HEG**						
	1	**4**	**6**	**10**	**14**	**18**	**22**
30%	3.8	6.5	8.4	14	21.5	29.6	30.0
25%	3.6	6.1	7.8	13.4	20.1	27.0	34.4
20%	3.5	6.0	7.6	12.8	18.9	25.3	31.5
10%	3.2	5.5	7.1	11.9	17.5	22.7	28.2
0%	3.0	5.1	6.7	11.2	16.1	21.1	26.0

External EGR	**O_2 Concentration (%) - HEG**						
	1	**4**	**6**	**10**	**14**	**18**	**22**
30%	12	13	14	14	14	14	15
25%	12	14	15	15	15	15	16
20%	13	15	15	16	16	17	17
10%	14	16	17	18	18	19	19
0%	15	18	19	20	20	21	21

E85 Engine

External EGR	**S_L (cm/s) - E85**						
	1	**4**	**6**	**10**	**14**	**18**	**22**
30%	29	28	26	22	19	19	18
25%	37	36	33	29	25	24	23
20%	43	44	41	37	32	31	30
10%	58	63	60	55	49	47	45
0%	76	85	82	76	70	67	65

External EGR	**δ_L (cm) - E85**						
	1	**4**	**6**	**10**	**14**	**18**	**22**
30%	0.0083	0.0051	0.0043	0.0033	0.0027	0.0020	0.0015
25%	0.0072	0.0043	0.0037	0.0029	0.0023	0.0017	0.0014
20%	0.0069	0.0039	0.0033	0.0025	0.0021	0.0016	0.0012
10%	0.0060	0.0032	0.0027	0.0021	0.0017	0.0013	0.0011
0%	0.0052	0.0029	0.0023	0.0018	0.0014	0.0011	0.0009

External EGR	Unburned Temperature (K) - E85						
	1	4	6	10	14	18	22
30%	851	786	763	739	738	764	790
25%	859	792	760	732	726	747	765
20%	853	791	759	732	715	733	744
10%	853	791	756	715	703	708	711
0%	852	783	753	711	691	695	693

External EGR	Pressure (bar) - E85						
	1	4	6	10	14	18	22
30%	11	16	20	28	39	58	82
25%	11	16	19	26	36	52	71
20%	10	15	18	26	33	47	63
10%	9	14	16	22	29	41	52
0%	8	12	15	20	27	36	46

External EGR	Total EGR (%) - E85						
	1	4	6	10	14	18	22
30%	46	38	36	34	34	34	34
25%	43	35	32	30	29	29	29
20%	41	31	28	25	24	24	23
10%	35	24	21	16	15	14	13
0%	30	17	13	9	7	5	4

External EGR	Unburned Density (g/m^3) - E85						
	1	4	6	10	14	18	22
30%	4.4	7.3	9.1	13.5	18.9	26.9	36.2
25%	4.3	7.1	8.8	12.7	17.2	24.2	32.6
20%	4.0	6.8	8.4	12.4	16.2	22.8	29.8
10%	3.7	6.3	7.7	11.1	14.6	19.9	25.8
0%	3.5	5.7	7.4	10.3	13.6	18.9	23.7

External EGR	O_2 Concentration (%) - E85						
	1	4	6	10	14	18	22
30%	11	13	13	14	14	14	14
25%	12	14	14	15	15	15	15
20%	12	14	15	16	16	16	16
10%	13	16	17	17	18	18	18
0%	15	17	18	19	19	20	20

Chapter 5: Lightweight materials and advanced combustion engines

5.1 Introduction

The combined potential of lightweight materials and advanced combustion engines to reduce life cycle energy and GHG emissions is evaluated by integrating the vehicle models developed in Chapters 2-3 with the engine models created in Chapter 4. Additionally, the life cycle performance of advanced engines must be incorporated in the LCA by modeling the vehicle-cycle impacts of downsized/turbocharged engines. Uncertainty due to assumptions regarding upstream production of fuels is included with a representative range of energy and GHG emissions intensities for various ethanol feedstocks and oil extraction processes from previous literature.

Since many combinations of mass reduction, engine technologies and vehicle platforms exist, the scope of this work is limited to answering the following three questions:

1. What level of mass reduction is required to match the life cycle GHG emissions reductions for a contemporary ICV due to downsizing/boosting an advanced gasoline engine?
2. What are the maximum life cycle energy and GHG reductions possible when lightweighting a contemporary ICV and replacing a baseline engine with an advanced gasoline or ethanol downsized/boosted engine?
3. What are the life cycle energy and GHG emissions reductions due to using an advanced downsized/boosted ethanol engine in a HEV and PHEV as compared to an ICV with a baseline engine?

It is important to note that while this framework enables an evaluation of the maximum increase in fuel economy for the mass reduction and engine scenarios

considered for the ICV, the fuel economy results for the hybrid vehicles are not the maximum value because controls have not been optimized. For this reason, the ICV is used to assess the individual versus combined application of lightweight materials and advanced engines in question one and two. Then, question three focuses on hybrid vehicles that utilize mass reduction and advanced engine technologies in order to demonstrate life cycle improvements possible even without optimal controls for each technology combination.

For ease of comparison of results, nomenclature is developed for the three engine/fuel technologies and vehicle-technology combinations. Engine/fuel strategies are referred to as follows: NA for the baseline naturally aspirated gasoline engine, HEG for the high efficiency gasoline engine, and E85 for the high efficiency E85 engine. Combinations of baseline/lightweight vehicles and engine type are identified by "X-YZ" where X is the engine name (e.g. NA, HEG, E85), Y is the vehicle name (e.g. ICV, HEV or PHEV), and Z is the percent body-in-white (BIW) mass reduction (e.g. 0, 10, 20, 25, or 35). For instance, HEG-ICV35 refers to the high efficiency gasoline engine ICV with 35% BIW mass reductions.

5.2 Engine production energy and GHG emissions

The life cycle impact of advanced engines is dependent on the energy and GHG emissions associated with their production, as well as the resulting fuel economy over the vehicle lifetime. Accordingly, a method is developed to convert the baseline naturally aspirated engine (equivalent to the baseline engine discussed in Chapter 4) to a downsized/boosted engine (equivalent to the HEG and E85 engines discussed in Chapter 4). First, the mass fractions of engine parts are determined based on teardown data from a representative naturally aspirated engine (1.8 L, 4-cylinders). (This is the same engine that was used for the vehicle materials and life cycle analyses in Chapters 2-3.) Then, these mass fractions are applied to the generic baseline engine to find the specific mass of each part. Next, the materials used for the engine block, cylinder head, pistons and crankshaft are evaluated to determine if higher strength materials are necessary to withstand the higher combustion pressures of the high efficiency engine. Then, the engine is modified by adding a turbocharger and reducing the number of cylinders, according to the size of the downsized/boosted engine. Lastly, the life cycle energy and GHG

emissions impact of these changes are assessed with the mass of materials and energy and GHG emissions intensities for each material.

The material composition and subsystem mass fractions for a typical naturally aspirated gasoline engine are determined from teardown data, as shown in Figure 44 [1]. A complete list of parts included in each engine subsystem is included in Table 31 of the Appendix. The engine block, cylinder head and crankshaft systems are the heaviest components, as they comprise 66% of the total engine mass. Accordingly, the material mass fractions of cast aluminum and steel are very significant, as the engine block and cylinder head are cast aluminum and crankshaft is steel. Additionally, much of the cooling system, engine mounts, lubrication system, front engine system, and components in the cylinder head system (e.g. camshaft) are composed of steel.

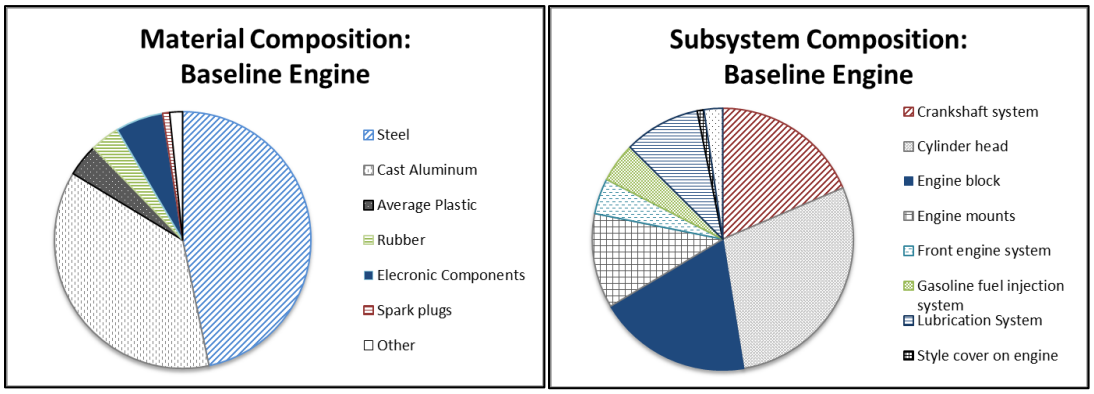

Figure 44: Materials and mass fraction of a typical naturally aspirated engine

In order to assess the design modifications required for a downsized/boosted engine, the materials of important load bearing components must be evaluated to determine if they are compatible with the higher cylinder pressures expected during engine operation. Specifically, the engine block and cylinder head are important structural components that must have adequate strength and stress qualities at a wide variety of temperatures and a high thermal conductivity in order to dissipate heat [2]. Also, the pistons must be designed to withstand high mechanical and thermal loads, as they are subjected to the peak cylinder pressures, high temperature gradients and significant inertial forces during acceleration events [2]. Similarly, the crankshaft must also have good strength and stress characteristics and be able to withstand the high forces due to combustion and piston accelerations.

The baseline engine is designed with a cast aluminum engine block, cylinder head and pistons, as well as a steel crankshaft. Based on current industry trends, it is assumed that these material choices are appropriate for the downsized/boosted engines as well [3], [4]. For instance, the materials for these parts are the same as used in the Ford EcoBoost 1.6 L and 2.0 L engines, two state-of-the-art downsized/boosted engines available in production vehicles today [3]. Also, BMW's 3.0 L triple-turbocharged duty diesel engine uses aluminum pistons designed by Federal-Mogul that can withstand cylinder pressures up to 200 bar [4]. However, it is important to note that the future trend of material application for significantly downsized engines is not certain, as new downsized/boosted engines are continually being released. For instance, the 1.0L, 3-cylinder Ford EcoBoost engine is the most recent and smallest of the EcoBoost engines and uses a cast iron engine block instead of aluminum [5]. This design choice was made in order to decrease the warm-up time, thereby decreasing fuel consumption during cold-start conditions [5]. While this may be a future trend of highly downsized/boosted engines, this work assumes that aluminum will remain one of the popular material choices for engine block design.

In addition to a materials analysis of critical engine components, the parts list of the baseline engine is assessed to determine if any additional parts are required or if any parts can be removed for the downsized/boosted engine model. The only additional components are included in the turbocharger system, which is characterized from teardown data of a representative turbocharged engine [1]. Accordingly, the turbocharger itself is composed of steel and cast aluminum alloys and has a mass of 2.4 kg. The turbocharger system weighs 7.0 kg in total and includes a wastegate (steel), valves (steel and electronic components), and piping for water and oil (steel, plastic and rubber) [1]. Since it is assumed that the number of cylinders is reduced for the downsized engine, the number of pistons, connecting rods, intake/exhaust valves and ignition coils/spark plugs decrease accordingly, as shown in Table 26 for a 4 to 3-cylinder reduction. It is assumed that the mass of the engine block, cylinder head and crankshaft do not decrease for the high efficiency engine due to the fact that these components are designed to meet the peak load demand or peak power, which is highly correlated with component mass (see Figure 50 in the Appendix). Since the peak power of the high efficiency engines is equivalent to the baseline engine, it is assumed that no downsizing occurs for these parts.

Lastly, before the engine production impact may be assessed, it is necessary to quantify the cylinder reduction between the baseline and downsized/boosted engines according to the displaced engine volume, calculated from the peak torque and power characteristics of the 0.5 L single cylinder engine models developed in Chapter 4. For instance, the baseline engine for the ICV must have a peak power of 117 kW (157 hp), as determined in Chapter 2, which corresponds to a peak torque rating of 231 Nm and a 2.6 L displacement (4-cylinders). Since the high efficiency engines must also meet the same acceleration requirements, they are sized for the same torque and power requirements. Accordingly, the high efficiency gasoline and E85 engines have a displacement of 1.5 L and 1.3 L, respectively. Based on current engine trends, it is assumed that the 2.6 L engine is a 4-cylinder engine, while the 1.5 L and 1.3 L each have 3-cylinders. A summary of the design changes from the 4-cylinder baseline engine to a 3-cylinder downsized/boosted engine is shown in Table 26.

Table 26: Material and parts for the baseline naturally aspirated and turbocharged/downsized engines

Engine Part	Material	No. of parts - Baseline	No. of parts - Turbocharged/downsized
Engine block	Aluminum	1	1
Cylinder head	Aluminum	1	1
Crankshaft	Steel	1	1
Pistons	Aluminum	4	3
Piston rings	Steel	12	9
Connecting rods	Steel	4	3
Intake valves	Steel	8	6
Exhaust valves	Steel	8	6
Spark plugs	Electronics	4	3
Ignition coil assembly	Electronics	4	3
Turbocharger	Steel + Aluminum	0	1

Engine production energy and GHG emissions are determined for the baseline 4-cylinder and downsized/turbocharged 3-cylinder engine based on the material energy and emissions factors and material masses for each engine. As done in Chapter 3, the energy

and GHG emissions intensities of steel and aluminum are adopted from the most recent published data from the steel and aluminum industries [6], [7]. Also, the energy and GHG emission factors for plastic and rubber are determined with GREET 2 [8]. However, since the material composition of electrical components, such as spark plugs, are not provided in the teardown data, these components are omitted from the engine production analysis.

The final mass of the downsized/boosted engines is determined to be 1 kg less than the baseline engine, due to the fact that the mass of the turbocharger system is only 1 kg less than the mass saved from downsizing. However, the mass fraction of cast aluminum is increased for the downsized/boosted engines because the addition of the cast aluminum portion of the turbocharger is larger than the cast aluminum removed from the engine due to downsizing.

As shown in Figure 45, downsizing and turbocharging the baseline engine results in a 3% increase in engine production energy and GHG emissions. The production burden increases despite the decrease in mass due to the fact that some of the steel in the baseline engine is replaced by cast aluminum. However, it is important to note that if the spark plugs and ignition coils were included in the energy and GHG emissions model, there would be less of a difference (relative and absolute) in energy and GHG emissions between the two engines. However, the difference between the baseline and high efficiency engines is negligible in the scope of the total vehicle life cycle analysis, as a 3% increase in engine production impacts would only increase the vehicle-cycle results by less than 1%.

While the engine production analysis shown here provides valuable insight on the life cycle comparison of naturally aspirated and downsized/boosted engines, it is important to note that there may be additional factors that would increase the vehicle production burden of downsized/boosted engines. For instance, advanced aluminum manufacturing techniques are likely to be used to create components (e.g. pistons) for engines with a high specific power [9]. These manufacturing techniques are likely more energy-intensive than the processes assumed in this model [9]. Also, as cylinders are removed from the engine it may be necessary to add balancing components, such as an unbalanced flywheel, as used in the 3-cylinder Ford EcoBoost 1.0 L engine [10].

However, it is expected that even with these considerations taken into account, the increase in total vehicle life cycle energy and GHG emissions would be minimal.

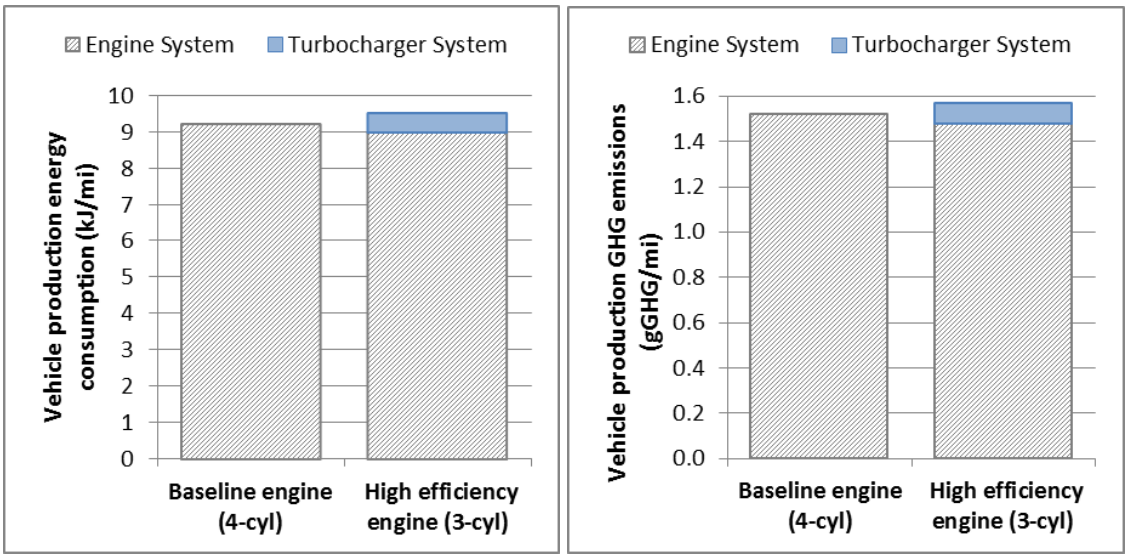

Figure 45: Vehicle production energy and GHG emissions for the baseline and downsized/boosted engines

5.3 Fuel-cycle analysis of gasoline and ethanol

To assess the life cycle impact of vehicles using gasoline and ethanol fuels, it is necessary to evaluate the range of fuel-cycle impacts that are possible due to differences in oil classification and extraction process, ethanol feedstock, and life cycle accounting method. Thus, current trends of gasoline and ethanol production are presented and previous fuel-cycle work is discussed. As done in Chapter 3, fuel cycle impacts from electricity are incorporated to the life cycle model using average US grid data from eGRID and the associated upstream impacts using GREET 1 [11], [12]. Based on this work, a range of energy and GHG emissions factors are identified to represent the span of fuel-cycle results for gasoline, ethanol and electricity (for PHEV charging). These values will be used in Section 4 for the total vehicle life cycle analysis.

5.3.1 Gasoline

Due to significant technology advancements in the oil industry and rising oil prices, the share of oil produced from unconventional sources is increasing rapidly [13]. Unlike conventional oil, unconventional oil requires either additional extraction or refining processes to achieve the same quality as light, liquid oil that is obtained from a

well drilling process [14]. For instance, oil shale is a sedimentary rock that contains kerogen, a pre-cursor of oil [15]. After the oil shale is mined and pre-processed, kerogen is extracted from the rock in a process that requires very high temperatures [15]. Similarly, oil (bitumen) derived from oil sands must be separated from sand, water and clay using high temperatures and additional water input. Most commonly, oil sands are mined with in situ technology (instead of surface mining), where steam is created by burning natural gas and pumped into the ground through horizontal wells [16]. After the bitumen becomes less dense, it is pumped to the surface. A similar process involving thermal heating is used to extract other types of heavy crude oil, such as the oil found in Venezuela (a significant crude oil import for the US) [17]. After these oils are extracted, they require significant refining processes to lower the sulfur content and density. On the other hand, shale oil is a light oil with low sulfur content, but is trapped in horizontal reservoirs at much deeper levels beneath the earth's surface [18]. Shale oil is mined using horizontal drilling and fracturing techniques, where a mix of water, sand and chemicals are pumped into the reservoir at a high pressure, causing fractures in the rock formation [18]. This releases the liquid shale oil that is subsequently pumped to the surface.

While oil shale remains uneconomical, the rate of extraction of oil sands and shale oil is rapidly increasing [18]. For instance, the Energy Information Administration (EIA) projects that due largely to shale oil recovery in the US and oil sand mining in Canada, liquid fuel production in non-OPEC nations will increase by 1.6 million bbl/d in 2014 [13]. In fact, in the US alone, crude oil production is expected to rise from 6.5 million bbl/d in 2012 to 8.1 million bbl/d in 2014, a 24% increase [13].

Previous work has shown that the fuel-cycle energy and GHG emissions for conventional and unconventional oils is dependent not only on the extraction process, but also the input assumptions and boundaries used in the life cycle analysis [15], [19], [20], [21]. For instance, work by Bergerson et al. found that when considering production of synthetic crude oil from oil sands with baseline assumptions, surface mining requires less energy and GHG emissions than in situ processes [19]. However, when best and worst case assumptions are included in the analysis, the range of possible emission intensities is very similar for the two processes [19]. Despite these uncertainties, most of the previous life cycle analysis of surface mining and in situ techniques for oil sands has found that

situ processes require increased energy and GHG emissions because to the natural gas required for bitumen extraction has a more significant impact than the electricity required for surface mining [12], [21]. Accordingly, the energy and GHG emissions intensities used in this work for gasoline derived from conventional oil and oil sands are adopted from GREET 1, as shown in Table 27 [12]. For reference, the GHG impact of Venezuelan crude oil is also shown in Table 27 [22]. While fuel-cycle information is not currently available for shale oil, it is expected that this will have a large variability based on the mining process and key assumptions, such as methane leakage during extraction [20].

Table 27: Energy and GHG emissions per MJ-gasoline for conventional and unconventional oils [12], [22]

	Energy (MJ/MJ)	GHG emissions (gGHG/MJ)
Conventional	0.21	19
Oil sands – surface	0.41	30
Oil sands – in situ	0.47	33
Venezuelan crude oil	-	22

5.3.2 Ethanol

Ethanol can be produced from any biological feedstock that is composed of sugars or materials that can be converted to sugar [14]. Thus, a range of feedstocks could be used, each requiring their own manufacturing processes [14]. For sugar crops, such as sugarcane, the sugar is removed from the crop and fermented into alcohol with yeast and other microbes [14]. Then, water is removed from ethanol and it is distilled to the desired concentration. However, if the feedstock is starch-based, such as corn, the starch must first be converted to sugar using a high temperature enzyme process before it is fermented into alcohol and distilled. Similarly, feedstock that is cellulosic biomass must be separated into cellulose, hemicellulose and lignin. Then, cellulose is converted into sugars with an acid hydrolysis process. While the process to convert biomass to ethanol is technically feasible, it remains limited by high cost and alternative processes are currently being investigated [14].

Motivated in part by the Renewable Fuel Standard and the recent E15 standard, ethanol production rates have increased from 800 to 1,100 million gallons per month

from 2009 to 2012 [23]. The majority of ethanol consumed in the US is derived from US grown corn, as 40% of the corn produced in 2011-2012 was used to produce ethanol or associated products, such as animal feed [23]. Aside from corn, some of the ethanol sold in the US is derived from sugarcane from Brazil. However, these imports are only a small fraction (less than 1%) of the total ethanol supply in the US [23]. To date, cellulosic ethanol has had a minimal role in US ethanol production, as financial barriers and technical scalability challenges have prevented high production volumes [24]. However, a recent study found that due to new ethanol plants coming online, 20,000 gallons of cellulosic ethanol was produced in late 2012 and their output is expected to rise to 5 million gallons by the end of 2013 [24]. However, this annual production rate would only be 0.4% of the total ethanol production in the US assuming 2012 production values [23], [24].

As compared to petroleum-derived fuels, biofuels present a unique set of challenges for typical attributional LCAs, such as the method used in this work. In attributional LCAs, environmental impacts are calculated according to industrial processes and it is assumed that the final destination of all carbon is known. However, this framework poses unique problems for biofuels. In biofuel LCAs, biogenic CO_2 is fully credited as it is assumed that the CO_2 uptake during feedstock growth exactly balances the CO_2 emitted due to combustion (during vehicle operation). This raises the issue of additionality because if the feedstock is earmarked for ethanol instead of food, no additional CO_2 is removed from the atmosphere by growing that feedstock. Also, leakages in GHG accounting occur due to the fact that the market will respond to a disruption in food sources and presumably, new land will be transformed into agricultural land to meet the market demands. Recent LCAs have attempted to capture this phenomenon, known as indirect land use change (ILUC), with a LUC factor that includes the impacts of deforestation, among other processes necessary to re-allocate land. However, there remains great variability due to the boundary used to find such LUC factors. Also, a discrepancy often exists between LCAs regarding co-product credits that are allocated by ethanol feedstock (e.g. animal feed, electricity) [25], [26], [27].

Due to biofuel-specific accounting difficulties as well as measurement uncertainties, such as N_2O emissions and soil organic carbon sequestration/emissions,

there is a great variability in the literature regarding life cycle impacts of ethanol [25], [26], [27]. For instance, Farell et al. performed a comparative study of select studies for corn ethanol and found that as compared to gasoline, corn ethanol GHG emissions results could range from +32% to -20% [27]. Also, Luo et al. assessed the impact of a range of assumptions on the environmental impact of corn stover-based ethanol and found that by incorporating the co-product impact of feed and fodder production, the GHG emissions changed from a positive to negative value [25]. Similarly, Wang et al. found that due to the lower fossil fuel energy required during farming and production of cellulosic ethanol, combined with the electricity credit, GHG emissions are very close to zero [26]. In the case of miscanthus, values are negative due to the CO_2 credits given due to LUC [26].

While the range of possible life cycle results is very large, the GREET 1 model provides a consistent method to compare ethanol derived from a range of feedstock options [12], [26]. As described in Wang et al., the model assumes specific co-products are derived for each feedstock (e.g. animal feed for corn ethanol, electricity for sugarcane and cellulosic ethanol) [12], [26]. Similar to other biofuel LCAs, it is assumed that there is no net change in biogenic CO_2 [26]. Also, land use changes are incorporated with global trade and soil organic carbon models that account for the differences in carbon emissions from specific crop types [26]. Accordingly, the energy and GHG emissions intensity of ethanol is shown in Table 28 with and without the inclusion of LUC impacts for GHG emissions. Overall, corn ethanol has the most significant GHG impact due to natural gas that provides power to the plant and nitrogen-based agricultural fertilizers that result in N_2O emissions [26]. Sugarcane has the next highest emissions and the highest energy requirement, largely due to increased transportation and distribution impact from Brazil to the US [26], [28]. Energy and GHG emissions for corn stover, switchgrass and miscanthus are minimal due to the low energy required during farming and the co-product credit for electricity production [26]. When considering the impact of LUC, results follow the same trend but are even less for corn stover and miscanthus, as carbon is assumed to be absorbed instead of released in the soil organic carbon model of these feedstocks [26].

Table 28: Energy and GHG emissions per MJ-ethanol for a variety of ethanol feedstocks [12]

	Energy (MJ/MJ)	GHG emissions (gGHG/MJ) [with LUC]	LUC
Corn	1.4	62 [65]	9.1 gGHG/MJ
Sugarcane	1.6	37 [53]	16 gGHG /MJ
Corn stover (cellulosic)	1.1	1 [0]	-1.2 gGHG /MJ
Switchgrass (cellulosic)	1.1	6 [7]	1.3 gGHG /MJ
Miscanthus (cellulosic)	1.2	1 [-11]	-12 gGHG /MJ

5.4 Results - Technology combinations

5.4.1 Mass reduction vs. advanced engines - ICV

The impact of using either lightweight materials or advanced gasoline engines to reduce life cycle energy and GHG emissions from an ICV is assessed using the aluminum-intensive and A/HSS vehicle designs, as described in Chapter 3, and the HEG engine model, presented in Chapter 4. Accordingly, the HEG engine model is integrated in the Autonomie ICV model and drive cycle fuel economy is determined. As previous described, the HEG engine is downsized from a 4-cylinder 2.6 L engine to a 3-cylinder 1.5 L engine to provide the same power and therefore, an equivalent 0-60 MPH acceleration time as the baseline ICV. Also, the vehicle-production energy and GHG emissions of the HEG engine is included in the life cycle model according to the results presented in Section 2.

The life cycle energy and GHG emissions for the NA-ICV0, A/HSS and aluminum lightweight ICVs (NA-ICV15-35) and HEG-ICV0 are shown in Figure 46. Error bars represent the variation in well-to-pump impacts for conventional oil and oil sands with surface and in situ mining processes. Results show that the life cycle energy and GHG emissions reduction achieved with the high efficiency gasoline engine exceeds the possible reduction by lightweighting the ICV up to 14%. This is due to the fact that life cycle results are strongly correlated to fuel economy and increase in fuel economy achieved by changing engines is much more significant than the lightweight BIW scenarios considered. Specifically, as compared to the baseline ICV, a 35% BIW mass

reduction reduces CAFE fuel consumption by 8.5% while simple changing engines reduces CAFE fuel consumption by 23%. Accordingly, well-to-pump and tank-to-wheel energy and GHG emissions are 23% lower for the HEG ICV as compared to the baseline ICV. Also, since vehicle production energy and GHG emissions are increased by only 1% by replacing engines, this results in a negligible increase in TVLC results. Thus, life cycle energy and GHG emissions are reduced by 7% and 22% for the ICV with 35% BIW mass reductions and high efficiency engine vehicle, respectively. Based on the trend of fuel economy with vehicle mass shown in Figure 46, it would require a 38% decrease in vehicle mass to achieve the same fuel economy, and therefore life cycle energy and GHG emissions, as the baseline ICV with the HEG engine.

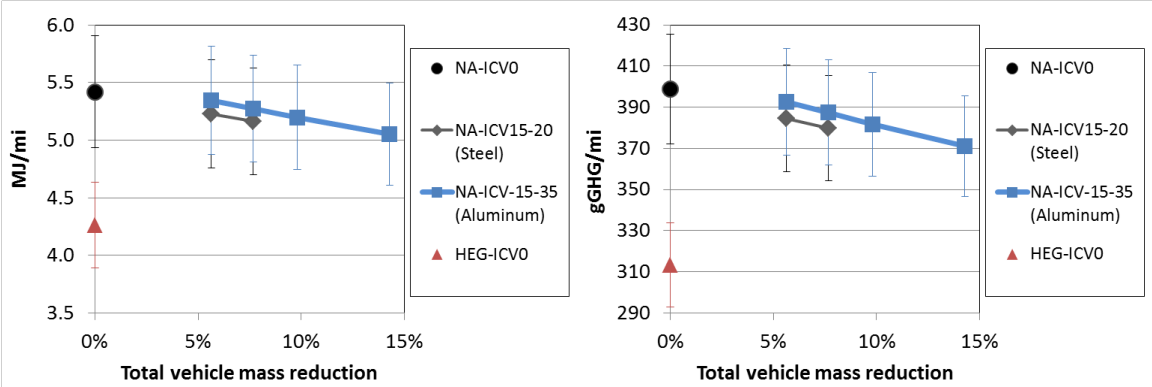

Figure 46: Life cycle energy and GHG emissions comparison of an advanced engine and lightweight ICVs. Error bars indicate well-to-pump variation of gasoline (conventional oil and tar sands).

While these results indicate expected trends based on the model, it is important to note that current downsized/boosted engines do not provide the fuel economy (and life cycle) benefits as shown in the model results. For instance, according to the EPA combined fuel economy for 2013 vehicles, the 1.6 L Ford Ecoboost Fusion achieves only a 7% decrease in fuel consumption as compared to the naturally aspirated 2.5 L Fusion [29].[4] This is due to two main reasons: 1) production engines require excess fuel at idle conditions, which was not incorporated in the engine model, and 2) the high dilution levels noted by Southwest Research Institute (SWRI) and used in the engine model are likely not realized in production engines, thus necessitating fuel enrichment and suboptimal spark timing to mitigate knock [30]. For instance, data published for the

[4] However, the 2014 2.0 L Ecoboost Explorer reduces fuel consumption by 13% as compared to the 2014 3.5 L Explorer [29]. Also, the 2014 1.4 L turbocharged Chevrolet Cruz reduces fuel consumption by 10% as compared to the 2014 1.8L version [29].

Ecoboost 1 shows that as load increases above 12 bar, brake specific fuel consumption (BSFC) begins to increase (e.g. about 10 g/kWh for a 10 bar BMEP increase), thus reducing some of the high load benefits assumed for downsized/turbocharged engines [31]. This increase in BSFC is likely due to lower dilution levels that are not significant enough to eliminate the need for knock mitigation, either by spark retard or fuel enrichment. On the other hand, experimental research at SWRI has shown that by using up to 25% dilution, fuel enrichment and spark retard can both be eliminated [30]. However, such dilution levels have been achieved by use of an advanced ignition system developed by SWRI which is currently not used in production engines [32].

Since the dilution levels used to create the HEG and E85 fuel economy maps are equivalent to those observed with SWRI's HEDGE engine, the brake specific fuel consumption for the HEG engine is consistent with the experimental fuel consumption results (see Chapter 4) [33]. Accordingly, life cycle results for the HEG ICV correspond to optimistic, but feasible engine/vehicle designs. Similarly, BIW designs using aluminum space frame or all A/HSS are most often used in luxury vehicles, such as the Audi A6 and Jaguar XL [34]. Since these designs are possible from a design and manufacturing perspective, they also are indicative of optimistic, but feasible life cycle results.

The sensitivity of life cycle results to fuel-cycle assumptions is evaluated by incorporating the range of possible well-to-pump values for gasoline, as identified in Section 3. Since the range of GHG emissions associated with oil shale is much larger than conventional oil or oil sands, the life cycle GHG reductions achieved by advanced engines or lightweight materials could be insignificant if oil shale is used with these vehicles. However, since current levels of oil shale production are minimal it is reasonable to assume the worst-case scenario of oil sands produced with in situ processes. Based on these results, life cycle emissions are still lower for the ICV with the high efficiency engine as compared to the lightest weight ICV with the baseline engine, as shown in Figure 46.

5.4.2 Mass reduction and advanced engines - ICV

The combined benefits of using advanced engines with lightweight ICVs is evaluated by applying the HEG and E85 engine maps to the Autonomie model for a

lightweight ICV with 35% BIW mass reductions (14% total vehicle mass reductions). Accordingly, the HEG and E85 engines are downsized from a 4-cylinder 2.6 L engine to 1.4 L and 1.1 L 3-cylinder engines and fuel economy results are obtained, as shown in Table 29. Similar to previous results, the change in vehicle production energy and emissions are negligible from downsizing from a 4 to 3-cylinder engine.

The life cycle impact of individual and combined applications of lightweight materials and advanced engines are shown in Figure 47 for the ICV. Error bars indicate the range of well-to-pump impacts for gasoline (conventional oil and oil sands) and ethanol (diverse feedstocks and LUC factors as identified in Table 28). Due to the previously described uncertainties with ethanol LCAs, the well-to-tank emissions (i.e. combustion emissions) are shown in the results for the E85-ICV35. However, since well-to-tank emissions would not be considered with typical life cycle accounting methods, the following analysis assumes this is excluded when comparing total vehicle life cycle results.

Results show that by using the advanced gasoline engine with the lightweight ICV, fuel consumption is decreased by 23% and life cycle energy and GHG emissions decrease by 26%. Note that the improvement in life cycle impacts due to lightweight materials and advanced engines is not directly additive, as this would have resulted in a 27% improvement. This is due to the fact that the baseline engine in the lightweight ICV is also downsized, resulting in additional fuel economy improvements. While not shown, a similar trend exists for the E85 engine, which has an even higher efficiency than the HEG engine.

Assuming that GHG emissions from combustion are negated by uptake of biogenic CO_2, the lowest life cycle GHG emissions are associated with the E85-ICV35, while the lowest life cycle energy consumption occurs for the HEG-ICV35. Energy consumption is significantly higher for the E85-fueled vehicle due to the increased energy required in the well-to-pump phase of the life cycle, despite the lower energy consumed on-board the vehicle (i.e. tank-to-wheel). Life cycle energy and GHG results are highly sensitive to the possible variation due to fuel-cycle impacts, particularly for ethanol. For instance, the magnitude of the uncertainty due to feedstock type and LUC for

the E85-ICV35 (180 gGHG/mi) is over three times higher than the greatest uncertainty for gasoline with the NA-ICV0 (54 gGHG/mi).

Table 29: Engine size and CAFE fuel economy (MPG) for ICV technology combinations

	NA-ICV0	NA-ICV35	HEG-ICV0	HEG-ICV35	E85-ICV35
Engine Size	2.6 L (4-cyl)	2.3 L (4-cyl)	1.5 L (3-cyl)	1.35 L (3-cyl)	1.1 L (3-cyl)
CAFE MPGe†	33	36	43	47	52
gge/100 mi†	3.0	2.8	2.3	2.1	1.9
kJ/m	2.3	2.1	1.8	1.6	1.5

†Miles per gallon equivalent (MPGe) and gallon of gas equivalent (gge) based on LHV of gasoline = 122.5 MJ/gal, LHV of E85 = 86.8 MJ/gal.

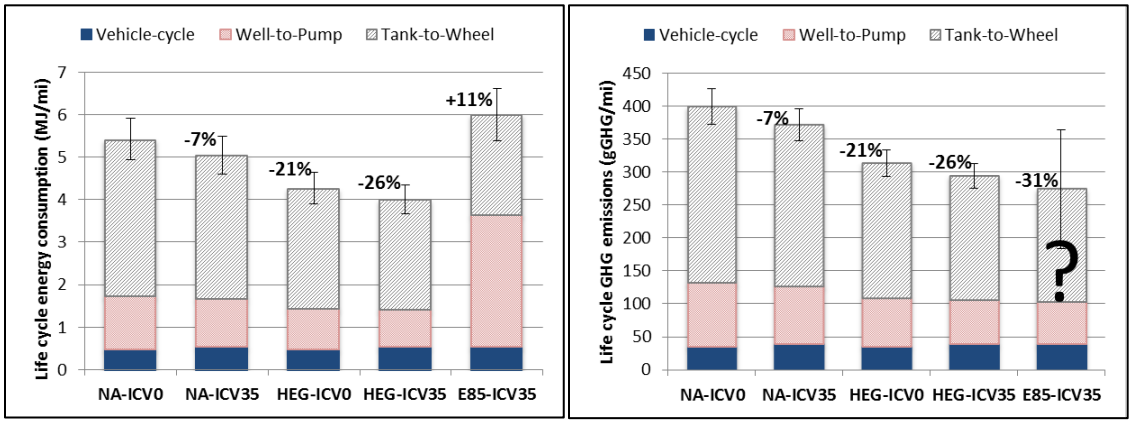

Figure 47: Life cycle results for lightweight ICVs using advanced gasoline and E85 engines. Error bars indicate well-to-pump variation of gasoline (conventional oil and tar sands) and ethanol (corn, sugarcane and biomass with and without LUC.

5.4.3 Mass reduction and advanced engines - HEV and PHEV

The impact of using advanced gasoline and E85 engines with lightweight HEVs and PHEVs is shown in Table 30 and Figure 48-Figure 49. Error bars indicate the range of fuel-cycle impacts for gasoline, ethanol and electricity, in the case of the PHEV. Similar to the trends shown for the ICV, the combination of mass reduction and advanced engine technologies provide the maximum benefits. However, since the hybrid vehicles rely on the engine for only a portion of the drive cycle, the impact of increasing engine efficiency is much less significant. For instance, while the HEG and E85 engines reduce fuel consumption of the ICV35 by 23% and 29% as compared to the NA engine, using

these engines in the HEV35 only reduces fuel consumption by 14% and 17%, respectively. The potential for fuel consumption reductions is even less for the PHEV because the total fuel economy is a weighted sum of blended and all-electric operation, and the efficiency in all-electric mode is constant regardless of engine type. Accordingly, even though the blended fuel economy results are very similar to those of the HEV, the total fuel consumption for the PHEV is only reduced by 6% with the HEG engine and 8% with the E85 engine.

As shown in Figure 5-6, the trend of HEV and PHEV life cycle energy and GHG emissions is highly correlated to fuel consumption and well-to-pump assumptions regarding ethanol, gasoline and electricity. Due to the higher efficiency of the E85 engine, tank-to-wheel GHG emissions are lowest for the ethanol-fueled HEV and PHEV. However, similar to the E85-ICV35, life cycle GHG emissions for the ethanol-fueled hybrids have a high degree of uncertainty. If it is assumed that biogenic CO_2 is fully credited and CO_2 from combustion is removed from the analysis, life cycle GHG emissions are lower for the E85-HEV35 as compared to the E85-PHEV35. The E85-PHEV35 results in slightly higher emissions (without combustion CO_2) due to the requirement that 27% of total miles traveled is fueled by electricity. Also, similar to the ICV results, the lightweight vehicles with the HEG engine achieve significant reductions in GHG emissions as compared to the NA-(P)HEV0 and have the lowest life cycle energy requirements.

Considering the ICV, HEV and PHEV technology combinations presented in Figure 4-6, life cycle energy consumption is lowest for the HEG-PHEV35 and GHG emissions are least for the E85-HEV35. For each vehicle, the trend of life cycle results is dependent on the fuel sources and corresponding assumptions, including the fuel source of electricity for the PHEV. For the well-to-pump scenarios considered in this work, ethanol has the greatest uncertainty followed by electricity and lastly, gasoline.

Table 30: CAFE fuel economy (MPG) for hybrid vehicle technology combinations

		NA-0	NA-35	HEG-35	E85-35
HEV	Engine Size	1.6 L (3-cyl)	1.4L (3-cyl)	0.8 L (2-cyl)	0.7 L (2-cyl)
	CAFE MPGe[†]	50	54	63	66
	gge/100 mi[†]	2.0	1.9	1.6	1.5
	kJ/m	1.5	1.4	1.2	1.2
PHEV	Engine Size	1.6 L (3-cyl)	1.5 L (3-cyl)	0.9 L (2-cyl)	0.7 (2-cyl)
	CAFE MPGe[†‡]	77	84	90	92
	gge/100 mi[†‡]	1.3	1.2	1.1	1.1
	kJ/m	1.3	1.2	1.0	1.0

[‡]Calculated with a utility factor (UF) of 0.271 and the EPA conversion that 1 gallon of gasoline is equivalent to 33.7 kWh.

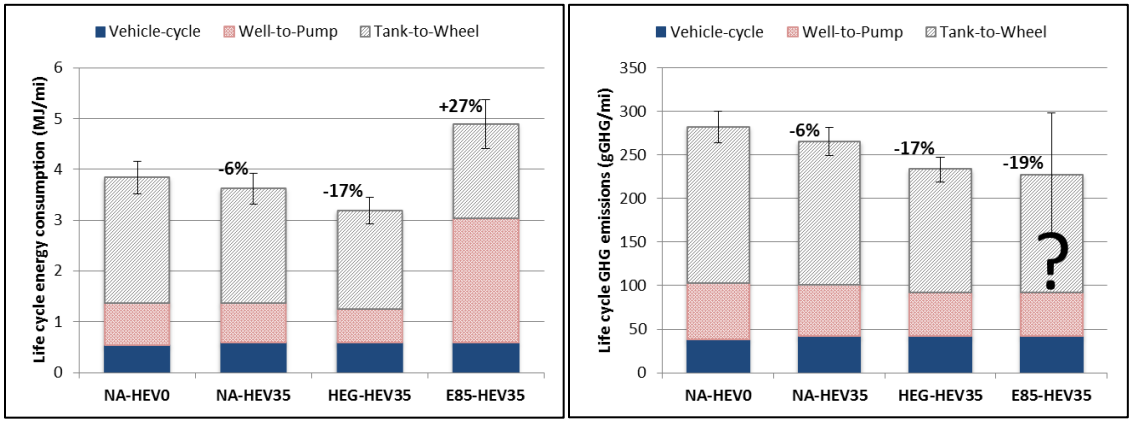

Figure 48: Life cycle results for lightweight HEVs using advanced gasoline and E85 engines. Error bars indicate well-to-pump variation of gasoline (conventional oil and tar sands), ethanol (corn, sugarcane and biomass with and without LUC), and electricity (greatest and least carbon intensive NERC grid regions).

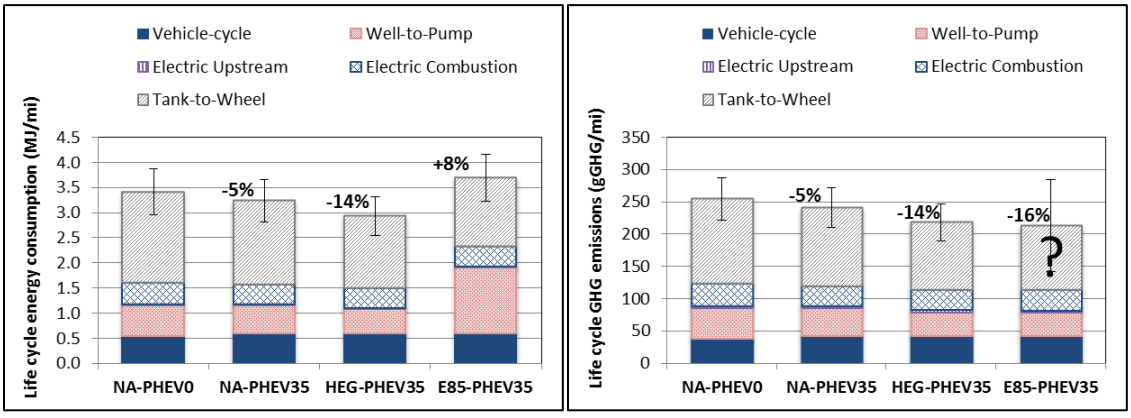

Figure 49: Life cycle results for lightweight PHEVs using advanced gasoline and E85 engines. Error bars indicate well-to-pump variation of gasoline (conventional oil and tar sands), ethanol (corn, sugarcane and biomass with and without LUC), and electricity (greatest and least carbon intensive NERC grid regions).

5.5 Conclusion

The life cycle energy and GHG emissions of an ICV, HEV and PHEV used with lightweight materials and/or advanced engines is evaluated with consideration of the plausible range of well-to-pump impacts associated with gasoline, ethanol and electricity. A model is developed to account for mass and materials changes necessary for downsized/boosted engines and is incorporated in the vehicle-cycle analysis of HEG and E85 vehicles. Also, a range of fuel-cycle impacts due to oil type / extraction method and ethanol feedstock / life cycle accounting method is included and represented by error bars in the analysis.

A life cycle comparison of using either lightweight materials or advanced engines for the ICV indicates that the most energy and GHG reductions are possible with the HEG engine. This is due to the fuel economy improvement observed with the HEG-ICV0 as compared to the NA-ICV35, which represents a total vehicle mass reduction of 14%. The fuel economy trends found in this work are consistent with previous work that has demonstrated a 7% improvement in fuel economy per 10% vehicle mass reduction and has predicted a 20% fuel economy improvement with an experimental version of the HEG engine (i.e. SWRI's HEDGE engine) [35], [36]. Based on the trend of fuel economy with mass determined in this work, a 38% decrease in vehicle mass would be necessary for the NA-ICV to achieve the same fuel economy and life cycle results as the HEG-ICV0.

Using mass reduction techniques and advanced engines in the same ICV platform further reduces life cycle energy and GHG emissions. For instance, while the NA-ICV35 and HEG-ICV0 reduces life cycle impacts by 7% and 22%, respectively, the HEG-ICV35 results in a 27% reduction. Since the impact of increased vehicle production energy and emissions is negligible, the decrease in life cycle impacts is due entirely to the reduction in fuel consumption, which is 9%, 24% and 30% for the NA-ICV35, HEG-ICV0 and HEG-IVC35 as compared to the NA-ICV0. Since the efficiency of the E85 engine is higher than the HEG engine, fuel consumption (based on gallons of gasoline equivalence) is reduced even further for the E85-ICV0 and E85-ICV35 (e.g. 30% and 35%). It is interesting to note that the benefit of combining lightweight and advanced engine technologies on fuel economy and life cycle results is not directly additive. This is due to

the fact that the NA-ICV35 engine is downsized to meet performance specifications, thus providing fuel economy benefits that are not included in the HEG-ICV35 or E85-ICV35 models. However, mass reduction and advanced engines are complementary technologies, as downsized engines are particularly desirable for vehicles with a lower total mass.

Hybrid vehicles show similar life cycle trends, but to a lesser extent, as compared to ICVs as lightweight materials and advanced engines are incorporated to their design. For instance, as compared to ICVs, the improvement from replacing the NA engine with the HEG or E85 engine is less for hybrid vehicles due to the fact that operation is split between the engine and motor. It is important to note that since controls were not optimized for each hybrid configuration, results are not representative of the maximum fuel consumption reduction possible. Thus, based on these assumptions, fuel consumption (on a MPGe basis) is reduced at most 24% and 16% for the E85-HEV35 and E85-PHEV35 as compared to the NA-HEV0 and NA-PHEV0. Furthermore, fuel economy and life cycle improvements for the PHEV are less than the HEV due to the dependence on all-electric consumption, which is constant regardless of engine efficiency.

Due to the higher fuel economy of hybrid vehicles, life cycle impacts are significantly lower for these vehicles. The least life cycle energy and GHG emissions occur for the lightest weight hybrid vehicles that use the HEG or E85 engine. Due to the high well-to-pump energy requirements of ethanol, energy consumption is lowest for the HEG as compared to the E85 in the PHEV35. However, assuming that the GHG emissions from combustion are negated by uptake of biogenic CO_2, GHG emissions are lower for the E85 as compared to the HEG in any vehicle. With GHG emissions from combustion excluded from the LCA, the relative impact of electricity increases, resulting in life cycle emissions that are higher for the E85-PHEV35 as compared to the E85-HEV35. Thus, life cycle GHG emissions are lowest for the E85-HEV35.

While the implementation rates of these technologies will depend on their cost and the price of fuel, it is clear that advanced downsized/boosted engines (with gasoline or ethanol) and lightweight materials provide complimentary benefits for both conventional and electric vehicles and will play a key role in meeting future CAFE

standards. Furthermore, reductions in life cycle energy and GHG emissions will take place as vehicles with these technologies are incorporated in the current fleet.

5.6 References

[1] www.A2Mac1.com, Automotive Benchmarking, Yipsilanti, MI, 2013.

[2] European Aluminum Association, "The aluminum automotive manual," 2011.

[3] Ford, "2013 Ford Fusion Technical Specifications," 2013.

[4] S. Birch, "Federal-Mogul's new 2D testing process helps diesel pistons stand the pressure," *SAE Vehicle Engineering Online*, 2012.

[5] E. Huw, "Ford Focus EcoBoost 1.0L Review," *AutoGuide.com*, 2012.

[6] I. Roy F. Weston, "Life cycle inventory report for the North American aluminum industry," 1998.

[7] R. Geyer, "Life Cycle Energy and Greenhouse Gas (GHG) Assessments of Automotive Material Substitution: WorldAutoSteel Energy and GHG Model," 2012.

[8] Argonne National Laboratory, "GREET 2 rev1." UChicago Argonne, LLC, 2012.

[9] Federal-Mogul, "Federal-Mogul: The Heart of Powertrains," *Powertrain overview brochure*, 2013.

[10] SAE International, "Ford 's new 1.0-L EcoBoost I3 is big on low-friction technology," *Automotive Engineering Online*, 2012.

[11] US Environmental Protection Agency, "eGRID2012 year 2009 Summary Tables," 2012.

[12] Argonne National Laboratory, "GREET 1 rev2." UChicago Argonne, LLC, 2012.

[13] U.S. Energy Information Administration, "Short-Term Energy Outlook - June 2013," 2013.

[14] U.S. Energy Information Administration, "Glossary," 2004.

[15] A. R. Brandt, "Converting Oil Shale to Liquid Fuels with the Alberta Taciuk Processor: Energy Inputs and Greenhouse Gas Emissions," *Energy & Fuels*, vol. 23, pp. 6253–6258, Dec. 2009.

[16] S. M. Jordaan, D. W. Keith, and B. Stelfox, "Quantifying land use of oil sands production: a life cycle perspective," *Environmental Research Letters*, vol. 4, pp. 15, 2009.

[17] U.S. Energy Information Administration, "U.S. Net Imports by Country," 2013. [Online]. Available: http://www.eia.gov/dnav/pet/pet_move_neti_a_ep00_imn_mbblpd_m.htm. [Accessed: 16-Jul-2013].

[18] L. Maugeri, "Oil: The Next Revolution," *The Geopolitics of Energy Project*, Belfer Center, Harvard Kennedy School, 2012.

[19] J. A. Bergerson, O. Kofoworola, A. D. Charpentier, S. Sleep, and H. L. Maclean, "Life cycle greenhouse gas emissions of current oil sands technologies: surface mining and in situ applications," *Environmental Science & Technology*, vol. 46, no. 14, pp. 7865–74, Jul. 2012.

[20] A. Burnham, J. Han, C. E. Clark, M. Wang, J. B. Dunn, and I. Palou-Rivera, "Life-cycle greenhouse gas emissions of shale gas, natural gas, coal, and petroleum," *Environmental Science & Technology*, vol. 46, pp. 619–27, 2011.

[21] S. Mui, L. Tonachel, B. Mcenaney, and E. Shope, "GHG Emission Factors for High Carbon Intensity Crude Oils," *Natural Resources Defense Council*, June, 2010.

[22] K. J. Gerdes and T. J. Skone, "An Evaluation of the Extraction, Transport and Refining of Imported Crude Oils and the Impact on Life Cycle Greenhouse Gas Emissions," *National Energy Technology Laboratory*, Project no. DOE/NETL-2, 2009.

[23] U.S. Energy Information Administration, "Biofuels Issues and Trends," October, 2012.

[24] U.S. Energy Information Administration, "Cellulosic biofuels begin to flow but in lower volumes than foreseen by statutory targets," *Today in energy*. [Online]. Available: http://www.eia.gov/todayinenergy/detail.cfm?id=10131. [Accessed: 17-Jul-2013].

[25] L. Luo, E. Voet, G. Huppes, and H. A. Udo de Haes, "Allocation issues in LCA methodology: a case study of corn stover-based fuel ethanol," *The International Journal of Life Cycle Assessment*, vol. 14, pp. 529–539, Jun. 2009.

[26] M. Wang, J. Han, J. B. Dunn, H. Cai, and A. Elgowainy, "Well-to-wheels energy use and greenhouse gas emissions of ethanol from corn, sugarcane and cellulosic biomass for US use," *Environmental Research Letters*, vol. 7, no. 4, p. 045905, Dec. 2012.

[27] A. E. Farrell, R. J. Plevin, B. T. Turner, A. D. Jones, M. O. Hare, and D. M. Kammen, "Ethanol Can Contribute to Energy and Environmental Goals," *Science,* vol. 311, pp. 506–508, January, 2006.

[28] J. Han, J. B. Dunn, H. Cai, A. Elgowainy, and M. Q. Wang, “Updated sugarcane parameters in GREET1_2012, Second Revision,” Argonne National Laboroatory, 2012.

[29] www.fueleconomy.gov, "EPA Fuel Economy,” 2013. [Online]. Available: http://www.fueleconomy.gov/.

[30] T. Alger and J. Gingrich, “Cooled EGR for Fuel Economy and Emissions Improvement in Gasoline Engines,” JSAE Paper 20105013, 2010.

[31] C. E. Weaver, “Advanced Gasoline Turbocharged Direct Injection (GTDI) Engine Development,” *2011 DOE Vehicle Technologies Program Review*, Project ID ACE065, 2011.

[32] T. Alger, J. Gingrich, B. Mangold, and C. Roberts, “A Continuous Discharge Ignition System for EGR Limit Extension in SI Engines,” SAE Paper 2011–01–0661, 2012.

[33] T. Alger, “SwRI’s HEDGE Technology for High Efficiency, Low Emissions Gasoline Engines,” in *DEER Conference*, September, 2010.

[34] N. Lutsey, “Review of technical literature and trends related to automobile mass-reduction technology,” *California Air Resources Board*, 2010.

[35] L. W. Cheah, “Cars on a Diet : The Material and Energy Impacts of Passenger Vehicle Weight Reduction in the U.S.,” MIT, Doctoral Dissertation, 2010.

[36] T. Alger, “SwRI HEDGE Program,” *(Presentation), Southwest Research Institute*, 2006.

5.7 Appendix

Table 31: Part list for the baseline engine

Crankshaft system	Cylinder head system	Engine block system	Engine mounts system
crankshaft, bearings crank seal housing, sensors, pulley, pistons system	cylinder head, bearings, camshafts rocker arms, valve train, Intake/exhaust valves, sprockets, cam sensor, spark plugs, ignition coil assembly	engine block, belts, knock sensor, starter motor	left and right mounts, oscillating mounts, motor mount stopper
Front engine system	**Gasoline fuel injection system**	**Lubrication system**	**Style cover system**
crankshaft sprocket, timing belt housing, timing system	injector rails, injectors, intake manifolds, throttle body	dip stick housing, oil pump/filter system, piston lubricators	noise insulation, style cover

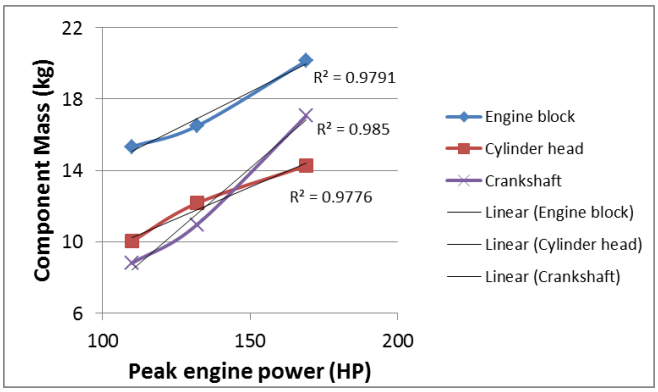

Figure 50: Correlation of peak engine power and mass of the engine block/head and crankshaft [1]

Chapter 6: Conclusions and recommendations for future work

6.1 Conclusions

The framework developed in this work enables an evaluation of vehicle technologies that have been proven as technically feasible but do not hold a significant share of the market. For instance, lightweight vehicle designs that use aluminum-intensive or advanced / high strength steel (A/HSS) body structures are technically feasible but remain limited to niche markets and proof-of-concept projects. Similarly, experimental research engines have shown brake thermal efficiencies exceeding 40%, but these efficiencies are not realized in current production vehicles. By incorporating lightweight materials and advanced gasoline and ethanol engines in the life cycle modeling framework, the individual and combined potential of these technologies are assessed, providing guidance for the future application of the technologies.

This work advances previous life cycle models by providing a further level of detail regarding advanced engines and hybrid electric vehicle models. For instance, fuel economy maps for downsized/boosted dilute gasoline and ethanol engines were developed and integrated in the vehicle simulations. Also, internal combustion vehicle (ICV), hybrid electric vehicle (HEV) and plug-in electric hybrid vehicle (PHEV) models were created using newly developed design harmonization techniques. Using a harmonized method to model vehicles with diverse powertrains ensures that vehicles are functionally equivalent and that hybrid vehicle models account for structural changes that are necessary to support the heavier mass of electric powertrains. Similar to previous work, lightweight vehicle models were created using primary and secondary mass reductions, and vehicle performance was maintained by re-sizing powertrain components. Primary reductions were evaluated with body-in-white (BIW) mass reduction scenarios ranging from 15%-35% for an aluminum-intensive design and 15%-20% for an optimized A/HSS structure.

Key findings from this work pertain to modeling methods, evaluation of technologies and implications for policy makers / automobile manufacturers, as follows:

MODELING METHODS

- DESIGN HARMONIZATION – As compared to previous techniques, a more streamlined and flexible method was developed to create equivalent vehicle models for vehicles with diverse powertrains. Based on a regression analysis of conventional and hybrid vehicle teardown data, a 1 and 2 fit correlation was determined using front track width and powertrain mass to predict vehicle mass. The design harmonization methods show that 0.2-0.3 kg of additional structural support is required per unit increase in powertrain mass. As compared to the constant glider or structural mass multiplier methods (using a ratio of 0.5:1), life cycle results obtained with the design harmonization method vary by -0.7% to +2%. Depending on the purpose of the study (e.g. if detailed vehicle modeling is desired) it may be acceptable to use the simpler approaches. However, if future work requires modeling the design trends of diverse vehicle platforms, the design harmonization method is most appropriate. The techniques presented in this work provide a flexible method to account for hybrid-specific design requirements and create comparable models of conventional and electrified vehicles.

- MASS ELASTICITY OF FUEL ECONOMY AND LCA – By modeling the fuel economy of the baseline and lightweight vehicles with forward-facing vehicle simulations, the mass elasticity of fuel economy (defined as the percent change in fuel economy per percent change in vehicle mass) is captured in the life cycle model for each powertrain-type vehicle. Thus, life cycle results show that for a unit decrease in mass, the maximum absolute and percent reductions occur for the ICV as compared to the HEV and PHEV. In other words, lightweight vehicle materials are most effective at reducing life cycle energy and GHG emissions for an ICV, as compared to HEVs or PHEVs. It is recommended that future work include this phenomenon when assessing the fuel economy or life cycle potential of mass reduction for various powertrain architectures.

EVALUATION OF TECHNOLOGIES

- TECHNOLOGY COMBINATION WITH THE LEAST LIFE CYCLE IMPACTS – The least life cycle energy and GHG emissions occur for the lightest weight hybrid vehicles that use an advanced gasoline or ethanol engine. Specifically, the least energy consumption occurs for the lightweight PHEV using a high efficiency gasoline engine. Energy consumption is lower for the PHEV fueled by gasoline instead of ethanol due to the high energy required to produce ethanol. Also, energy requirements are lowest for PHEVs because they have the highest vehicle efficiency. As compared to the gasoline fueled vehicles, life cycle GHG emissions are lowest for the lightweight PHEV with the high efficiency gasoline engine. While the E85 engine reduces GHG emissions during the vehicle operation, life cycle GHG emissions are indeterminate for biofuels.

- ADVANCED ENGINES - The potential of advanced engines to decrease life cycle energy and GHG emissions is significant, as dilute downsized/boosted gasoline and ethanol engines increase fuel economy by 24-30% for ICVs and 6-17% for hybrid vehicles. A comparison of mass, materials, and production energy/GHG emissions for a 4-cylinder naturally aspirated and 3-cylinder downsized/turbocharged engine reveals that the impact on vehicle production energy and GHG emissions is negligible (less than 1%). Overall, advanced gasoline and ethanol engines reduce life cycle GHG emissions by up to 26%, depending on vehicle type. Energy consumption is also reduced by up to 26% for the advanced gasoline engine, but increased by 6-14% for the ethanol engine due to the increased energy required to produce ethanol.

- LIGHTWEIGHT MATERIALS – Life cycle results show that by reducing the BIW mass by 35% with an aluminum-intensive design decreases life cycle impacts by 5-7%, despite the fact that the energy and GHG emissions intensity of aluminum is higher than steel. Similarly, as compared to aluminum A/HSS results in 5% life cycle energy and GHG reductions. The energy and GHG reduction

from aluminum and A/HSS are similar because while there is less potential for mass reduction with A/HSS, the energy and GHG emissions to produce A/HSS are much lower than for aluminum. Furthermore, the potential to reduce life cycle impacts per unit mass removed is higher for A/HSS than aluminum. Therefore, A/HSS is more advantageous for BIW mass reduction scenarios up to a 20%, while maximum life cycle reductions are achieved with a 35% reduction in BIW mass using aluminum.

- ADVANCED ENGINES VS. LIGHTWEIGHT MATERIALS – For the scenarios considered in this work, advanced gasoline and ethanol engines provide significantly more life cycle energy and GHG emissions reductions than achieved with lightweight vehicle materials due to the higher fuel economy realized with advanced engines. For instance, using the high efficiency gasoline engine in the ICV with no BIW mass reduction results in a 24% reduction in fuel consumption as compared to the baseline vehicle. However, if the BIW mass is reduced by 35% and the ICV is operated with the baseline engine, fuel consumption is reduced by only 9%. Also, while certain lightweight materials, such as aluminum, increase vehicle production energy and GHG emissions, there is no noted increase for advanced engines. Thus, advanced engines offer more dramatic reductions in life cycle energy and GHG emissions, while reductions from lightweight materials are more modest. While the advanced engine/fuel strategies considered in this work are currently not available in production vehicles, aluminum and A/HSS are presently being implemented in vehicle design, particularly for luxury vehicles.

- CONVENTIONAL VS. HYBRID ELECTRIC VEHICLES - As compared to ICVs, HEVs and PHEVs offer significant reductions in life cycle energy and GHG emissions, corresponding to the higher fuel economy of hybrid vehicles. Since controls were not optimized in this work, it is expected that the attainable fuel economy and life cycle improvements are even higher for hybrid vehicles in the market. When lightweight materials and advanced engines are used with

ICVs, HEVs and PHEVs, ICVs show the greatest potential for life cycle reductions due to their higher mass elasticity of fuel economy. Also, since ICVs are propelled entirely by power from the engine, increasing engine efficiency results in more significant fuel consumption and life cycle reductions for these vehicles. While advanced engines and lightweight materials have less of an impact for hybrid vehicles, there is an opportunity to significantly reduce life cycle GHG emissions from PHEVs if the vehicle is charged in an electric grid region with a low carbon intensity.

- LIFE CYCLE TRADEOFFS WITH ETHANOL - The fuel properties of ethanol enable up to an 18% improvement in peak engine efficiency as compared to a baseline naturally aspirated gasoline engine, even when considering knock limitations. This results in a 8-30% decrease in fuel consumption (on a MPGe basis) for each vehicle type, with maximum reductions occurring for the ICV. However, these reductions in energy consumption are offset to some extent by the significant energy requirements to produce ethanol. Final life cycle results are indeterminate due to the inherent difficulties of using LCA to evaluate biofuels.

IMPLICATIONS FOR POLICY MAKERS / AUTOMOBILE MANUFACTURERS

- STRUCTURAL MASS REQUIREMENTS FOR HYBRID ELECTRIC VEHICLES – This work has evaluated vehicle teardown data and developed correlations that account for the increased structural mass that may be necessary for electrified powertrains. If the structural mass increase is significant, fuel economy would decrease and the energy and GHG emissions associated with vehicle production would increase, thus negating some of the benefits of hybrid vehicles. This work finds that 0.2-0.3 kg of structural support is required for a 1 kg increase in powertrain mass, resulting in a less than 1% increase in vehicle production energy and GHG emissions.

- MASS REDUCTION FOR CONVENTIONAL VS. ELECTRIFIED VEHICLES – Since the mass elasticity of fuel economy is greatest for ICVs, these vehicles have the greatest potential to reduce life cycle energy and GHG emissions per unit

of mass removed from the vehicle. Thus, it is recommended that automakers aggressively incorporate mass reduction techniques in the design of ICVs. Such techniques should also continue to be applied to hybrid vehicles, as this will also provide fuel economy benefits and enable smaller batteries to be used with no reduction in performance or range. Smaller batteries are desirable because they can reduce the environmental impact of hybrid vehicle production and also lower the cost of hybrid vehicles, thus increasing their market penetration. Overall, while vehicle mass reduction has the potential to reduce life cycle impacts for all powertrain type vehicles, maximum fuel economy improvements are achieved for lightweight ICVs.

6.2 Recommendations for future work

Based on the findings of this work, the following questions could be posed for future work:

1. *What are the life cycle trade-offs of using ethanol vs. a petroleum-based high octane fuel with a high heat of vaporization?*

This work has demonstrated the potential of ethanol to increase engine efficiency when used with a downsized/boosted engine with a high compression ratio (14:1) and significant amount of dilution (25% EGR). However, the life cycle impacts of ethanol are uncertain, as cellulosic ethanol is currently uneconomical and corn-based ethanol results in competition with food resources. Also, from a life cycle perspective, the GHG emissions for biofuels are debatable, since the impacts of dedicating farmland for an energy crop are not straightforward. Thus, it may be desirable to produce a petroleum-based fuel with the beneficial fuel properties of ethanol, namely a high octane number and high heat of vaporization. Future work could compare the energy and environmental impacts of manufacturing this petroleum-based fuel as compared to ethanol and assess the trade-offs over the total vehicle life cycle. If the increased GHG emissions associated with fuel production do not outweigh the GHG reductions due to increased fuel economy, the petroleum-based fuel could provide a more certain pathway to reduce life cycle GHG

emissions. Thus, results of this analysis could be used to inform future policies regarding optimal fuels for light-duty vehicles.

2. *What policies could encourage the production and use of engines and fuels that are optimized for each other?*

There remains a potential to create policies that encourage the use of advanced engines and fuels that are optimized for each other. Current policies, such as the renewable fuel standard and CAFE credits for flex fuel vehicles (FFV), have not produced the desired effects. E85 is not widely available and flex fuel vehicles are often fueled by gasoline instead of ethanol. Furthermore, due to the uncertainty of E85, most FFV engines are not optimized for ethanol and the fuel economy improvements that are possible with a high octane/heat of vaporization fuel are not being realized. Thus, future work could propose a policy solution that encourages the production of fuels and engines that are tailored for each other and the use of these technologies together.

3. *To reduce life cycle energy and GHG emissions, is it more desirable to have one or more than one vehicle platform for conventional and electrified vehicles?*

While electrified vehicles may require design modifications to account for powertrain component changes and provide the support necessary for heavier powertrains, it remains unclear if it is more advantageous to create a new vehicle platform for electrified vehicles, such as the Toyota Prius, or use an existing platform, such as the GM Volt. With one platform, fewer modifications may be required to the existing vehicle manufacturing process. However, a trade-off exists when considering conventional vehicles that share the same platform as electrified vehicles. Since vehicles must be designed to support the heaviest powertrain, any increase in structural mass would reduce the fuel economy of the conventional vehicles in a one-platform approach. To evaluate these trade-offs, an assessment should include vehicle manufacturing processes and life cycle analyses of vehicles sharing the same platform. Also, trends in vehicle design may be modeled using the regression analysis method proposed in this work, which should be updated as more electric vehicle data becomes available.

4. *What are the implications of using distinct regression correlations for electrified vehicles to predict vehicle mass instead of one aggregated correlation to describe all vehicles?*

This work has discussed the differences of using 1 vs. 2 regression correlations to predict vehicle mass from powertrain mass and front track width. However, as more data becomes available on electrified vehicles, the regression analysis method should be updated to capture the differences between each powertrain-type vehicle. For instance, future work could model different powertrain type vehicles with separate regression equations or the degree of hybridization could be included in the analysis as a parameter. This will provide further insight in the unique design characteristics of diverse powertrain vehicles and increase the level of modeling detail included in the design harmonization method.

5. *Based on technology adoption scenarios, what is the potential of lightweight materials, advanced engines, and electrified vehicles to reduce GHG emissions in the US by 2050?*

While this work has evaluated the current potential of lightweight materials, advanced engines and electrified vehicles to reduce life cycle GHG emissions, the future potential of these technologies should be evaluated to provide a roadmap for achieving GHG reduction targets. Since there is an increased cost associated with clean vehicle technologies, their adoption will depend on their current price, balanced by any subsidies, and the price of fuel. Thus, technology adoption pathways should be evaluated under reasonable economic and policy scenarios. Since the same life cycle goals may be achieved by using different technologies or technology combinations (as shown in this work), such an analysis could provide insight to the most affordable pathway to an equivalent reduction in GHG emissions.